GOME-2 Error Assessment Study

Phase V: Final Report

Version 1-1

Study Team

Dr Brian Kerridge
    (Science Coordinator)
Dr Richard Siddans
Mr Barry Latter

Prof. Dr Ilse Aben
Dr C. Tanzi
Dr W. Hartmann

Prof. Dr. J. P. Burrows
Dr Mark Weber
Dr Ruediger de Beek
Dr Vladimir Rozanov
Dr Andreas Richter

Space Science Department
Rutherford Appleton Laboratory
Chilton, Didcot
Oxfordshire
OX11 0QX
UK

SRON
Earth Oriented Science Division
Sorbonnelaan 2
NL-3584 CA Utrecht
The Netherlands

FB1 Institute for Environmental Physics (IUP)
University of Bremen
Postfach 33 04 40
D-28334 Bremen
Germany

Eumetsat Technical Officer:

Dr R Munro

EUMETSAT ·
Am Kavalleriesand 31
Postfach 10 05 55 ·
D-64295 Darmstadt
Germany

Study Manager

Mr M.G. Wickett

Serco Europe Ltd
Kempton Point
68 Staines Road West
Sunbury-on-Thames
Middlesex TW16 7AX
UK

Date: April 2004

List of Contents

7   Task 3: Optimal operational settings and error mitigation

List of Tables

List of Figures

Supporting CD-ROM

CD-ROM: GOME-2 Error Assessment Study
– Phase V: Final Report and supporting documents

The CD-ROM, which is supplied with this Final Report, contains the following files:

Phase V:

Executive Summary	`GOME-2_FR_Ph__V___Exec_Summary.pdf`
Final Report	`GOME-2_FR_Ph__V___Final_Report.pdf`
Appendices (A – F)	`GOME-2_FR_Ph__V__Appendices_A-F.pdf`

Phase I - IV:

Executive Summary	`GOME-2_FR_Ph_I-IV__Exec_Summary.pdf`
Final Report	`GOME-2_FR_Ph_I-IV__Final_Report.pdf`
Appendices (A – E)	`GOME-2_FR_Ph_I-IV_Appendices_A-E.pdf`

All these files are intended primarily for viewing on a PC, but they are in a suitable format for printing as separate documents.

Contents of Phase V Appendices A to F

GOME-2 Error Assessment Phase V

Executive Summary

1   Introduction to Phase V

In Phase I to Phase IV of the GOME-2 Error Assessment Study, a number of issues of potential importance to GOME-2 operational settings and error mitigation were investigated. The findings raised additional issues which required further work. The methodology and findings of Phase I to Phase IV were reported in main Final Report [Kerr&Al02]. This present Executive Summary outlines the findings from the work conducted under the Phase V study extension, which was added to the main study to consolidate the findings from Phase I to Phase IV. In the main part of Phase V (Task 2) five specific topics were addressed:

1. **Type of Diffuser Plate**
    The potential improvement in trace gas column retrieval, when using a quasi-volume diffuser (QVD) in place of the originally proposed ground aluminium diffuser, was assessed.

2. **Uncertainty in Characterisation of Diffuser BSDF**
    Information from the GOME-2 FM1, FM2 and FM3 calibration activities was used to quantify current uncertainties in characterisation of diffuser BSDF.

3. **Residual Error from Polarisation Correction**
    The analysis performed in the main study was based on information from GOME-1 and GOME-2 (at component level). This was updated by using new information at instrument level from the GOME-2 calibration activities [TPD01, TPD03] and a polarisation study [Har&Al03].

4. **Spatial Aliasing via Polarisation Monitoring Detectors**
    Spatial aliasing via the spectrometer (FPA detectors) had been analysed in the main study. In Phase V, spatial aliasing via the PMDs was analysed in an analogous way

5. **Requirements for Characterisation of Slit Function Shape**
    The main study determined that slit function knowledge at sub detector pixel resolution was required to avoid serious errors in ozone profile retrieval. In Phase V, requirements were derived for laboratory measurements of the slit function shape.

As in the main study, most simulations in Phase V were performed for a set of realistic and representative geo-temporal scenarios (12 in total) which spanned a diverse range of observing conditions, including several surface albedos (typically 0.05 and 0.8), for view angles of nadir and the two (1920 km) swath extremes. The conclusions and recommendations from this study are therefore expected to be applicable to GOME-2 observing conditions generally (though not universally).

In all cases, the methodology was to:

a. Generate spectral signatures for a particular error or uncertainty
b. Propagate error signatures onto retrieved tracegas columns and O_3 profiles by *linear mapping*.

The significance of estimated errors was gauged by comparing these to the User Requirements, and to the Estimated Standard Deviations and Baseline Error Budgets, which had been compiled in the main study.

In support of these Task 2 activities, preparatory work to develop necessary software and datasets was conducted under Task 1.

In Task 3, recommendations were made in relation to operational settings and error mitigation, based on a review of the recommendations from the main study (Task I - IV) and the new results from Task 2 of Phase V.

Phase V of the study was conducted by a consortium comprising the following members:

Serco Europe Ltd	Prime Contractor; Study Administrator
RAL	Technical Coordinator; Ozone Profile Analysis; Methodology to Derive Slit-Function Measurement Requirements; Generation of Spectral Signatures of Diffuser BSDF Measurement Uncertainty
IUP/IFE-UB	Trace Gas Column Analysis; Analysis of Errors from different Diffuser Types
SRON	Generation of Residual Polarisation Error Signatures with/without Spatial Aliasing

2   Choice of type of diffuser plate

The diffuser type baselined for GOME-2 is made of ground aluminium. For GOME-1, this type of diffuser has been demonstrated to exhibit small-scale spectral structures which vary with sun-angle, and therefore season. The wavelength scales of these structures are comparable to those of trace gas absorption signatures, and their amplitudes are significant in relation to the fitting precision and the absorption amplitudes of trace gases other than ozone. Spectral correlation with trace gas absorption signatures has therefore been found to cause serious, seasonally dependent biases in trace gas columns retrieved from GOME-1[1].

For the quartz quasi-volume diffuser (QVD), the amplitudes of these BSDF spectral structures have been measured to be four times smaller than the ground aluminium diffuser baselined for GOME-2. Errors on trace gas columns were estimated in Phase V of this study to be correspondingly lower for the QVD than the aluminium diffuser. These reductions were found to be worthwhile and important for O_3 (visible), NO_2, BrO and H_2CO.

Recommendation V1   *The quasi volume diffuser should be used for GOME-2*

	DIFFrms / DODrms*100 [%]	
	GOME-1	QVD
O_3 UV	0.5	0.1
O_3 VIS	15	4
NO_2	82	22
BrO	255	67
H_2CO	82	22
DIFFrms	1.64e-4	0.43e-4

Table 1:   Estimated percent error on trace gas columns from the RMS ratio of diffuser over differential optical depth (DOD) and RMS of differential spectral structures for different diffuser types

With the new diffuser mounted, seasonally-dependent biases in minor trace gases should be reduced by a factor of ~ 4. However, these biases will still not be negligible, and so will need to be carefully quantified. It is assumed that a dedicated validation campaign will be conducted for each GOME-2 flight model in the period soon after launch, and that this will reveal any biases in columns of the minor absorbers NO_2, BrO, OClO, H_2CO, and SO_2 arising from this and other error sources. To characterise the *seasonal-dependence* of errors arising from diffuser spectral structures, ground-based measurements of these minor absorbers will need to be made regularly for each flight model at a range of latitudes for several years[2].

Recommendation V2:   Measurements of NO_2, BrO, OClO, H_2CO and SO_2 columns should be made regularly for several years by ground-based instruments to characterise the *seasonal-dependence* of errors arising from diffuser spectral structures for each FM in flight.

---

[1] Structures of this magnitude may also cause a seasonally-dependent tropospheric ozone bias in profile retrieval, as indicated in this study by simulations of BSDF error (see Sect 3).

[2] Extending the existing NDSC network to make regular column measurements of these minor absorbers in the free troposphere and stratosphere would enable the quality of GOME-2 trace gas column data to be maintained over the entire MetOp-1,-2 & -3 mission duration. When tropospheric concentrations of HCHO, SO_2 and NO_2 are elevated by pollution, their tropospheric columns can be derived from GOME-2. Extending the existing ground-based network to include (DOAS) measurements of these trace gases would therefore enable tropospheric columns derived from GOME-2 to be validated

3   Uncertainty in characterisation of diffuser BSDF

The bi-directional spectral distribution function (BSDF) of the GOME-2 QVD has been measured with two different optical stimuli during calibration activities for FM1, FM2 and FM3: (i) the FEL lamp, and (ii) the sun-simulator (SS)[3]. In the ideal case, these two measurements would be identical, but in practice they are not.

The deviation of the FEL:SS ratio from 1 was taken as a measure of the current uncertainty in BSDF. The magnitude and wavelength dependence of this deviation was different for FM1, FM2 and FM3, although in all three cases its magnitude was ~ few %. From the Baseline Error Budgets for retrieved products derived in the main study, it could be anticipated that broad-scale BSDF errors of this magnitude in Band 1 would cause significant errors in stratospheric O_3 profile retrieval, and this was confirmed to be the case in Phase V.

In addition, fine-scale spectral structure in the FEL:SS deviation in other bands was also discovered to cause errors in retrieved products, depending on the degree of spectral correlation with trace gas absorption signatures. In the Huggins bands, the spectral signature of FEL:SS deviation was found to give rise to large errors in tropospheric O_3 profile retrieval. Deviations in Bands 2 and 3 were found to also give rise to errors in columns of BrO and NO_2, respectively, which were significant in relation to their baseline error budgets.

The above approach has identified the potential importance of erroneous fine-scale spectral structure in GOME-2 BSDF characterisation[4]. However, propagated errors on O_3 profile and trace gas column retrievals should be considered as indicative, at best.

It is important that measurements by the FEL and the sun-simulator (and also NASA integration sphere) are mutually consistent within their respective error bars, and also that the sun-angle dependence of the diffuser BSDF is accurately characterised on fine spectral scales. Pre-flight measurements on ground of zenith-sky and direct-sun spectra should permit diffuser BSDF and the Level-1 radiometric calibration algorithm to be verified to a useful level.

> *Recommendation V3*:   *Realistic error budgets should be defined for FM1, FM2 and FM3 diffuser BSDF, paying particular attention to fine-spectral scales.*
>
> *Recommendation V4*:   *Zenith-sky and direct-sun measurements should be made with flight models on ground to verify BSDF calibration and to test the Level-1 algorithm[5].*

4   Residual error from Polarisation Correction

Residual error signatures, in sun-normalised radiance spectra arising from the polarisation correction, depend upon the polarisation responses of the FPAs and PMDs, and errors in their pre-flight measurement (i.e. errors in polarisation Key Data). An important aspect of Phase V was to use the polarisation responses, which had been measured at *instrument level[6]* for FM2, in place of information on individual *optical components,* which had been combined together in a theoretical way for use in the main study.

The location of the lowest wavelength PMD near 311 nm (c.f. ~ 350 nm for GOME-1) means that wavelength interpolation yields smaller polarisation errors for GOME-2 in Band 1. In the main-study, errors simulated for GOME-2 were almost always better than for GOME-1 and always less than 20% (in almost all cases < 10%).

The unpolarised radiation from the sun becomes polarised when scattered/reflected. The type and degree of polarisation depends on the nature of the scattering/reflecting medium and therefore on height. *The polarisation signatures in monochromatic spectra of backscattered solar radiation are therefore controlled by the absorption of ozone and other trace gases.* To the extent that the GOME-2 PMDs under-resolve and under-sample these atmospheric absorption signatures (e.g. ozone in the Huggins bands), smooth wavelength interpolation of the derived polarisation correction will be in error. Residual errors from application of the current

---

[3] A third stimulus, NASA's integrating sphere, has also been used but results were not available in time for Phase V.
[4] This is consistent with the previous finding in regard to diffuser type.
[5] Measurements need to be made and analysed early enough for a feasible response to be possible, if necessary (e.g. repeat measurement).
[6] This also included the measured U sensitivity, which was not accounted for in the main part of the study.

polarisation correction algorithm (PCA) were synthesised using calculations on a sufficiently fine spectral grid by a polarisation-dependent radiative transfer model.

Because residual errors are spectrally correlated with the O_3 Huggins bands, the tropospheric part of the O_3 profile retrieval and the O_3 total column retrieval, which both make use of differential structures in the Huggins bands, were both found to be very sensitive to propagation of residual polarisation errors.

The possibility was assessed to reduce these errors by reading out every PMD detector, instead of the currently-selected sub-set. However, this was found to give very little improvement, because of the more fundamental problem of limited spectral resolution, ~ 4 nm in the Huggins bands, which is not sufficient.

The main findings from Phase V can be summarised as follows:

1. The new, more reliable, simulations for GOME-2 indicate that mapping errors can be much larger than simulated in the main study, particularly for eastward pixels. In some cases, errors are unacceptably high in the troposphere.

2. It was originally expected that residual errors from the polarisation correction would be most serious in the Band 1 region, due to the interpolation from the theoretical point to the lowest wavelength PMD ~ 311 nm. However, the mapped errors showed that, for GOME-2 FM2, the largest contributions are actually from Band 2. This is driven by the large amplitude in some cases (notably extreme east pixels) of fine-structure in the error signatures which is correlated with the Huggins bands.

3. Although GOME-2 improves on GOME-1 in capturing polarisation on broad spectral scales, it does not improve on GOME-1 in capturing the fine-scale polarisation signature caused by atmospheric absorption in the Huggins bands, because the spectral resolution of the PMDs is not sufficient.

4. Errors in polarisation Key Data were not addressed explicitly in Phase V. However, the residual errors depend also on the Q/I ratio[7], and noise in the measured polarisation responses "blows up" when Q/I tends to zero[8].

5. GOME-2 views much closer to 90° scattering angle towards the eastern edge of the 1920 km swath and earlier local time of observation than does GOME-1 in its 960 km swath.

6. Errors due to low Q:I ratio are generally large, but not as significant as those driven by large amplitude Huggins structure.

It is recommended that further work be carried out with respect to residual errors in sun-normalised radiance arising from polarisation because, although these are generally quite small (< 1%), in a number of cases they cause errors in O_3 total columns and profiles which exceed User Requirements. At present, for example, errors of 10's% are found in tropospheric ozone retrieved from the extreme east view. These large errors are caused by Huggins structure in the residual polarisation error which cannot be corrected with the current scheme, even if all PMD pixels were to be made available and used in the correction. This is a consequence of the low spectral resolution (~ 4 nm) of the PMDs in the Huggins range.

Possible approaches to mitigate these errors would be:

a. Ideally, to improve the spectral resolution of the PMDs in the Huggins bands. A resolution of order 1 nm (c.f. PMD pixel sampling in this region of 0.7 nm) would be expected to largely remove these errors. However, it is recognised that neither an across-the-board increase in PMD spectral resolution nor a preferential focusing in this spectral range of the PMDs would be practical at this time.

b. Shifting the 1920 km swath to the west would reduce the occurrence of the largest errors[9]. Further work would be required to model fully the across-track dependence of this error[10], in order to define

---

[7] Q/I is the ratio of Stokes parameters defining the linearly-polarised and total intensities.

[8] This is because, when Q/I tends to zero, the Stokes parameter U and FPA and PMD sensitivities to this component become important. Although the FPA and PMD responses to U have been measured, there are uncertainties in these key data.

[9] Selecting a (symmetric) 960km swath instead of the 1920km swath could also alleviate this problem at tropical latitudes, though not at middle and high latitudes where scattering angles ~ 90° are not confined to the most easterly pixels.

[10] Across-track scanning strategy should also consider recommendations from the main study to alleviate scan-angle dependent errors from sun-glint (low latitudes) and the pseudo-spherical approximation (high latitudes).

an optimum across-track scan, which would be asymmetric about the nadir point and would vary around the orbit and the annual cycle.

c. Low Q:I ratio occurs in at least 1 across-track ground pixel throughout most of the orbit. It is important to implement a polarisation correction algorithm which can cope with this specific condition.

d. A more sophisticated polarisation correction scheme can be envisaged, which would make use of knowledge of the ozone profile[11] to model the wavelength dependence of polarised radiation at finer scales than can be captured by the PMDs. It would require significant further work to assess whether such an approach might be feasible.

Recommendation V5:   *The base-line polarisation correction scheme for Level 1 processing should be improved to accommodate low Q:I cases.*

Recommendation V6:   *To mitigate residual polarisation errors correlated with the Huggins absorption features, the following strategies should be investigated: (a) devise across-track scan pattern to avoid 90° scattering angle, (b) devise scheme to correct for fine structure in polarisation.*

5   Spatial aliasing via polarisation monitoring detectors

Because spectral pixels in the GOME-2 detector arrays are read-out sequentially, and this takes a finite time, the scene over which each spectral pixel integrates is slightly different. The possibility therefore exists for spatial variability in the scene to be aliased into the measured spectrum. The most extreme difference in scene is between spectral pixels at the ends of the arrays, which causes spectral discontinuities at band boundaries. This had provided clear evidence of spatial aliasing in GOME-1 flight data. The ratio of integration time to read-out time is smaller for GOME-2 than for GOME-1, so GOME-2 is more susceptible to this phenomenon.

During the main part of the study (Phase I to Phase IV), this error source had been assessed by mapping the impact on FPA signals of spatial variations in surface reflectance (derived from a limited number of LANDSAT images) onto the constituent retrieval. An important finding from this work, which had not previously been appreciated, was that the GOME-2 instantaneous fields of view (IFOV: 0.29° ~ 4 km across-track on ground) will effectively filter out structure at high spatial frequencies in the scene (i.e. spatially-aliased noise). In Phase V, the investigation of spatial aliasing has been extended to the PMD detectors.

The realistic simulation of spatial-aliasing via the PMDs was complicated and involved a number of steps. The first step was to generate time-series of the Stokes parameters I(t), Q(t) and U(t) from a set of five LANDSAT images using a polarised radiative transfer model. The second step was to calculate PMD and FPA signal time-series, integrating and sampling in time as appropriate and applying time and wavelength interpolation as necessary to synchronise FPA and PMD signals as closely as possible. The polarisation correction algorithm was then applied to the time series of FPA signals.

At wavelengths < 310 nm, ozone absorption hides clouds and other sources of scene inhomogeneity, so spatial aliasing via the PMDs (as well as directly via the FPAs) is only seen in the signatures at longer wavelengths. So the O_3 profile retrieval is affected exclusively through Band 2, except when the selected interval of Band 1 is extended from 306 nm to 314 nm.

Key points arising specifically from the exercise to linearly-map signatures of additional spatial-aliasing via the PMDs (i.e. additional to residual errors from the PCA reported in preceding section) were:

1. The signature of aliasing via PMDs has little impact over and above that of error in the polarisation correction algorithm itself (see preceding section).

2. Results from the main study on the direct impact of spatial aliasing via the FPAs are therefore still considered representative of the spatial-aliasing problem as a whole (subject to the limited number of cases represented by the chosen LANDSAT images).

---

[11] It might be desirable to incorporate a correction for polarisation fine structure into the L2 processor since this could exploit real-time O_3 information rather than depend on an O_3 climatology, as would be necessary in the L1 processor.

In summary, the consequences for ozone profile retrieval of perturbations to the polarisation correction caused by spatial aliasing are minor compared to: (i) direct impact of spatial aliasing on the signals recorded by the FPAs and (ii) other errors from the PCA. It should, however, be recalled that although (i) was found not to be a source of significant additional random error, this would not be true for a profile algorithm which used composite spectra from Bands 1 and 2. Inhomogeneity within the scene is also known to cause two problems in addition to spatial aliasing: (a) radiative transfer non-linearity means that significant retrieval errors are inevitable for a mixed scene comprising both high and low intensities, as shown in the main study, (b) variation in instantaneous pattern of illumination along the cross-dispersion axis of the slit (i.e. the along-track direction) will cause GOME-2's true response to differ subtly from that characterised on the ground with uniform illumination, e.g. spatial inhomogeneity in detector pixel sensitivity and/or slit-function shape.

6   Requirements for measurement of slit-Function shape

The main study had demonstrated unequivocally that characterisation of the slit-function shape in the relevant wavelength interval of Band 2 was of critical importance to ozone profile retrieval, in order to avoid errors in excess of 100% in the troposphere which would otherwise occur. Pre-flight measurements of slit-function shape were therefore recommended so as to meet User Requirements on the accuracy of GOME-2 ozone profile retrieval. Such measurements would also offer a major advance on GOME-1, for which errors in knowledge of slit-function shape can now be identified to be a limiting factor on accuracy.

In Phase V, trace gas column retrieval was considered in addition to ozone profile retrieval and requirements have been defined for laboratory measurements of slit-function to satisfy both applications.

6.1   Approach

The approach employed in this part of Phase V was based on a development of the linear-mapping methodology used elsewhere in the study. In summary, this involved propagating errors associated with the laboratory set-up for measuring the slit-function onto retrieved ozone profiles and trace gas columns. By exploiting the matrix algebra for linear mapping, the following three steps were conveniently combined into a single mathematical step:

1. Propagation of errors in laboratory set-up onto errors in retrieved slit-function shape
2. Propagation of errors in slit-function shape onto errors in calculated, sun-normalised spectra
3. Propagation of error signatures in sun-normalised radiance onto retrieved O_3 profiles and trace gas columns

The representation of the slit-function was, of course, a critical issue in this analysis. A piece-wise linear representation was used on a wavelength grid with 0.01 nm spacing, since this offered the degree of flexibility which would be needed in practice to analyse laboratory measurements of slit function and avoided pre-selection of a particular functional form[12]. Of equal importance was the degree of spectral correlation permitted in the representation. A *spectral correlation length* was defined from measurements of the GOME-2 slit-function width, which was assumed to result from the convolution of three functions:

1. The detector pixel spatial response
2. The image of the slit on the detector array if perfectly focused
3. A Gaussian spot function

The width of the spot function was adjusted until the convolution of the three functions gave the measured FWHM for the FM2 slit function (~ 0.3 nm).

The laboratory set-up assumed to apply for GOME-2 was similar in concept to that used recently for OMI: a quasi-monochromatic source with Gaussian spectral shape was scanned in wavelength at steps of 0.005 nm. The FWHM of this source was varied from 0.005 nm to 0.500 nm to assess sensitivity to this parameter.

---

[12] The primary reason for laboratory measurements is that the GOME-2 slit-function shape cannot be specified from theoretical considerations alone and is unlikely to follow a simple functional form.

Four sources of error on laboratory measurements, each with four different assumptions regarding their spectral correlation, were propagated onto trace gas columns and ozone profiles.

Propagated errors were found to be large for a source whose width was comparable to or larger than the slit function itself. Errors were found to decrease as source width was reduced from 0.1 nm to 0.01 nm (the resolution at which monochromatic radiance/irradiance spectra had been simulated).

6.2   Derivation of requirements

(a) O$_3$ profile analysis

The propagated errors were translated into stability / knowledge requirements on the lab set-up, taking into account the observation time required to achieve the necessary signal to noise. This translation was done by scaling propagated errors such that the End User Requirements on O$_3$ profile were satisfied at all altitudes, for both albedos and for all three geo-temporal scenarios. The table below presents requirements for the case of errors which are uncorrelated over a GOME-2 detector pixel but fully correlated from one detector pixel to the next (worst case of the four simulated). Assumptions common to all derived requirements in the table are: (1) that the source width is 0.04 nm (comparable to the OMI stimulus) and (2) that observations are scanned across the detector array in 0.005 nm steps[13].

It is important to note that requirements in the table apply to a GOME-2 spot width of 0.21 nm, which corresponds to a GOME-2 slit-function width of 0.3 nm, as pertains to FM2 after defocusing. Calculations performed within the study show that more stringent requirements would have to be imposed for a more focused instrument. It is therefore recommended that FM1 and FM3 be defocused to at least 0.3 nm slit-width for this reason, in addition to those given in the main study.

(b) Trace gas column analysis

For retrieval of trace gas columns using the DOAS algorithm, the slit-function enters explicitly into the so-called under-sampling correction. This allows structure in the sun-normalised spectrum, which originates from fine structure in the solar spectrum together with wavelength misregistration between backscattered and direct-sun spectra, to be compensated using calculations from a high-resolution solar reference spectrum convolved with the slit-function. Doppler shift of the solar irradiance spectrum incident at GOME-2 ensures that there is typically a misregistration of ~ 0.007 nm, as has been simulated here.

Slit-function convolution can also enter explicitly into the trace gas column retrieval, if high-resolution laboratory measurements of absorption cross-section are used instead of absorption cross-section measurements by the GOME-2 instrument itself. Using the proper slit-function will permit the assessment of the error from using an under-sampling correction scheme as proposed for GOME-1.

On the trace gas column side, requirements on the slit-function measurement set-up were driven by the End User Requirement on O$_3$ accuracy, which is quite strict (< 4%). They were found to be comparable to those derived from the O$_3$ profile retrieval side, which were driven by an End User Requirement of < 30% accuracy in troposphere.

Table 2 below also refers to information supplied by ESA in regard to the OMI slit-function measurement set-up. Quantitative requirements derived for GOME-2 appear to be reachable with a set-up of this kind.

Recommendation V7:   *The slit function of GOME-2 (all flight models) should be determined according to the quantitative requirements specified in this study, with particular attention to the Huggins bands (315 - 335 nm).*

Recommendation V8:   *FM1 and FM3 should be defocused to at least the level implemented in FM2 (slit width of 0.3 nm in Huggins bands), with the same physical slit dimension.*

---

[13] A larger step size could be used instead. However, the S/N requirement would then need to be increased by the square root of the ratio of the new step size to 0.005nm.

Source error type	O₃ Profile	Trace gas column	OMI Source
Signal:Noise	700	100	~ 1000[14]
Power	1%	2 %	0.5-1%[15]
Shift	3% of width (0.0012 nm)	8% of width (0.0032 nm)	0.003nm[16]
Width	40%	20%	~ 10's%[17]

Table 2:   **Requirements for laboratory measurements derived from O3 profile and trace gas column analyses assuming defocused slit and FM2 spot size**

7   Recommendations from Phase V and from the Main Study

7.1   Summary

The eight new specific recommendations for operational settings and error mitigation arising from Phase V are listed in the table below (V1 – V8):

	New recommendations from Phase V of study
V1	The quasi volume diffuser should be used for GOME-2.
V2	Measurements of NO₂, BrO, OClO, H₂CO and SO₂ columns should be made regularly for several years by ground-based instruments to characterise the *seasonal-dependence* of errors arising from diffuser spectral structures for each FM in flight.
V3	Realistic error budgets should be defined for FM1, FM2 and FM3 diffuser BSDF, paying particular attention to fine-spectral scales.
V4	Zenith-sky and direct-sun measurements should be made with flight models on ground to verify BSDF calibration and to test the Level-1algorithm
V5	The base-line L1 polarisation correction scheme should be improved to accommodate low Q:I cases.
V6	To mitigate residual polarisation errors correlated with the Huggins absorption features, the following strategies should be investigated: (a)devise across-track scan pattern to avoid 90° scattering angle; (b) devise scheme to correct for fine structure in polarisation.
V7	The slit function of GOME-2 (all flight models) should be determined according to the quantitative requirements specified in this study, with particular attention to the Huggins bands (315 - 335 nm).
V8	FM1 and FM3 should be defocused to at least the level implemented in FM2 (slit width of 0.3 nm in Huggins bands), with the same physical slit dimension.

---

[14] A basic S/N of ~ 1000 can be achieved at the stimulus central wavelength.

[15] For sufficiently long integration times, and Echelle angles within 1° of the nominal angle (at 75° angle of incidence)

[16] Relative accuracy near 335 nm arising from motor drive. Bias of ~ 0.01 nm is also expected from the alignment procedure, but is not important to derivation of slit-width since it would apply to all wavelengths.

[17] Uncertainty in knowledge of stimulus width has been inferred indirectly by comparison of measured and predicted OMI slit-function widths to be ~ 10's %.

The specific recommendations from the original study (Phases I to IV) were reviewed in the context of the new findings from Phase V. As a result of this review, the following have been retained in their original or modified form:

	Retained recommendations from Phases I to IV of study
A1	For O_3 profile retrieval, it is recommended to not use Band 1B wavelengths above 307 nm.
A2	For O_3 profile retrieval, it is recommended that the integration times for Bands 1A and 1B be 1.5 sec and 0.1875 sec, respectively.
A4	It is recommended that the impact of spatial aliasing be assessed more thoroughly: a) Global statistical analysis of O_3 profiles and trace gas columns using ATSR-2 images b) Impact on geophysical products retrieved directly from PMD measurements c) Impact on multi-wavelength aerosol retrieval.
A5	It is recommended that an Observing System Simulation Experiment (OSSE) be undertaken for GOME-2 to decide on optimum ground-pixel size and swath width[18].
B2/C3	It is recommended to review the feasibility of doubling the number of ground pixels sampled across-track, so as to halve ground pixel size for a given swath-width, in order to maximize the number of cloud-free scenes observed and hence the quality of O_3 and minor trace gas distributions in the troposphere[19].
C2	It is recommended to quantify the impacts of: (a) scene inhomogeneity on radiometric response and slit-function shape[20] and (b) errors in knowledge of slit-function shape on aerosol and cloud retrievals using the O_2 A-band.
C5	Assess possible use of onboard white light source to monitor wavelength-dependent degradation in UV
C6	Implement and quantify the benefits to ozone profile and trace gas column retrievals of algorithm improvements to mitigate errors due to sun-glint.
C7	Quantify errors arising from non-linear radiative transfer in conjunction with static scene inhomogeneities in cloud and surface reflectance.
C8	Assess errors on ozone profiles from the assumed vertical distribution of aerosol more thoroughly, in order to better gauge instrumental errors
C9	Assess the impact on ozone profile and ozone column error budgets of adding visible wavelengths
C10	Assess errors from uncertainties in absorption cross-sections of ozone and other trace gases, the high-resolution solar reference spectrum and polarised atmospheric radiative transfer, in order to better gauge instrumental errors

---

[18] It is envisaged that although such an OSSE might be conducted using the O_3 assimilation scheme of an NWP centre, the "figure of merit" should be the 4D O_3 field itself, and possibly the surface UV flux, rather than the usual NWP forecast variables. Ie ground-pixel size and swath would be optimised by minimizing (time-evolving) deviations between assimilated and true O_3 fields, taking into account the likelihood of cloud obscuration for different ground pixel sizes and known variations with integration time and scan-angle of random and systematic errors on retrieved O_3.

[19] This would require Band 2B, 3 and 4 integration times to be halved from 0.1875 sec to 0.09375 sec. Onboard data compression could offer a practical means to double the number of ground-pixels without doubling the GOME-2 data downlink capacity. If not, an alternative would be to halve the integration times and downlink alternate ground-pixels across the swath. This would still permit the frequency of cloud-free pixels to be increased substantially, although at the expense of losing half the total measurement time. In the redesign of a future UV/VIS satellite-borne spectrometer, it would benefit photometric S/N on trace gas column retrievals for individual ground pixels to have a slit-function wider than that of GOME-2: ~ 0.5 nm in Band 2 and ~ 1 nm in Band 3.

[20] Non-uniform illumination of the entrance slit in conjunction with non-uniform detector pixel spatial response will modify signal level and variation in illumination along the cross-dispersion axis (i.e. along-track direction) will modify slit-function shape.

7.2   Selection of swath and ground-pixel size

In Phases I – IV and V of this study a number of factors have been identified which, for one of two reasons, need to be taken into account in selecting an operational swath and ground-pixel size:

- A number of significant errors vary in an asymmetric way with view-angle across-track (and therefore on swath width), as well as solar geometry (latitude and season)
    1. Residual error from the polarisation correction algorithm
    2. Error from Lambertian surface approximation in presence of sun-glint
    3. Error from pseudo-spherical approximation at high solar zenith angles

- Other key factors depend upon ground-pixel size (and therefore on swath width).
    1. Frequency of cloud-free scenes
    2. Non-linearity error for a scene of mixed (i.e. high and low) albedo

A simple recommendation concerning the operational swath and ground-pixel size is not forthcoming on the basis of information from this study. Further work is therefore needed to support this selection, as indicated in preceding sections:

1. View-angle dependence of the residual error from the polarisation correction algorithm (PCA) should be quantified in detail (i.e. at angles in addition to the three assessed so far: nadir plus the two extreme view angles of the 1920 km swath)
2. The alternative option, to mitigate residual PCA errors by modifying Level 2 algorithms, should be investigated
3. Investigate the feasibility to double downlink data rate (e.g. by onboard data compression) or to downlink alternate ground-pixels, so as to halve the ground-pixel size for a given swath width
4. An OSSE with realistic prescription of cloud statistics and retrieval errors as functions of view angle, latitude, season and ground pixel size is recommended in order to select an operational swath and ground-pixel size in an objective manner.

7.3   References

[Kerr&Al02]   Kerridge, B.J., R. Siddans, B.L. Latter, J.P. Burrows, M. Weber, R. De Beek, I. Aben and W. Hartman,   GOME-2 Error Assessment Study, Final Report EUMETSAT Contract No EUM/CO/01/901/DK, 2002

[Har&Al03]   Hartmann, H.W, C.P. Tanzi, J.M. Kruger, I. Aben, GOME-2 Polarisation Study – phase C/D, SRON RP-GOME2-003SR, 2003

[TPD01]   TNO-TPD, Gome-2 FM1 Instrument Calibration "CRR Data Pack", MO-AD-TPD-GO-0012 issue 1, 2001

[TPD03]   TNO-TPD, Gome-2 FM2 Instrument Calibration "CRR Data Pack", MO-AD-TPD-GO-0017 issue 1, 2003

GOME-2 Error Assessment Study

Phase V: **Final Report**

1   Introduction to GOME-2 Error Assessment Study Phase V

1.1   Scope of Phase V

In Phase I to Phase IV of the GOME-2 Error Assessment Study, a number of issues of potential importance to GOME-2 operational settings and error mitigation were investigated, raising a number of issues which required further work. The methodology and findings of Phase I to Phase IV are reported in [Kerr&Al02].

This present report describes work conducted under the Phase V study extension, which was added to the main study to consolidate the findings from Phase I to Phase IV.

In Phase V four specific topics are addressed[1]:

Task 2a	**GOME-2 Diffuser Plate**
	To compare the performance of the originally specified Aluminium diffuser with the proposed, alternative quasi-volume diffuser (QVD) and recommend whether the latter should be base-lined in the GOME-2 design
Task 2b	**Aliasing of Spatial Variability into Spectral variability**
	To extend the analysis of spatial aliasing to include Level 1 calibration errors induced by spatial aliasing of PMD observations
Task 2c	**Requirements for Characterisation of Slit Function Shape**
	The main study determined that slit function knowledge at sub detector pixel resolution was required to avoid serious errors in ozone profile retrieval. This task is to define requirements for laboratory measurements of the slit function which would mitigate trace-gas retrieval errors (profile and column).
Task 2e	**Re-Assessment of Key Instrumental Errors**
	To assess specific errors based on new information from the GOME-2 CRR activities [TPD01, TPD03] and polarisation study [Har&Al03], namely:

- Knowledge of instrument polarisation response
- Knowledge of (absolute) BSDF

Preparatory work to develop the necessary software and datasets was conducted in Task 1.

Recommendations relating to operational settings and error mitigation were derived in Task 3, based on a review of the recommendations from the main study and results from Task 2 of this phase V extension.

---

[1] In the SoW (2 September 2002), a Task 2d was identified to investigate the sensitivity of aerosol retrieval algorithms to key instrument parameters and operational settings. After negotiation this task was replaced by Task 2e, above.

1.2   Consortium responsibilities in Phase V

The consortium has available the specialist expertise and, subject to the modifications identified below, also the software tools needed to accomplish Tasks 2a, 2b, 2c and 2e. The division of responsibilities within the consortium for Phase V was broadly similar to that of the main study:

Serco Europe Ltd

Prime contractor and study administration

RAL

Study technical co-ordination and ozone profile retrieval analysis

Generation from LANDSAT images of spatially-aliased spectral signatures in FPAs and PMDs
(Task 2b)

Definition of requirements for laboratory measurements of slit-function shape, simulation of lab measurements of slit-function shape and generation from these of slit-function shapes
(Task 2c)

Generation of spectral signatures of errors in knowledge of (absolute) BSDF
(Task 2e)

IUP

Trace gas column retrieval analysis

Generation of spectral signatures due to sun-angle dependent differential structures in Al and QVD diffusers
(Task 2a)

SRON

Propagation of spatially-aliased spectral signatures in FPAs and PMDs onto Level-1 products (sun-normalised, polarisation corrected radiances and Stokes parameters)
(Task 2b)

Provision of spectral signatures of errors in knowledge of instrument polarisation response
(Task 2e)

1.3   References

[Kerr&Al02]   Kerridge, B.J., R. Siddans, B.L. Latter, J.P. Burrows, M. Weber, R. De Beek, I. Aben and W. Hartman,   GOME-2 Error Assessment Study, Final Report EUMETSAT Contract No EUM/CO/01/901/DK, 2002.

[Har&Al03]   Hartmann, H.W, C.P. Tanzi, J.M. Kruger, I. Aben, GOME-2 Polarisation Study – phase C/D, SRON RP-GOME2-003SR, 2003.

[TPD01]   TNO-TPD, Gome-2 FM1 Instrument Calibration "CRR Data Pack", MO-AD-TPD-GO-0012 issue 1, 2001

[TPD03]   TNO-TPD, Gome-2 FM2 Instrument Calibration "CRR Data Pack", MO-AD-TPD-GO-0017 issue 1, 2003

2   Task 1: Tool Adaptation and Definition of Test Data

2.1   Adaptation of software tools

Some adaptations to existing software and several new software developments were required to enable Task 2a, Task 2b, Task 2c and Task 2e to be carried out. The work required was carried out under the headings of the following sub-tasks:

WP1100	Preparations for measurement and analysis of slit-function shape simulations (RAL)
WP1200	Spatial aliasing signatures in PMD Channels (RAL)
WP1300	Development of scheme to propagate spatially-aliased signatures (SRON)
WP1400	Development of scheme to generate diffuser error characteristics (IUP)

Details are given under the relevant Task 2 work description, below:

Task 2a

IUP	Scheme to synthesise differential structures as a function of solar elevation and azimuth angles from available information on Al and QVD diffusers

Task 2b

RAL, SRON	Scheme to assign polarisation "p" to each LANDSAT pixel Adaptation to PMDs of scheme to generate spatially-aliased signatures in FPAs
SRON	Scheme to propagate spatially-aliased signatures on FPAs and PMDs through polarisation correction algorithm onto calibrated, sun-normalised radiances and Stokes parameters

Task 2c

RAL	Scheme to simulate laboratory measurements of slit-function shape Scheme to derive slit-function shape from analysis of simulated measurements

No software development was required for Task 2e.

2.2   Geo-temporal scenarios

The same geo-temporal and observational scenarios as in the main study were used as a basis for all retrieval simulations conducted here. These consisted of the following basic cases:

Four seasons:	represented by January, April, July, October
Three latitudes:	5°N, 55°N and 75°N
Two Lambertian surface albedos:	0.05 and 0.8

Twelve geographical/temporal scenarios, simulated with 2 surface albedos gave 24 basic cases. Since the January 75°N case is not observed in daylight by GOME-2, this case was replaced by October 75°S (Antarctic spring).

Trace gas and temperature / pressure profiles assigned to each scenario are described in Section 6 of the main study report (Phase 1 to Phase IV).

GOME-2 solar / observing geometry was taken from orbit propagator data provided by ESA / M. Eisinger and is summarised in the table below.

For ozone-profile simulations, results are generally considered for nadir, and the two extremes of the 1920 km across-track. For column retrievals the full variation across-track is generally considered.

N	Month	Latitude deg	SZA Deg	Rel. azmth Deg *east / west*	Albedo %
1	January	5 N	46.5	23.3 / 156.7	5
2					80
3		55 N	79.8	46.8 / 133.2	5
4					80
5	April	5 N	36.7	22.0 / 158.0	5
6					80
7		55 N	49.5	39.6 / 140.4	5
8					80
9		75 N	65.0	50.4 / 129.6	5
10					80
11	July	5 N	40.4	40.0 / 140.0	5
12					80
13		55 N	39.0	31.8 / 148.2	5
14					80
15		75 N	53.4	48.5 / 131.5	5
16					80
17	October	5 N	35.8	10.0 / 170.0	5
18					80
19		55 N	66.3	49.4 / 130.6	5
20					80
21		75 N	83.4	54.3 / 125.7	5
22					80
23		75 S	76.0	55.0 / 125.0	5
24					80

Table 2-1:   **Viewing geometry for the 24 geo-temporal scenarios**

3 Task 2a: GOME-2 Diffuser Plate

3.1 Introduction to Task 2a *(RAL/IUP)*

3.1.1 General

In the proposal the following work packages were planned:

WP2110	Spectral Signatures from Aluminium and QVD Diffusers	(IUP)
WP2120	Mapping onto Trace Gas Columns	(IUP)
WP2130	Mapping onto Ozone Profiles	(RAL)

3.1.2 Background

From the technical note provided by Richter and Wagner [RW], it was concluded in the original GOME-2 Error Assessment Study that the current baseline GOME-2 diffuser, a wet-sanded Ground Al Diffuser plate as in GOME-1, leads to slant column errors larger than 50% for trace gases other than ozone.

These errors are strongly dependent on the elevation and azimuth angle of the incoming solar beam, which vary around the annual cycle. These errors are the largest contributor to DOAS trace gas column retrievals, except in the case of ozone. From integrated ozone profiles using GOME-1 data, an error of only a few tenths of a percent were inferred based on a very limited test [B&Al]. In the original study, the replacement of the Ground Al Diffuser with one having differential structures below 10^{-4} was recommended. From industry, a new Quasi-Volume Diffuser (QVD) has been proposed; this is expected to have much reduced differential structures.

Information, which specifies the sun-angle dependent differential structure in diffuser BSDF for the current baseline Aluminium Diffuser and for the proposed replacement Quasi-Volume Diffuser, has been acquired from EUMETSAT/ESA [TPD]. Using the available information for the new and old diffuser types, it was planned to estimate the differential error spectra for mapping onto retrieval errors. Since these residuals may be fairly small, care must be taken not to introduce numerical noise into the error patterns. The differential spectral structures were supposed to be "linearly mapped" onto trace gas columns and ozone profiles using the same methodology as employed in the original study. The annual cycle of the elevation and azimuth angle was planned to be simulated, if possible.

The urgency of the scientific assessment required by EUMETSAT of the current diffuser in comparison to the proposed replacement diffuser was recognised by the consortium. A technical report was urgently delivered in time for the first progress meeting, which was scheduled for early December 2002. This technical report is summarised in Section 3.2 below.

Following the initial investigations into the alternative diffuser plate types, the Ground Al Diffuser and Quasi-Volume Diffuser, it was decided that it was unnecessary to carry out the error mapping onto tracegas columns and ozone profiles. This was because there were only measurements available where incident angle changes were small compared to the seasonal variation observed in space. Results from the TPD measurements clearly demonstrated qualitatively a reduction in the differential structure (using a pair of incident angles in the experimental set-up)

3.2   Scientific justification for diffuser replacement *(IUP)*

3.2.1   Introduction

The detection of BrO, NO_2, HCHO, OClO, and SO_2 by GOME are of fundamental importance for the understanding of stratospheric (ozone depletion) and tropospheric (air-pollution) chemical processes.

Several independent investigations have confirmed that the Ground Al Diffuser setup in GOME-2 will lead to large errors in retrieved minor tracegas total column amounts that clearly exceed scientific user requirements for long-term monitoring.

In order to take advantage of the unique capability of GOME-2 to detect trace gas species other than ozone, it is strongly recommended to replace the Ground Al Diffuser with the proposed Quasi-Volume Diffuser (QVD).

3.2.2   Description of the problem

The Differential Optical Absorption Spectroscopy (DOAS) retrieval of tracegas column amounts is applied to the ratio of nadir earthshine radiance over the solar irradiance. GOME measures the extraterrestrial irradiance using a diffuser mounted in the calibration unit. The purpose of the diffuser is to evenly illuminate the entrance slit of the GOME spectrometer.

In a recent study [RW] it was shown that the solar irradiance from GOME-1 (containing no atmospheric absorption) has differential structures that strongly correlate with atmospheric tracegas absorption. According to [RW] a maximum error of up to 100% in the NO_2 and BrO total columns in the tropics can be induced by the GOME-1 diffuser. This error appears as a bias with a strong seasonal cycle [RW]. This can be explained by the solar elevation and azimuth incidence angle of the diffuser, which has a distinct seasonal cycle related to the sun-synchronous near-polar orbit.

The scientific user requirements for long-term trend analysis as outlined in [WMO] requires for NO_2 a precision (RMS error) less than 10%, and an accuracy (bias error) of less than 20%. For BrO a precision of 20% (or better), and an accuracy of 40% (or better) are targeted. See Table B.4A and Table B.4b in [WMO].

It is obvious that the Ground Al Diffuser type planned for GOME-2, which is the same as used in GOME-1, will not be able to meet these requirements. From the extensive earlier part of the GOME-2 Error Assessment Study (Phase I to Phase IV), it was concluded that the diffuser error is by far the largest error source in tracegas column retrieval for all tracegases except ozone [ES].

The spectral features in the diffuser reflectivity have been confirmed by laboratory measurements for different diffuser types [TPD01]. Additional investigation using in-flight measurements from SCIAMACHY confirmed the results from [RW] as summarised in [DB].

SCIAMACHY aboard ENVISAT uses the same diffuser type as GOME-1 and it was, for the above reasons, decided to reduce the spectral features by adding a second diffuser on the back of the azimuth scan mirror, whilst leaving the first GOME-1 type diffuser in place. This replacement occurred after integration of the instrument to the platform, which underlines the significance of this problem.

The need for replacing the Ground Al Diffuser in the GOME-2 set-up has been recognized by ESA and a justification has been given in [SSST]. The proposed replacement is the Quasi-Volume Diffuser (QVD), which has been qualified at TPD and which shows differential structures with an RMS improvement by a factor of four (0.4×10^{-4} 1-σ RMS) [QVD].

3.2.3   Quantification of errors for different diffuser types

Table 3-1 summarises the errors to be expected for the Ground Al Diffuser type.

The detector noise level was determined from [ES] assuming low albedo, tropical conditions, and an integration time of 0.1875 sec (GOME-2 setup). Signal-to-noise ratios (SNR) are averages in the fitting windows and can be improved by increasing the integration time. Typical column densities for each tracegas were taken from tropical scenarios as described in [ES]. Largest errors are expected in the tropics due to minimum optical paths at low solar zenith angles.

To convert these vertical column amounts into SCDs a geometric air mass factor of 2.1 was assumed. The SCD diffuser error, which is given in Table 3-1, is derived from the SCIAMACHY diffuser investigation [DB]. The errors should be considered correct only in the order of magnitude and may be larger in other circumstances, because the diffuser investigations with SCIAMACHY were limited in the range of diffuser incidence angles [DB].

However the errors found for BrO and NO_2 are in qualitatively good agreement with results from [RW]. The differential optical depths (DOD) are obtained by multiplying the molecular absorption spectrum with the typical SCD. For the quantification of the diffuser error the RMS of DOD (DODrms) should be compared with the RMS spectral noise derived from the diffuser characterisation [SSST, QVD].

In Table 3-1 this error estimate (last column) is given for the SCIAMACHY diffuser, which is the same as the Ground Al Diffuser in both GOME-2 and GOME-1.

This error estimate has been translated to the other diffuser types: this is summarized in Table 3-2. DIFFrms are taken from Table 2 in [SSST], which is based upon test results reported in [TPD, QVD].

Trace	Fitting window	Detector noise	Typical SCD	SCD diffuser error	DODmax	DODrms	DIFFrms/DODrms
Gas	nm	10^{-4}/SNR	cm^{-2}	cm^{-2}	-	-	%
O_3 UV	325-335	6/1600	1.6e19 (280DU)	9.0e16 / 0.6%	0.14	0.03	0.5
O_3 Vis	450-497	6/1600	1.6e19	4.5e17 / 3%	4.2e-3	1.1e-3	15
NO_2	425-450	8/1300	2.0e15	1.1e15 / 55%	7.9e-4	1.9e-4	82
BrO	344-366	7/1500	4.0e13	6.0e13 / 150%	2.6e-4	6.4e-5	255
H_2CO	338-359	7/1500	2.1e16	1.0e16 / 48%	1.5e-3	2.0e-4	82

Table 3-1:   **GOME-1 diffuser type error assessment**

Trace	DIFFrms / DODrms*100 [%]		
Gas	GOME-1	QVD	Al_2O_3
O_3 UV	0.5	0.1	<0.1
O_3 VIS	15	4	2
NO_2	82	22	13
BrO	255	67	39
H_2CO	82	22	13
DIFFrms	1.64e-4	0.43e-4	0.25e-4

Table 3-2:   **Estimation of Error for different diffuser types (DIFFrms/DODrms)**

3.2.4   Conclusions

It is clear that the Quasi-Volume Diffuser (QVD) diffuser brings the errors close to the accuracy requirement of 20% and 40% for NO_2 and BrO. The total ozone error figure is well below the user requirement of 3% [WMO] for all diffuser types.

One may be tempted to dismiss the diffuser replacement because the detector noise level given in the third column of Table 3-1 is higher than the spectral noise of the diffuser. However it is important to note that the detector noise represents random noise, while the diffuser noise introduces a bias, which does not cancel.

There is strong evidence that significant improvement in minor trace gas column retrieval is to be expected with the new Quasi-Volume Diffuser (QVD).

3.3   References

[RW]   Richter, A., and T. Wagner, Diffuser Plate Structures and their Influence on GOME Slant Columns, Technical Note, January 2001 (http:///www.iup.physik.uni-bremen.de/gome/data/diffuser_gome.pdf)

[B&Al]   K. Bramstedt, J. Gleason, D. Loyola, W. Thomas, A. Bracher, M. Weber, and J. P. Burrows, Comparison of total ozone from the satellite instruments GOME and TOMS with measurements from the Dobson network 1996-2000, Atmos. Chem. Phys., 3, 1409-1419, 2003

[TPD03]   GOME-2-CU-QVD: Spectral Features Test Report, MO-RP-TPD-GO-0044, TPD Space Instrumentation, 2003

[DB]   de Beek, R. , SCIAMACHY Diffuser Characteristics and End-to-end Analysis, Technical Report, IFE- SCIA-TR-280601, Issue 2, ESA/ESTEC, 2002

[QVD]   GOME-2-CU-QVD: Spectral Features Test Report, MO-RP-TPD-GO-0044, TPD Space Instrumentation, 2003

[ES]   Kerridge, B., et al., Study – GOME-2 Error Assessment, EUMETSAT Contract EUM/CO/01/901/DK, Draft Final Report V 1.1, 2002

[TPD01]   Interim Report on Spectral Features of Test Diffuser Items, Doc. No. HOI-T1cal-comp-01, Issue 1, TPD Space Instrumentation, 2001

[SSST]   Single Space Segment - Scientific Justification for the Proposed Diffuser Change in the GOME-2 CU, ESA Technote MO-TN-ESA-GO-0325, Issue 1, 2002

[WMO]   WMO/CEOS Report on Strategy for Integrating Satellite and Ground-based Observations of Ozone, WMO/GAW Technical Document 140, World Meteorological Organization, Geneva, Switzerland, 2000

4 Task 2b: Aliasing of Spatial Variability into Spectral Variability

4.1 Introduction to Task 2b *(RAL)*

Because spectral pixels in the GOME-2 detector array are read-out sequentially and this takes a finite time, the scene over which each spectral pixel integrates is slightly different. The possibility therefore exists for spatial variability in the scene to be aliased into the measured spectrum.

The most extreme difference in scene is between spectral pixels at the ends of the arrays, and spectral discontinuities at band boundaries. This had provided clear evidence of spatial aliasing in GOME-1 flight data. The ratio of integration time to read-out time is smaller for GOME-2 than for GOME-1, so GOME-2 is more susceptible to this phenomenon.

During the main part of the study (Phase I to Phase IV), this error source had been assessed by mapping the impact on FPA signals of spatial variations in surface reflectance (derived from a limited number of LANDSAT images) onto the constituent retrieval. An important finding from this work, which had not previously been appreciated, was that the GOME-2 instantaneous fields of view (IFOV: 0.29° ~ 4 km on ground) will effectively filter out high-frequency structure (i.e. spatially-aliased noise).

The retrieval schemes implemented were shown to be relatively insensitive to remaining errors, after the IFOV was accounted for. It was noted, however, that spatial aliasing would also impact observations of the PMD channels, thereby causing additional error in constituent retrieval, via erroneous polarisation correction.

It was proposed to quantify this additional error contribution in Task 2b of this Phase V extension.

The work required was carried out under the headings of the following sub-tasks:

WP2210	Generation of spatially-aliased signatures in PMD Channels	SRON
WP2220	Propagation of spatially-aliased signatures in PMD Channels on to Level 1 Products	SRON
WP2230	Mapping of Spatially-Aliased Signatures onto Trace Gas Columns	IUP
WP2240	Mapping of Spatially-Aliased Signatures onto Ozone Profiles	RAL
WP2210	Generation of Spatially-Aliased Signatures	RAL

LANDSAT Images 1, 6, 7, 10, and 13 from Phase I - IV of the study [Kerr &Al] were used to construct spatial reflectance variations as observed by GOME-2 as in the main study:

 ➢ Uncalibrated LANDSAT data were converted to an effective Lambertian surface albedo by scaling the image data linearly to span the range 0 - 1.

 ➢ The images were convolved with a 4 km by 40 km box-car function to represent the GOME-2 instantaneous field of view.

 ➢ The images were sampled every 40 km in the long-IFOV direction (corresponding to along the orbit track) and 20 m in across-track / dispersion direction.

The resulting albedo-variation signatures were delivered to SRON via the IUP ftp server.

4.2   WP2210: Generation of spatially-aliased signatures in PMD channels *(SRON)*

4.2.1   Introduction

This work involved the update of radiance errors due to the GOME-2 polarisation correction algorithm calculated in the previous phase of the GOME-2 error study. Before the end of 2002 radiance errors had to be calculated using instrument responses based on component simulations. By the beginning of 2003 a complete set of calibration key data had become available to perform the update reported here. The calculation of radiance errors due to the polarisation correction algorithm involves a sequence of steps. The most important of these are described below.

To simulate the Earth's radiance model, radiances and polarisation need to be calculated first. Spatial aliasing is mimicked by application of a scene-varying (time dependent) albedo. Instrument characterization data is applied for the simulation of detector signals. The polarisation correction algorithm starts with calculation of the Stokes Q/I polarisation ratio from PMD band measurements and wavelength interpolation. Next spatial aliasing synchronization is applied to the polarisation measurement. The derived Q/I polarisation curve and instrument characterization data are implemented in the polarisation correction term for the radiances which are measured by the main channels.

The origin of more and less typical radiance error spectral structures are highlighted by demonstrating variations of the polarisation correction theme.

4.2.2   Calculation of model reflectivities and polarisation

To simulate representative GOME-2 measurements, a series of model reflectivities and polarisations are calculated from 12 geo-temporal scenarios which have already been selected by RAL in the previous phase of the GOME-2 error study. The models act as input to the polarisation correction algorithm. The scenarios are indicated by month and latitude:

Jan_05n	Apr_05n	Jul_05n	Oct_75s
Jan_55n	Apr_55n	Jul_55n	Oct_05n
	Apr_75n	Jul_75n	Oct_55n
			Oct_75n

Information about the viewing geometry of each scenario, necessary for the calculation of the model radiances and polarisation, is obtained from the GOME-2 orbit propagator. Each model is calculated for extreme-East, Nadir and extreme-West view. The reflectivities are multiplied with a Kurucz solar spectrum to obtain the radiances [Kur&Al]. The spectral resolution of the models is 0.2 nm over the full spectral range of 260 - 400 nm. Two ground albedos of 0.05 and 0.8 are applied for the clear-sky models. Considering the computing time of more than one week a single cloud model is computed. The spectral resolution of the cloud model is 0.2 nm over the spectral range 295 – 350 nm and 1 nm otherwise. For each scenario and viewing angle the single scattering ratios Q/I and U/Q of the cloud model, which are applied in the polarisation correction algorithm, are scaled such that they match the single scattering values of the clear sky model, see Figure 4-2.

Note that it is not possible to scale the cloud reflectivity as well, since the single scattering reflectivity is wavelength dependent.
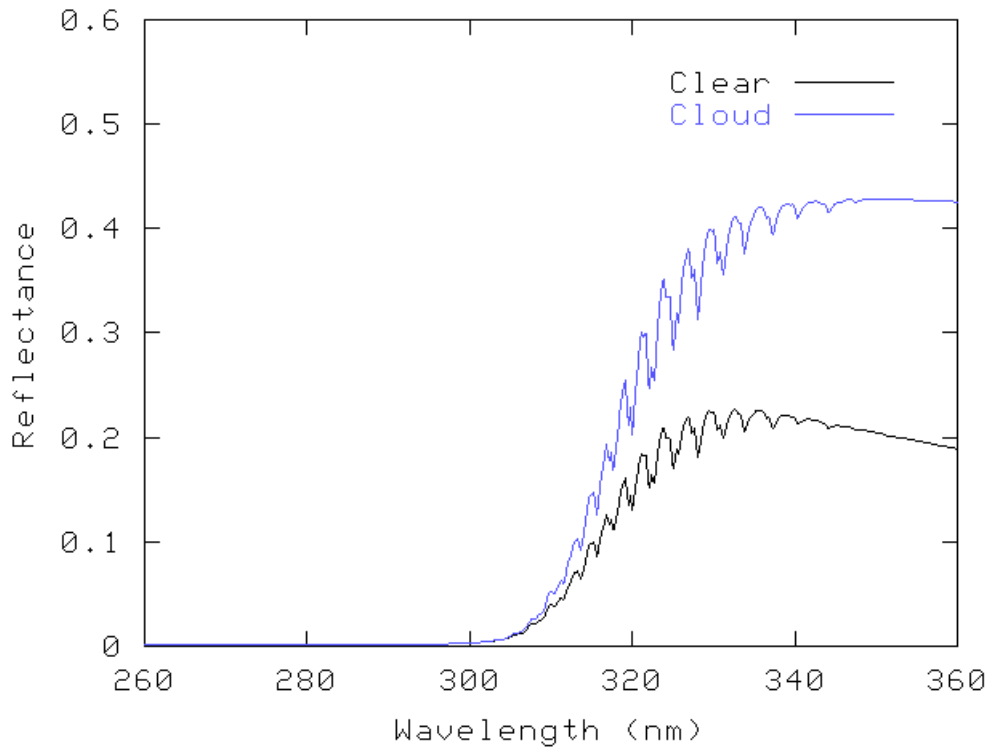
Figure 4-1: **Example reflectances of a clear model (Jan_05n) and the cloud model**
The high reflectance of the cloud is apparent at longer wavelengths

The cloud and clear-sky models are combined in the study to the propagation of the aliasing signatures by weighting the clear and (scaled) cloud model with a time variable albedo A(t). The albedo is obtained from a set of 5 selected LANDSAT images, some examples are shown in Figure 4-3. The weighting of the model radiances and polarisation with the albedos is necessary since the albedos themselves are monochromatic and contain no polarisation information. Each image provides roughly seven albedo time series which are used for weighting. Thus a total of 37 different time series are applied to each scenario and viewing angle. An albedo of 0 corresponds to a clear scene, an albedo of 1 corresponds to a fully clouded scene:

$$I(t) = I_{clear} + A(t) \cdot \left(I_{cloud} - I_{clear} \right)$$
$$Q(t) = Q_{clear} + A(t) \cdot \left(Q_{cloud}^{scaled} - Q_{clear} \right)$$
$$U(t) = U_{clear} + A(t) \cdot \left(U_{cloud}^{scaled} - U_{clear} \right)$$

Note: when no spatial aliasing is considered, only the clear-sky models are used. This can be achieved in the equations above by setting A(t) to 0.
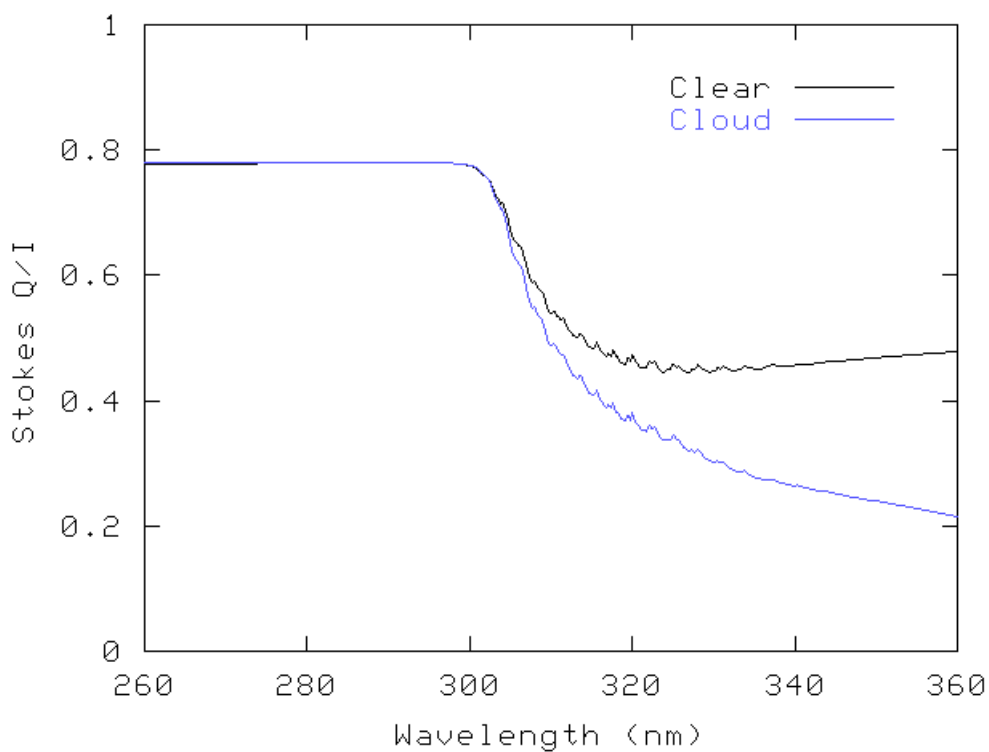
Figure 4-2:   **Example of Stokes Q/I of a clear model (Jan_05n) and the scaled cloud model**
        The cloud has a strongly depolarising effect at longer wavelengths.
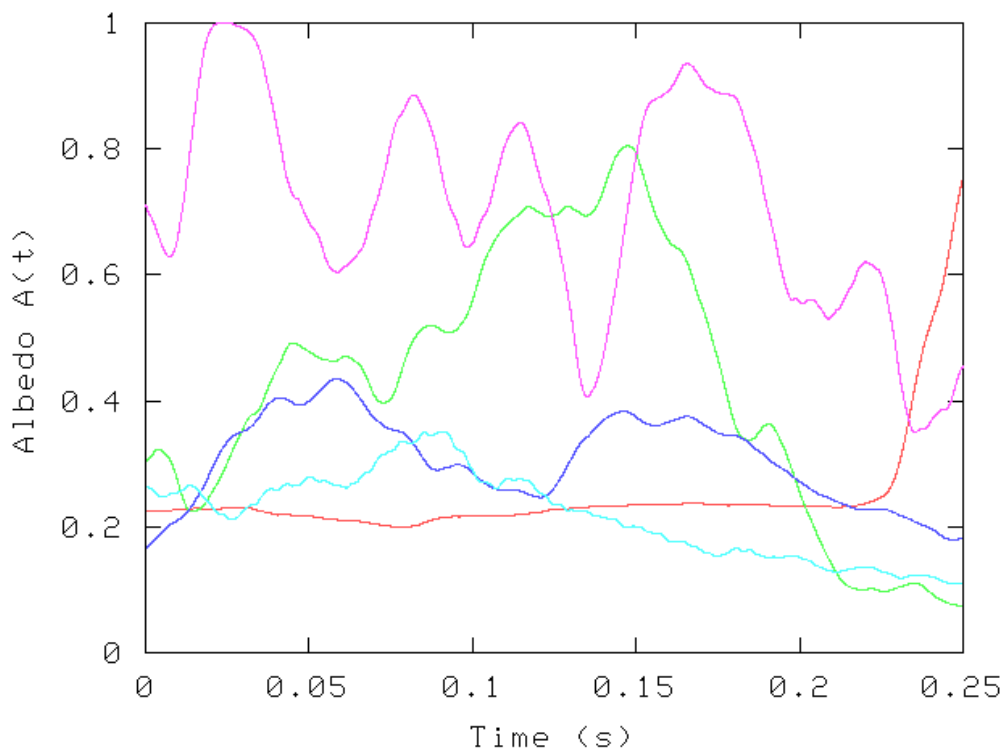
Figure 4-3:   **Example albedos as derived from the LANDSAT images**

4.2.3   The polarisation correction algorithm

4.2.3.1   Simulation of PMD detector signals

In the calculation of the PMD detector signals the model radiances (I, Q and U) are first folded with the wavelength dependent PMD slit function. Next, the folded radiances are multiplied with the corresponding instrument responses in the following general equation to obtain the detector signal [Har&Al]]:

$$Sig^{p-PMD} = R^{p-PMD} \cdot \left(I + \mu_2^{p-PMD} \cdot Q + \mu_3^{p-PMD} \cdot U\right)$$
$$Sig^{s-PMD} = R^{s-PMD} \cdot \left(I + \mu_2^{s-PMD} \cdot Q + \mu_3^{s-PMD} \cdot U\right)$$

where $RPMD$ indicate the radiometric responses of the corresponding PMDs and

$$\mu_2^{p-PMD} = \frac{\beta \cdot \chi - 1}{\beta \cdot \chi + 1} \qquad ; \qquad \mu_2^{s-PMD} = \frac{\alpha \cdot \chi - \gamma}{\alpha \cdot \chi + \gamma}$$

$$\mu_3^{p-PMD} = \frac{\zeta^p - 1}{\zeta^p + 1} \qquad ; \qquad \mu_3^{s-PMD} = \frac{\zeta^s - 1}{\zeta^s + 1}$$

The quantities a, β, γ, χ and ζ are instrument polarisation response functions which are part of the calibration keydata [TPD02]. Calibration measurements of the GOME-2 PMD U polarisation sensitivity ζPMD have shown that this sensitivity is small but significant and can no longer be ignored as was done in the previous phase of the GOME-2 error study.

Due to limited bandwidth the PMD signals are downloaded in approximately 13 PMD spectral bands. The individual PMD pixel signals within a spectral band are co-added aboard the spacecraft. The spectral bands do not always connect and do not cover the complete PMD spectral range. In the wavelength range up to ~ 400 nm the baseline band selection includes 6 PMD spectral bands starting at ~ 311 nm [Har&Al]. The central wavelength of the band is assigned to the band signal.

The PMDs integrate ~ 23.4 msec after which the detector pixels are read out one-by-one, 45.8 µsec per pixel. As a consequence of the sequential pixel readout, the integration of each detector pixel starts at a slightly different time. This results in spatial aliasing between the individual PMD signals. In simulating the PMD signals scene variation during the integration time is introduced in the model radiances and polarisation by weighting clear and cloud model I, Q, and U with LANDSAT albedos, as described in the previous section, such that the weighting albedo corresponds in time with the integration time of each individual PMD pixel.

4.2.3.2   Co-adding of PMD band signals

In order to match the main channel integration time of 187.5 msec 8 consecutive PMD readouts are co-added. For each PMD spectral band this is done in four sets of 8 co-added readouts, i.e. 0 - 7, 1 – 8, 2 - 9 and 3 - 10, which are 23.4 msec apart.

See the readout scheme in Figure 4-4, where: the dashed lines in the λ-t plane indicate the readout of the PMD detector array, Number 0 corresponds to the readout prior to the main channel readout, The thick dots indicate the co-added band signals (or Q/I values later on). The shaded areas indicate the readout time of the main channel pixels. Note that none of the PMD band readouts in Figure 4-4 is time and wavelength synchronous with the main channel pixel readouts. In fact, the occurrence of any such time and wavelength synchronicity is a pure coincidence.
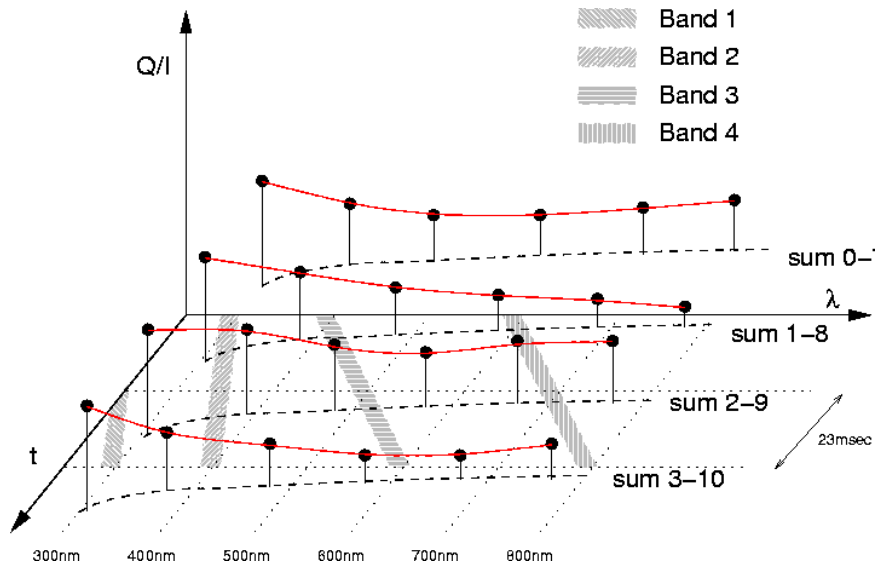
Figure 4-4: **Main channel and PMD readout scheme**
The thick dots indicate the co-added PMD measurements.
The red lines indicate the interpolated Q/I polarisation curves.

4.2.3.3 Calculation and wavelength interpolation of Q/I

For each co-added band readout, the Stokes fraction Q/I band is calculated using the following equation:

$$\left.\frac{Q}{I}\right|_{band} = \frac{\alpha'_{band} - Z_{band}}{Z_{band} \cdot \left(\mu^{p-PMD}_{2,band} + \mu^{p-PMD}_{3,band} \cdot \left.\frac{U}{Q}\right|_{ss} \right) - \alpha'_{band} \cdot \left(\mu^{s-PMD}_{2,band} + \mu^{s-PMD}_{3,band} \cdot \left.\frac{U}{Q}\right|_{ss} \right)}$$

where

$$Z_{band} = \frac{Sig^{s-PMD}_{band}}{Sig^{p-PMD}_{band}} \quad ; \quad \alpha'_{band} = \left.\frac{\alpha \cdot \chi + \gamma}{\beta \cdot \chi + 1}\right|_{band}$$

$$\mu^{p-PMD}_{2,band} = \left.\frac{\beta \cdot \chi - 1}{\beta \cdot \chi + 1}\right|_{band} \quad ; \quad \mu^{s-PMD}_{2,band} = \left.\frac{\alpha \cdot \chi - \gamma}{\alpha \cdot \chi + \gamma}\right|_{band}$$

$$\mu^{p-PMD}_{3,band} = \left.\frac{\zeta^p - 1}{\zeta^p + 1}\right|_{band} \quad ; \quad \mu^{s-PMD}_{3,band} = \left.\frac{\zeta^s - 1}{\zeta^s + 1}\right|_{band}$$

The quantities α, β, γ, χ and ζ are PMD instrument polarisation response functions which are part of the calibration keydata [TPD02]. Note that the Stokes U-polarisation is not measured by GOME-2. Instead it is assumed that both Q and U have similar spectral shapes and therefore that the ratio U/Q is to first order wavelength independent. The ratio U/Q can then be approximated by its single scattering value, which is an analytical function of the viewing geometry. The single scattering value is indicated by the subscript ss.

The four sets of co-added PMD band measurements of Q/I are wavelength interpolated by Akima interpolation to the spectral scale of the main channels. Akima interpolation is a local smooth curve fitting

procedure based on a cubic spline. The interpolation is indicated in Figure 4-4 by the red lines connecting the measured Q/I values (thick dots).

4.2.3.4   The spatial aliasing synchronization step   (time interpolation of Stokes fractions Q/I)

The four sets of 8 co-added PMD detector signals are ~ 23.44 msec apart, i.e. one PMD integration time. The main channel signals are 187.5 msec apart, i.e. one main channel integration time. Moreover, the PMD detectors are read out reversely. As a result the readout of the main channel and PMD pixels at a particular wavelength are in general not time-synchronous. This is demonstrated in Figure 4-4: only at the intersections of the PMD and main channel readout curves in the λ–t plane the readout is synchronous. Thus, spatial aliasing is introduced between the PMD signals which make up the polarisation correction factor and the main channels signals which are to be polarisation corrected.

To minimize the effect of spatial aliasing between the radiances measured by the main channels and the Stokes fractions Q/I measured by the PMDs an additional synchronization step is introduced. The synchronization is a time interpolation between the four sets of co-added PMD readouts to synchronize the polarisation measurements with the main channels at each wavelength. Given a main channel detector pixel the PMD detector pixel closest in wavelength is determined, using the main channel and PMD dispersion equations. For this PMD detector pixel, the time of the four readouts is calculated relative to the corresponding main channel pixel. By repeatedly adding 23.44 msec the relative timing of the remaining three PMD readouts can simply be determined.

Thus having obtained all the necessary time labels the Q/I curves (which had already been wavelength interpolated to the main channel scale) are next linearly interpolated in time such that they are synchronized both in time and wavelength with the readout of the main channels.
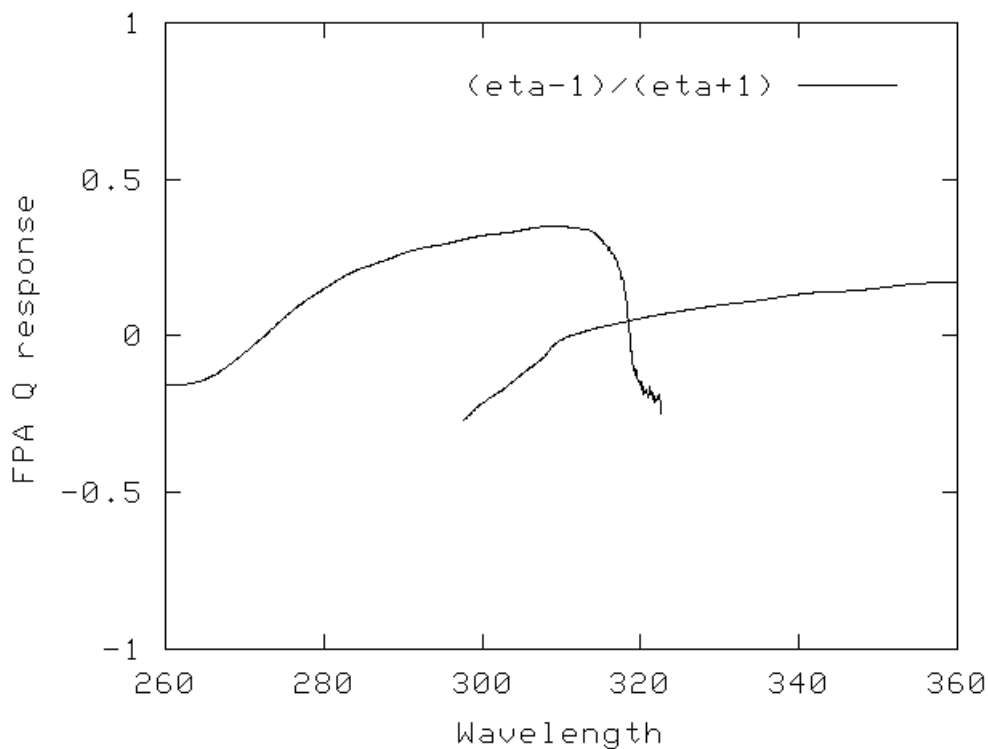
Figure 4-5:   **Main channel Q-polarisation response as applied in polarisation correction term**

4.2.3.5 Application of the derived Q/I in the polarisation correction term

The main channel signal is constructed similar to the PMD signals. The model radiances (I, Q and U) are folded with the main channel slit function. The folded radiances are multiplied with the corresponding instrument responses:

$$Sig^{main} = R^{main} \cdot \left(I + \mu_2^{main} \cdot Q + \mu_3^{main} \cdot U\right)$$

Where R^{main} indicates the radiometric response of the main channels and

$$\mu_2^{main} = \frac{\eta - 1}{\eta + 1} \qquad ; \qquad \mu_3^{main} = \frac{\zeta^{main} - 1}{\zeta^{main} + 1}$$

Where η and ς^{main} are the main channel Q and U polarisation responses respectively, which are part of the calibration keydata [TPD02].

The polarisation sensitivities are shown in Figure 4-5 and Figure 4-6.

Note from Figure 4-5 that the Q polarisation sensitivity between 300-320 nm of Band 1 is significantly higher than that of Band 2. In Figure 4-6 only the noise-like structure in the U polarisation sensitivity of Band 2 is demonstrated. Both features will be discussed in the next sections.

The polarisation correction of the measured radiance is a correction factor c_{pol} to the radiance response R of the main channels. The correction factor contains the polarisation information as it is derived from the PMD measurements:

The Q/I values obtained after the wavelength interpolation and spatial aliasing synchronization described in the previous section are applied in the polarisation correction term. Also, the single scattering ratio for U/Q has again been used. These radiance errors obtained by including PMD measurement and spatial aliasing synchronization errors have the extension 'total' added to their filenames.

To separate the error introduced by the spatial aliasing synchronization from the error due to the band approximation of the PMD measurements and wavelength interpolation, a complete set of radiance errors have been calculated where the PMD measurements are excluded from the calculations. Instead, the spatial aliasing synchronization step is applied to the Q/I model values corresponding to the readout times of the PMD detector arrays. The resulting Q/I aliasing corrected model values are applied in the polarisation correction term. These radiance errors obtained by including only spatial aliasing synchronization errors have the extension 'clean' added to their filenames.

$$I^{main} = \frac{Sig^{main}}{R^{main} \cdot c_{pol}}$$

$$c_{pol} = 1 + \frac{Q}{I} \cdot \left(\frac{\eta - 1}{\eta + 1} + \frac{\zeta^{main} - 1}{\zeta^{main} + 1} \cdot \frac{U}{Q}\bigg|_{ss}\right)$$

The relative radiance error due to application of the polarisation correction scheme is defined with respect to reference radiance:

$$Rad\_err = \frac{I^{main} - I^{ref}}{I^{ref}}$$

The reference radiance Iref is obtained when the model values for Q/I and U/Q, corresponding to the readout times of the main channel detector arrays, are directly applied in the polarisation correction term. Thus Iref represents the case without spatial aliasing synchronization and polarisation measurement errors.
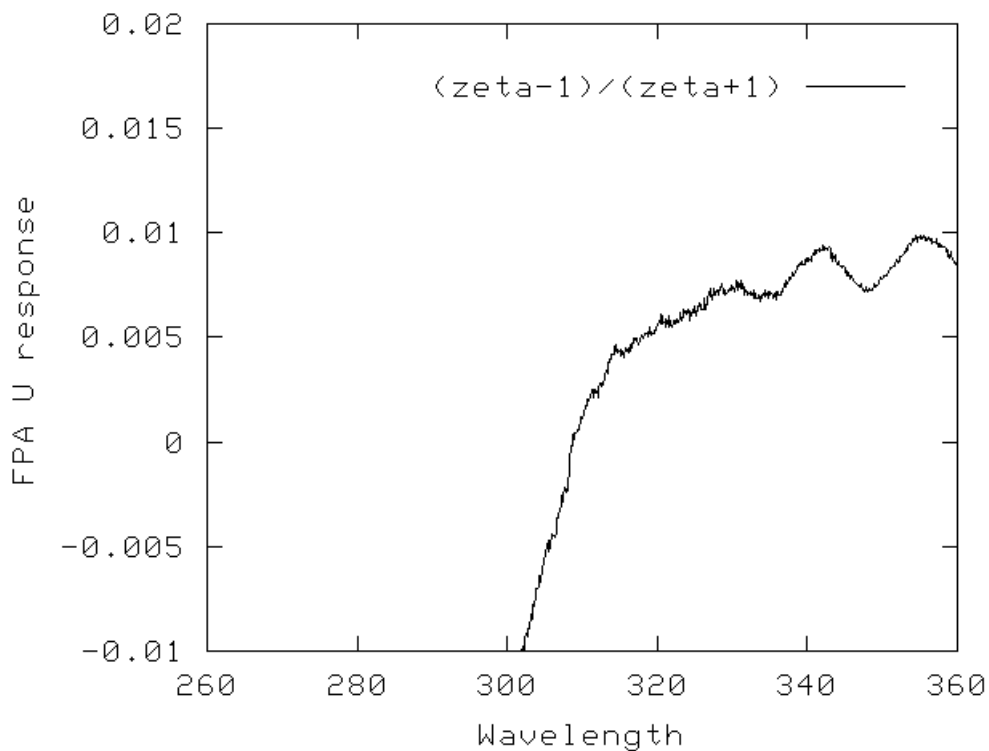
Figure 4-6:　　　　**Detail of main channel U-polarisation response as applied in polarisation correction term**

4.3 Delivered error signatures from PMD Channels *(SRON)*

4.3.1 Delivered spatially aliased signatures for WP2200

The 10656 data files delivered for Task 2b, WP2220 "Propagation of PMD spatially-aliased signatures", are labelled:

GEOM_VIEW_ALB_IMAGE_INDX_READ_ERR

Where:

GEOM	indicates the geo-temporal scenario
VIEW	indicates the ground pixel (East, Nadir, and West)
ALB	indicates the model ground albedo (0.05 or 0.8)
IMAGE	indicates selected LANDSAT image
INDX	indicates column from that LANDSAT image
READ	indicates readout direction (n = nominal, r2 = reverse readout Channel 2)
ERR	indicates the type of radiance error ('total' or 'clean')

The files include three columns for wavelength, radiance error and 1σ accuracy of the radiance error.

The full range of these signatures is illustrated in Appendix A: Task 2b – Error signatures from spectral aliasing

4.3.2 Delivered residual polarisation error signatures for WP2400

The 72 files delivered for Task 2e "Reassessment of key instrumental errors" are labelled:

GEOM_VIEW_ALB

Where:

GEOM	indicates the geo-temporal scenario
VIEW	indicates the ground pixel (East, Nadir, and West)
ALB	indicates the model ground albedo (0.05 or 0.8)

The files include three columns for wavelength, radiance error and 1σ accuracy of the radiance error.

The full range of these signatures is illustrated in Appendix B:
"Task 2b – Signatures from residual polarisation errors"

Appendix B is to be found on the supporting CD-ROM:
"GOME- 2 Error Assessment Study – Phase V: Final Report and Supporting Documents"

4.3.3 Medium for deliverables

The deliverables for both WP2220 and WP2400 are provided to EUMETSAT on:
"GOME-2 Error Assessment Study - Phase V - Data DVD"

This DVD is delivered separately to the EUMETSAT Technical Officer, Dr Rosemary Munro.
Eml: Munro@eumetsat.de

4.4 WP2220: Propagation of PMD spatially-aliased signatures into Level 1 products *(SRON)*

4.4.1 Typical radiance error spectral structures

Radiance errors due to the polarisation correction algorithm are a combination of polarisation sensitivity of the instrument and errors in the polarisation measurement. For the given calibration keydata set two types of typical spectral structures are present in general when the current baseline PMD band selection is applied. The first is a 'bulk' error with a relatively long wavelength between 300 nm and 310 nm. The second is relatively the short wavelength 'oscillations' which correspond to the Ozone Huggins spectral structures.

Both typical structures are a result of wavelength interpolation of the polarisation band measurements. The steep polarisation gradient from the single scattering region to the first PMD band measurement, between 300 - 310 nm in the baseline band selection, is not represented by any measurements, this is indicated by the red lines in Figure 4-6.

 The wavelength interpolation of such a steep gradient is likely to introduce a 'bulk' error in the measured polarisation curve. This error is mainly present in Band 1 since the polarisation sensitivity is relatively large, whereas the polarisation sensitivity is closer to zero in Band 2, see Figure 4-4.

Since the wavelength interpolation is smooth, details like the Ozone Huggins spectral structure will disappear in interpolated PMD band measurements. The corresponding radiance errors are present in both Band 1 and Band 2 but the amplitude is again higher in Band 1 due to the larger polarisation sensitivity, see Figure 4-7 and Figure 4-8.

In an effort to eliminate the Ozone Huggins spectral structures from the radiance errors a set of radiance errors is calculated assuming full PMD readout, hence removing the need for a wavelength interpolation of the PMD band measurements. However, as is demonstrated in Figure 4-8, it appears that the spectral resolution of the PMDs (typically 3 - 4 nm between 300 nm and 400 nm) is not sufficient to resolve the Ozone Huggins structures, although the bulk error due to wavelength interpolation of the steep gradient of the polarisation curve has disappeared.

Due to the strong ozone absorption which 'hides' any low clouds from being observed the reflectivities and polarisations of the cloud and clear models are very similar up to ~ 310 nm. This is already shown in Figure 4-1 and Figure 4-2. As a result, the effect of spatial aliasing in the measured Q/I, and of the radiance error, becomes apparent only at wavelengths beyond 310 nm. This is shown in Figure 4-11 to Figure 4-14 where the measured Q/I and radiance errors of different ground scenes diverge toward 360 nm. In general spatial aliasing does not seem to have much effect between 300 - 400 nm on the radiance error caused by the polarisation correction algorithm.

Due to spatial aliasing, a tiny discontinuity in the calculated Q/I appears between Band 1 and Band 2, this is seen in Figure 4-11. The discontinuity is caused by the maximum time difference in the readout of the last pixels of Band 1 and the first pixels of Band 2, and the corresponding difference in ground scene.

This discontinuity can be artificially removed by reversing the readout sequence of one of the bands. Usually it is suggested to reverse the readout sequence of Band 2, since not only the discontinuity between Band 1 and Band 2 is removed, but also that between Band 2 and Band 3. Figure 4-12 and Figure 4-14 show the result of the readout reversal of Band 2. Note that this reversal only removes discontinuities in the measured Q/I between adjacent bands, not the spatial aliasing over the band itself.

Note: the individual radiance errors due to the spatial aliasing synchronization and the PMD band measurements and wavelength interpolation do not add up quadratically like, for example, random noise. The total radiance error is occasionally reduced by a combination of positive and negative contributions in the polarisation measurement and aliasing synchronization steps. See Figure 4-10, where the total error (blue line) between ~ 310 - 320 nm is smaller than the error without the aliasing synchronization (black line).
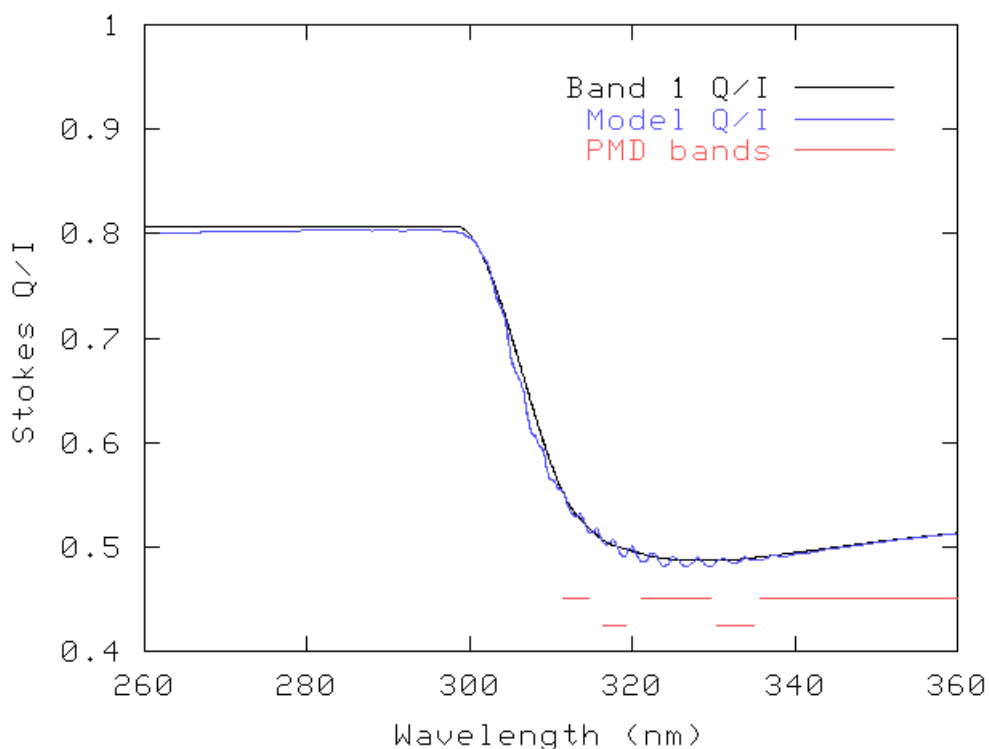
Figure 4-7: **Example of model and measured Q/I**

Example of model (blue line) and measured (black line) Q/I. Systematic differences between model and measurements between 300 - 310 nm determine the bulk radiance error. Varying differences between 310 - 330 nm strongly affect the O_3 profile error in the lower troposphere.
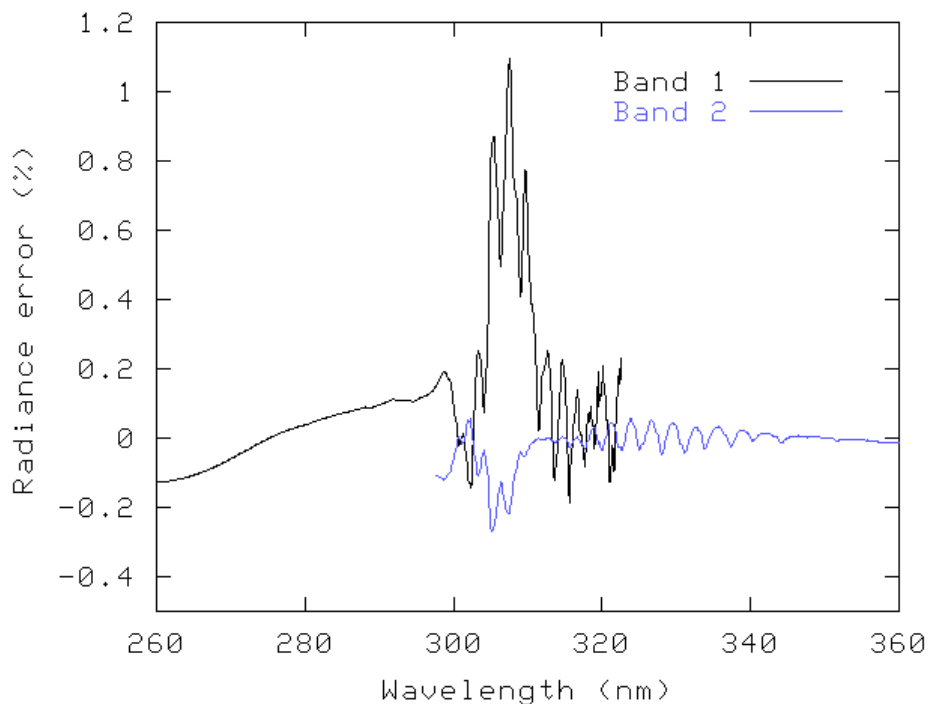
Figure 4-8: **Radiance error without spatial aliasing - Apr_05n extreme East pixel case**

Typical example radiance error without spatial aliasing for Apr_05n extreme East pixel case .The characteristic spectral shape is explained in the text.
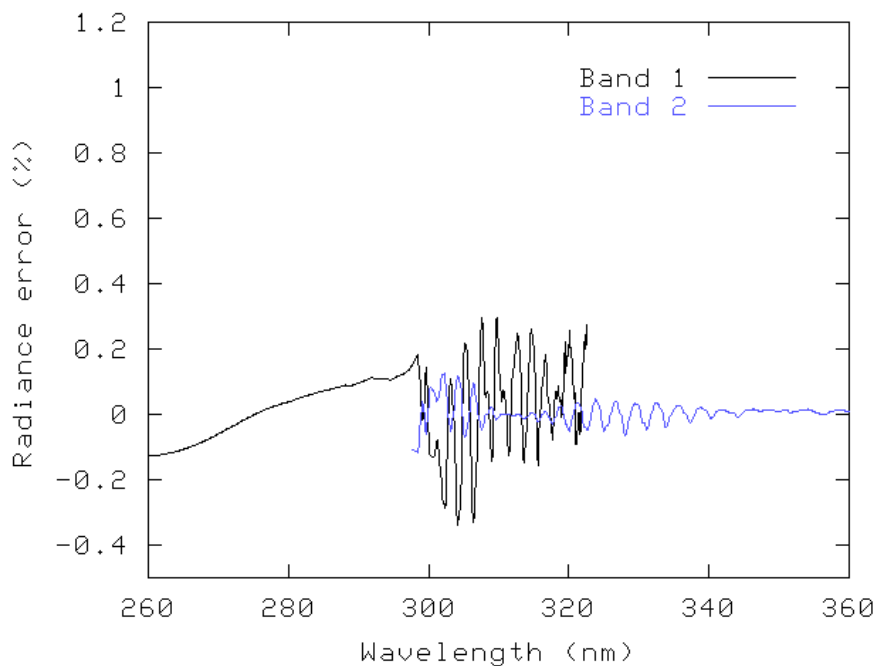
Figure 4-9: **Radiance error without spatial aliasing - PMDs in single pixel readout mode**

Example radiance error without spatial aliasing - Apr_05n extreme East pixel case, with PMDs in single pixel readout mode

Bulk error between 300 - 310 nm has disappeared, Ozone Huggins spectral structures remain.
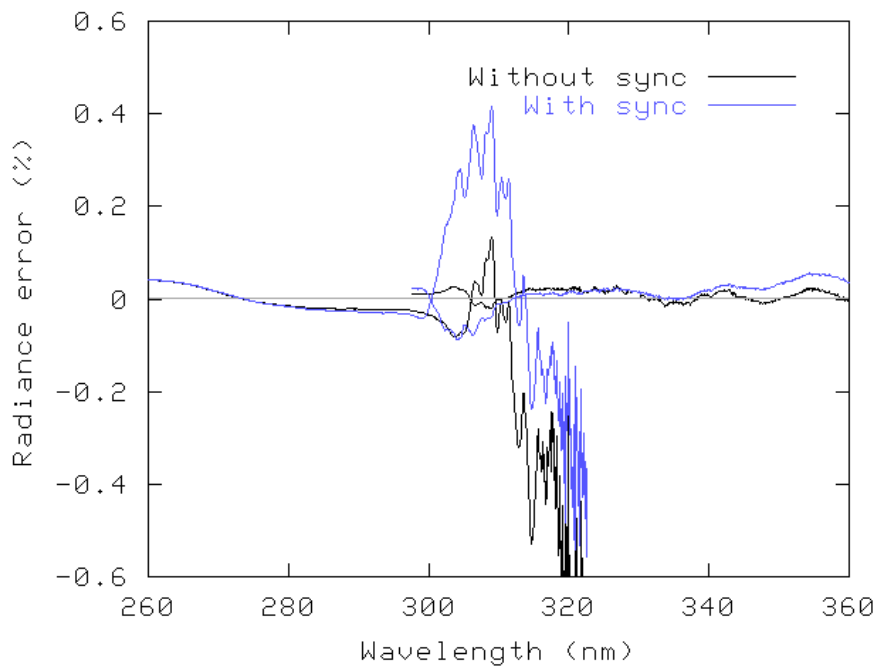
Figure 4-10: **Example radiance errors – with and without errors from aliasing sync**

Black line: only contributions from Q/I measurement and wavelength interpolation errors
Blue line: with additional errors from the aliasing synchronization step
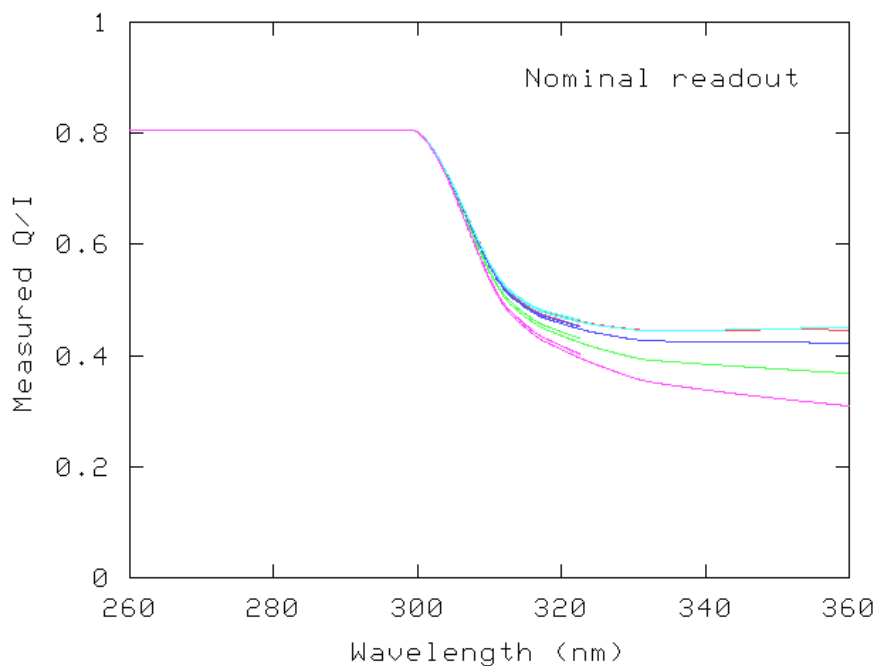
Figure 4-11: **Examples of calculated Q/I corresponding to aliasing albedos in Figure 4-3**

Note a tiny discontinuity between Band 1 and Band 2 (near 320 nm) as a result of spatial aliasing.
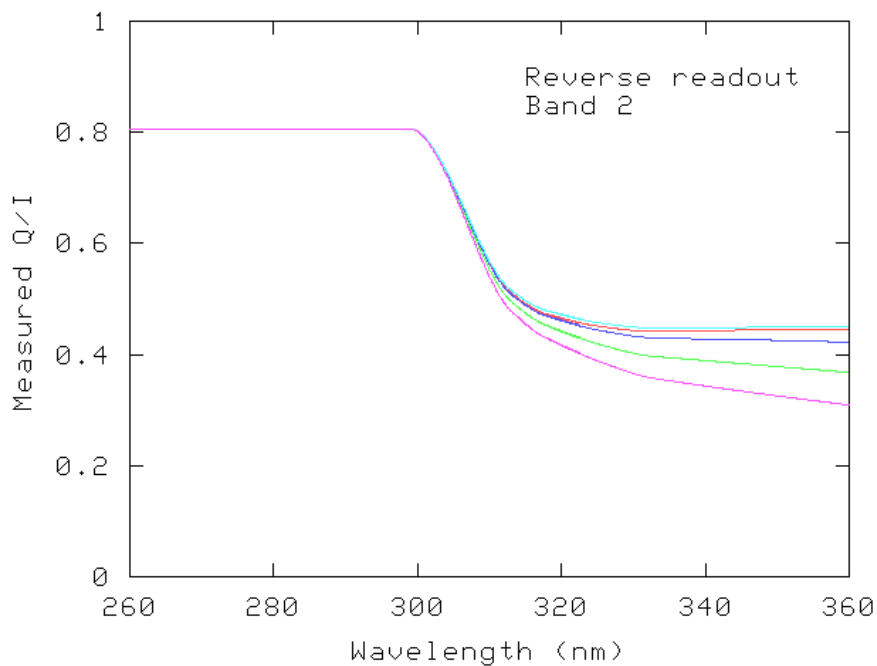
Figure 4-12: **Example calculated Q/I as in Figure 4-13, - but reverse readout of Band 2**

Examples of calculated Q/I corresponding to the aliasing albedo shown in Figure 4-3
The discontinuity shown in Figure 4-11 has disappeared due to the reverse readout of Band 2.
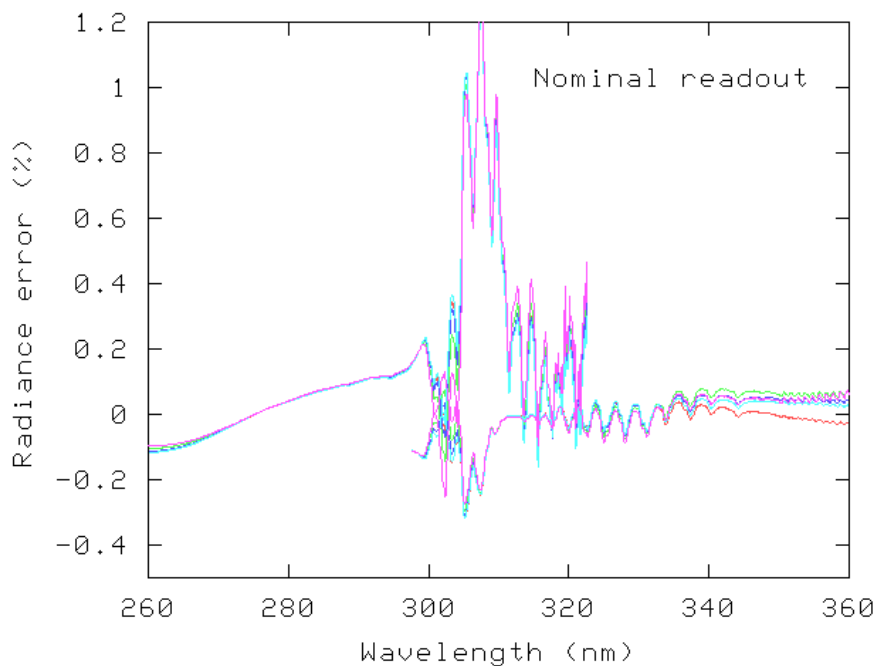
Figure 4-13: Example radiance errors corresponding to aliasing albedos in Figure 4-3
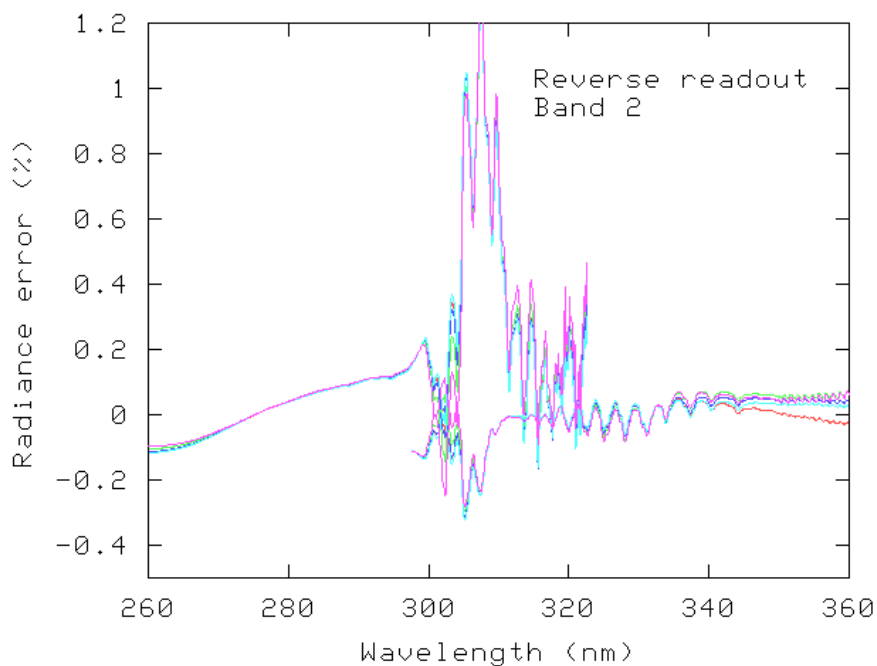
Figure 4-14: Example radiance errors as in Figure 4-13, but with reverse readout of Band 2

Example radiance errors corresponding to aliasing albedos in Figure 4-3, with reverse readout of Band 2. There is almost no difference with the error in nominal readout mode in Figure 4-13.
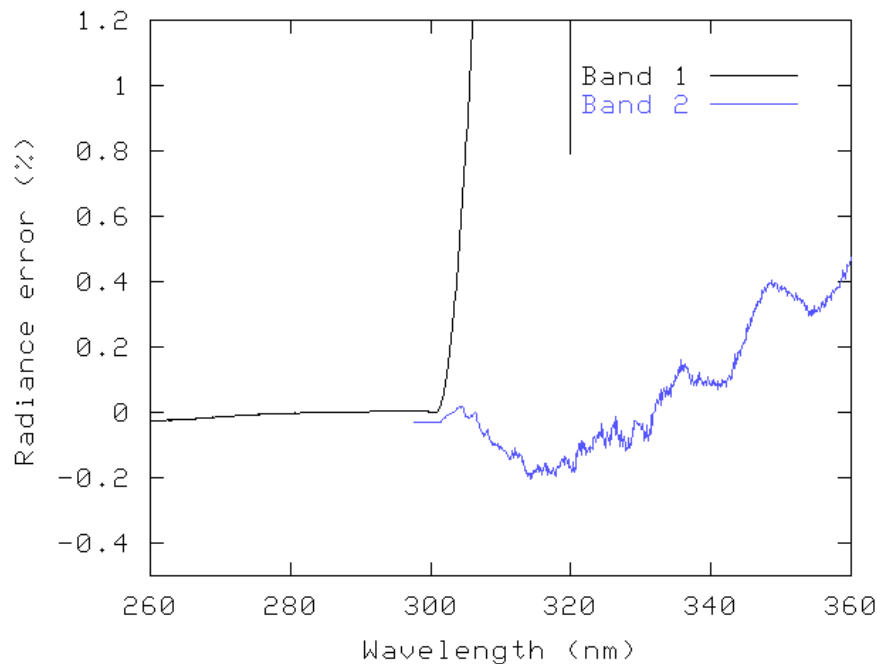
Figure 4-15:   **Radiance error corresponding to the Oct_55n scenario**

The main channel U polarisation response shown in Figure 4-6 is reflected in the radiance error
due to the huge error in the U/Q assumption for this scenario.

4.4.2   Atypical radiance error spectral structures

In a few cases, e.g. Apr_05n West, Apr_75n East and Oct_55n East, the radiance error displays an atypical
behaviour. The error in Band 1 explodes to several percent. The error in Band 2 no longer shows clear Ozone
Huggins spectral structures but is rather noisy instead, see Figure 4-15. Both features have the same origin.
For those particular geo-temporal scenarios the single scattering Q/I ratio is very close to zero, typically less
than 0.01, see Figure 4-16. As a result the single scattering approximation for U/Q becomes extremely large,
typically larger than 100, see Figure 4-17. Outside the single scattering wavelength region the Q/I value has
some small but non-zero value causing the true value for U/Q to drop. Although the Q/I ratio is properly
measured by the PMDs, the high single scattering value for U/Q is maintained in the polarisation correction
algorithm. As a result the U polarisation sensitivity μ^{main_3} is given a huge weight and its own spectral
structure is reflected as a large radiance error in Band 1 and noise in Band 2. For comparison, see Figure 4-6.
The amplitude of the Ozone Huggins structures in the Q/I ratio is small and does not contribute much to the
radiance error.

Currently, a protocol is under development that will improve situations where Q/I has an extremely low
single scattering value, and in the current algorithm a large error in U/Q is introduced.
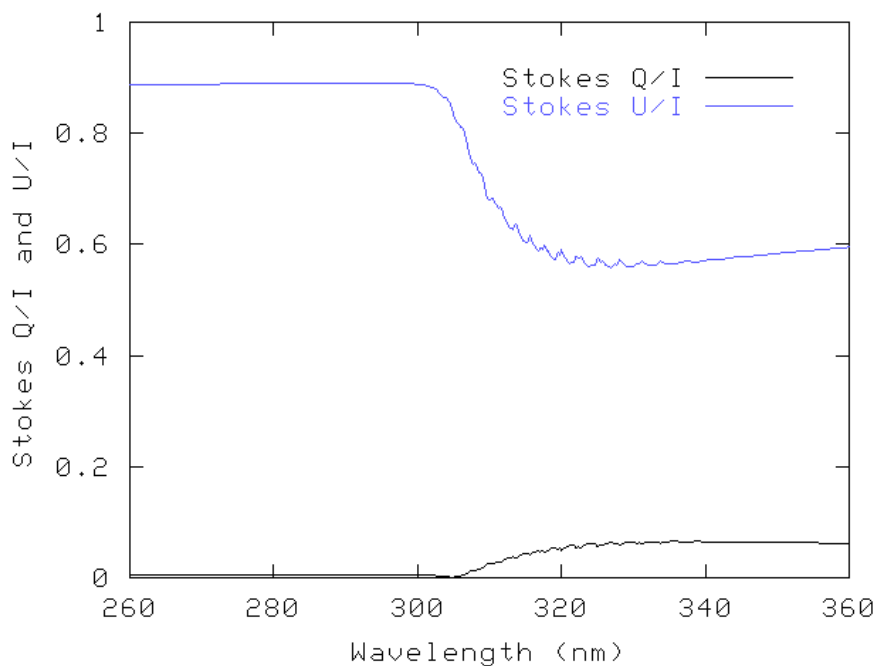
Figure 4-16: **Example of single scattering Q/I close to 0, but increasing toward longer λs**

Example (Oct_55n) where the single scattering Q/I is very close to 0, but is increasing significantly toward longer wavelengths. As a result the single scattering approximation of U/Q fails dramatically.
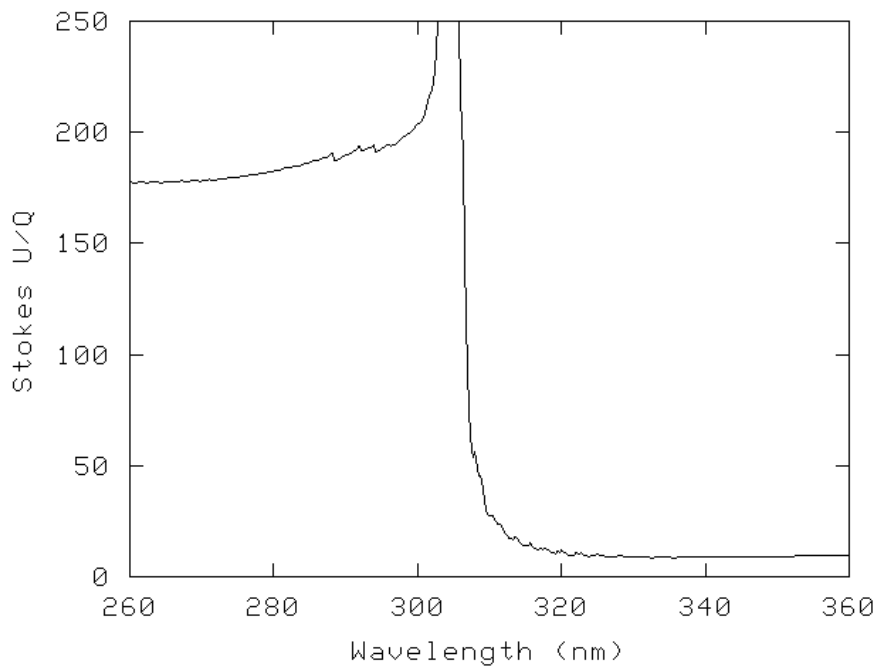
Figure 4-17: **U/Q ratio for the Oct_55n case**

In the wavelength region of interest (300-340 nm) this ratio deviates strongly from the assumed single scattering value.

4.5 WP2240: Aliasing of spatial variability into spectral variability - Ozone Profile results *(RAL)*

4.5.1 Introduction

SRON has modelled the propagation of spatially-aliased polarised radiances through the GOME-2 calibration equations to arrive at errors in estimated sun-normalised radiance due to imperfect polarisation correction, including the effect of spatial aliasing. Error signatures were provided for the following cases:

- ❑ All geo-temporal scenarios

- ❑ With and without a reversal in the read-out of Band 2 with respect to Band 1.

- ❑ With and without errors associated with the polarisation correction scheme itself, referred to here as "clean" and "full" error cases.

- ❑ For nadir and extreme East/West viewing (scanner angle -45° and +45°, respectively): i.e. a total of 12 x 2 x 2 x 3 cases (144 cases, each with many signatures derived from the set of images).

All cases are simulated for the 1920 km swath.

4.5.2 Results

Results for each of the above 144 cases, have been produced using the quasi-nonlinear model used in the main study for the analysis of spatial aliasing, with the following measurement vector options:

- ❑ B1 spectral coverage 265 - 314 nm. Illustrated in Figure 4-18 to Figure 4-21

- ❑ B1 spectral coverage 265 - 307 nm. Illustrated in Figure 4-22 to Figure 4-25

In the main study, it was found that restricting wavelength coverage of B1 to 265 - 307 nm resulted in insignificant spatial aliasing errors, whereas using the range to 314 nm led to significant spatial aliasing errors in some extreme cases.

Figure 4-18 to Figure 4-21 show results for the B1 range extended to 314 nm, Figure 4-22 to Figure 4-25 show results for the standard range adopted in this study (265 - 307 nm). In each case, results for error signatures for nadir and extreme East and West viewing are included. The four figures for each wavelength range correspond to the two options for B2 read-out order and error case (full or clean). Figure 4-23 shows the total error for the nominal B2 readout and standard B1 wavelength range.

It is noted that:

- ❑ Results for certain geotemporal / scan angle combinations should be treated with caution due to low Q/I ratio leading to relatively high polarisation correction error which might be corrected algorithmically (see previous section). These cases are Apr5N (West /+45° pixel), Apr75N (East /-45°) and Oct55N (East).

- ❑ The mapped errors are referenced to the true, aliased intensity, so the direct impact of spatial aliasing on the FPA signals is not included, only the impact propagated via the polarisation correction. Results from the main study are still considered representative of the direct impact of spatial aliasing (subject to the limited number of cases represented by the chosen LANDSAT images).

- ❑ The spread of the results for each scan angle is very small compared to the mean error over all scan scenarios, indicating that the aliasing signature itself has little impact on the error mapped. The mean error is caused by errors in the polarisation correction itself as quantified with the linear mapping scheme under Task 2e. (Mean errors reported here have similar geo-temporal and scan angle behaviour but are generally slightly smaller than the straightforward

polarisation correction error, without spatial aliasing, reported under Task 2e, presumably because the results presented here are based on the quasi-non linear scheme.)

❑   Errors sometimes appear larger in the "clean" case than in the "full case". This is presumably due to a compensation of errors. The "clean" cases should be considered illustrative only; the "full" simulations are considered to represent the errors which would be experienced in practice.

Errors are somewhat larger for the extended B1 wavelength range (as expected).

4.5.3   Conclusions

The consequences for ozone profile retrieval of perturbations to the polarisation correction caused by spatial aliasing are minor compared to:

➢   The direct impact of spatial aliasing on the signals recorded by the FPAs
(Modelled in the main study)

➢   Other errors in polarisation correction
(See Task 2e)
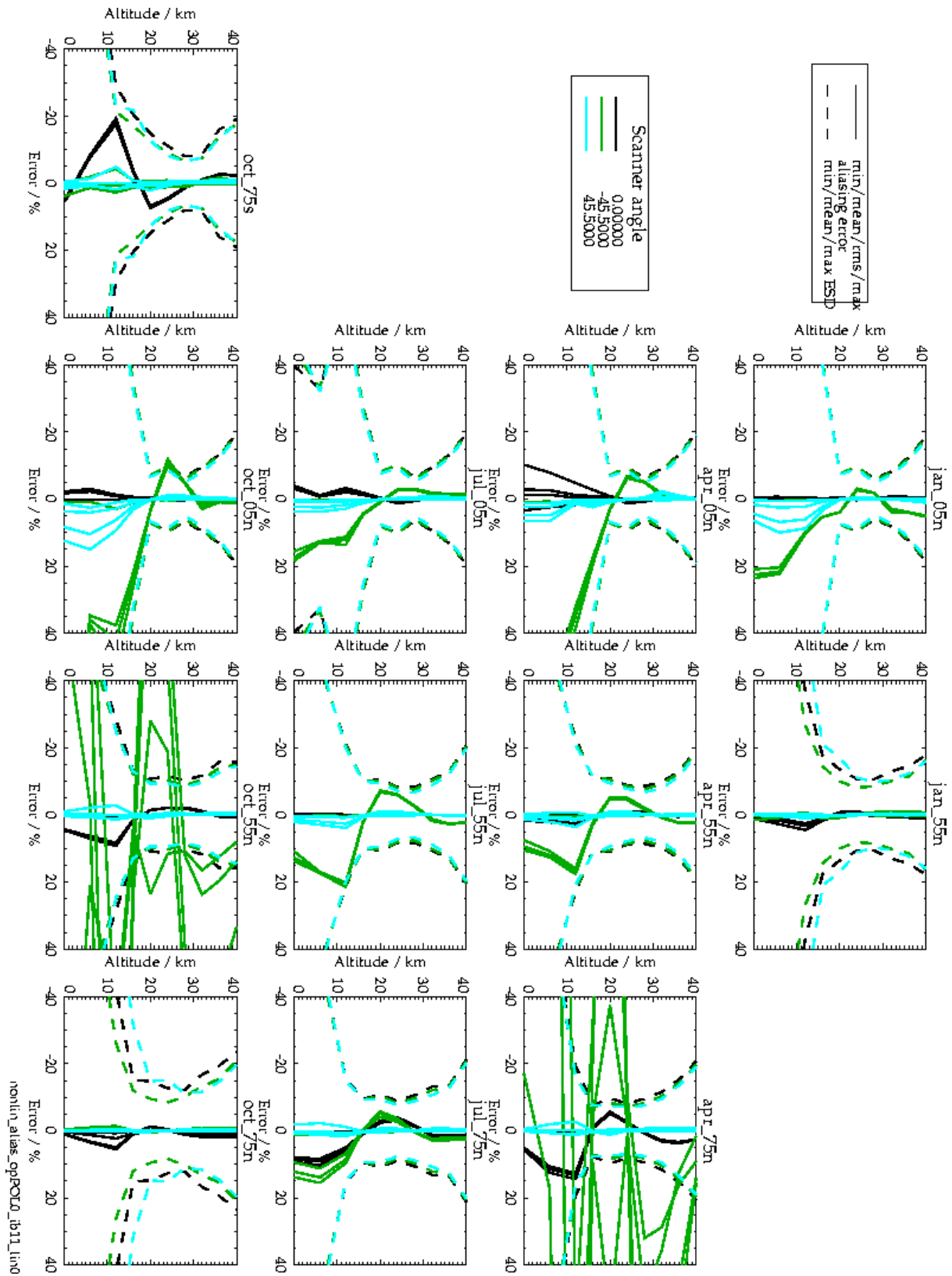
Figure 4-18: Aliasing errors: B1 – 265 - 314 nm; nominal readout direction B2; "clean" case

Task 2b: Aliasing of spatial variability into spectral variability
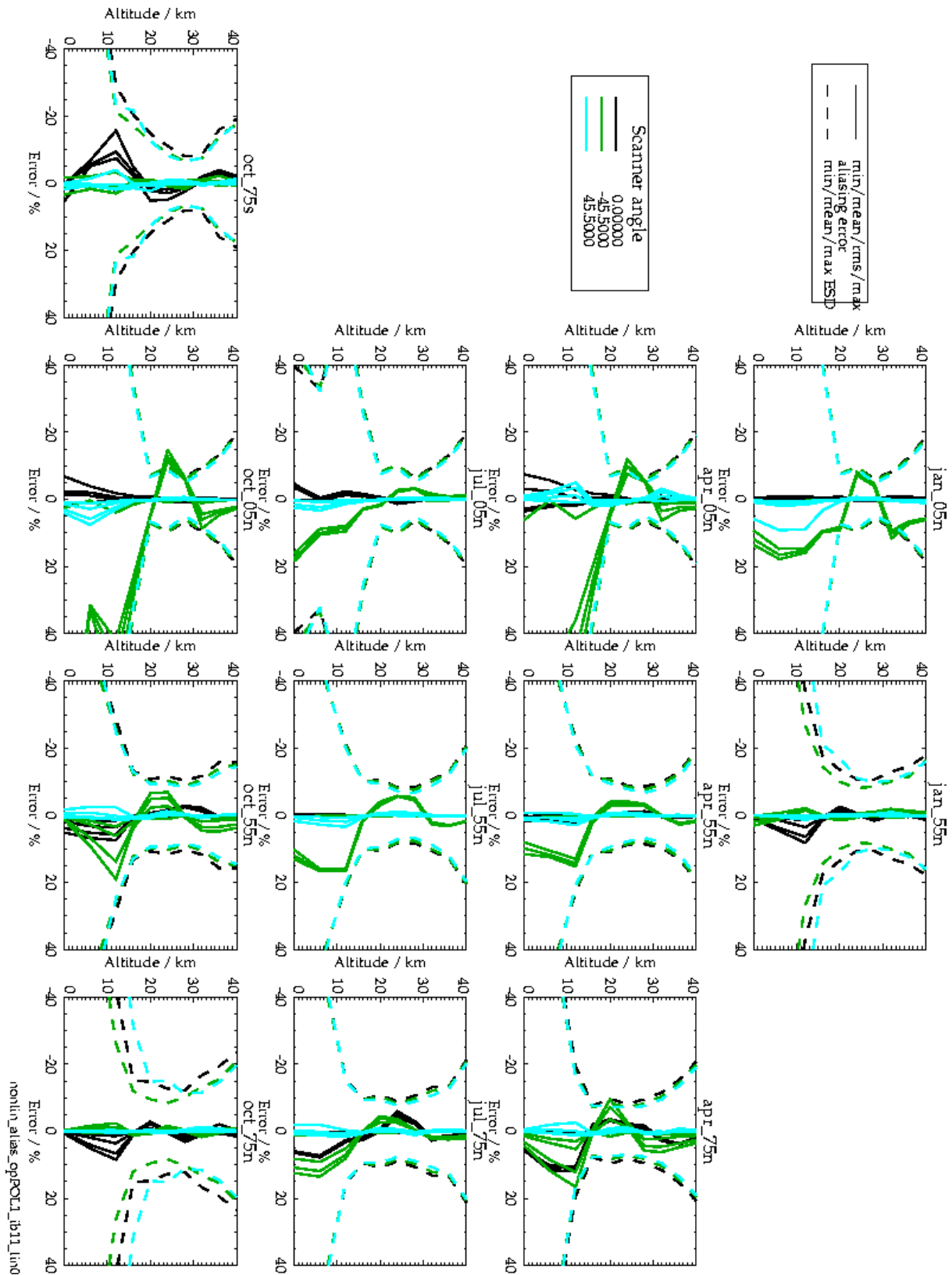
Figure 4-19: Aliasing errors: B1 – 265 - 314 nm; nominal readout direction B2; full errors case
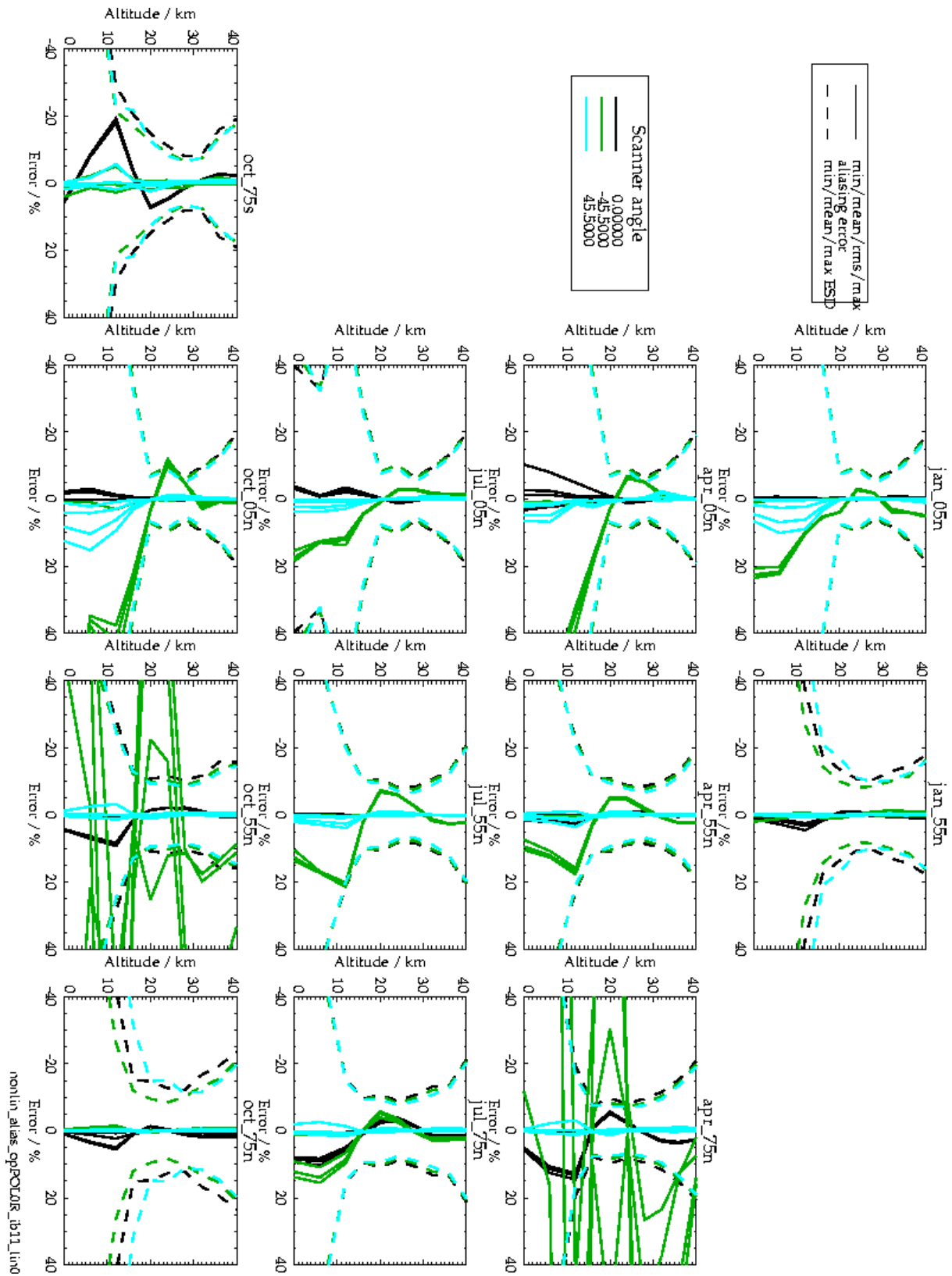
Figure 4-20: Aliasing errors: B1 – 265 - 314 nm; reverse readout direction B2; "clean" case
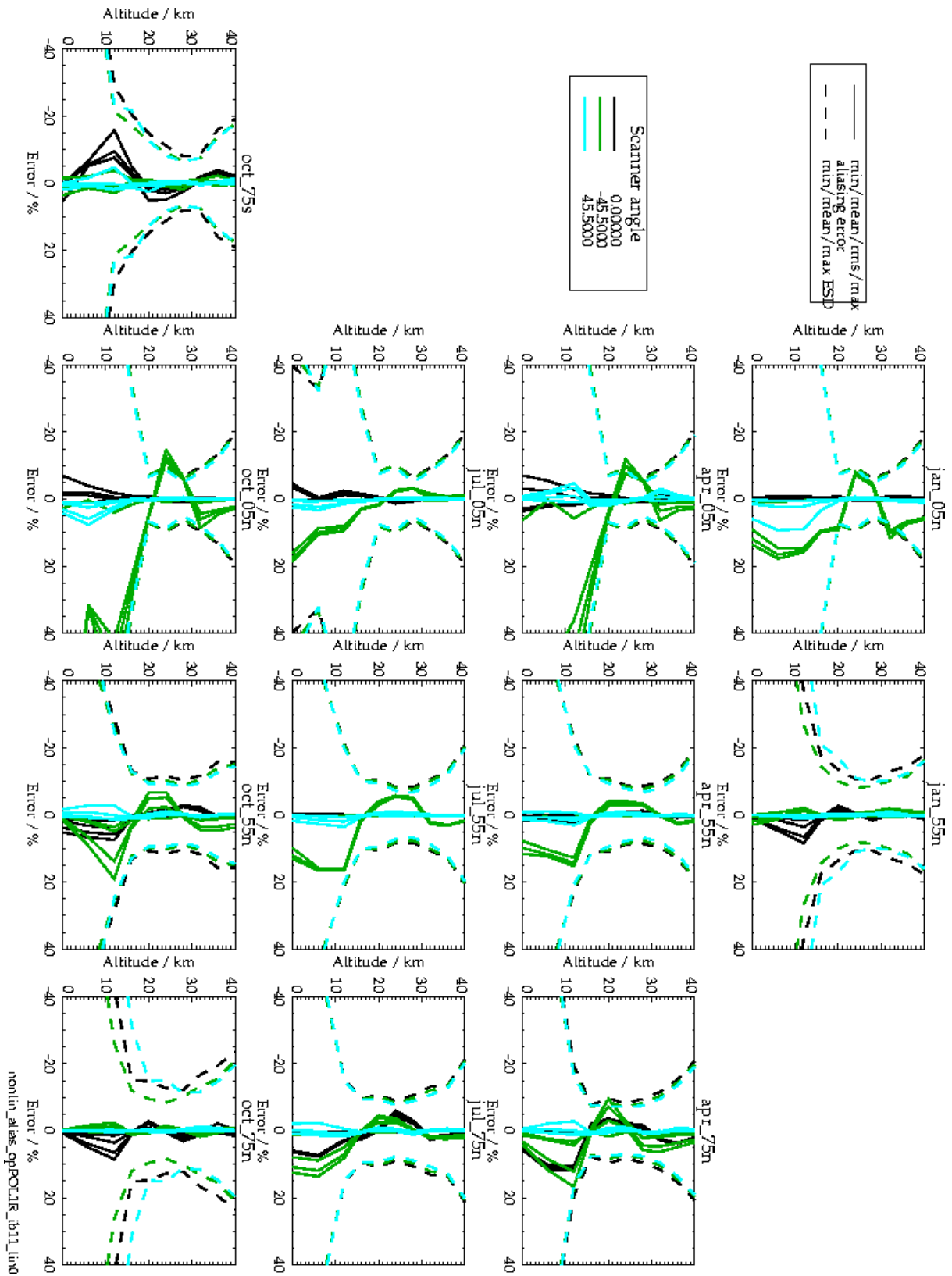
Figure 4-21: Aliasing errors: B1 – 265 - 314 nm; reverse readout direction B2; full error case

Figure 4-22: Aliasing errors: B1 – 265 - 307 nm; nominal readout direction B2; "clean" case
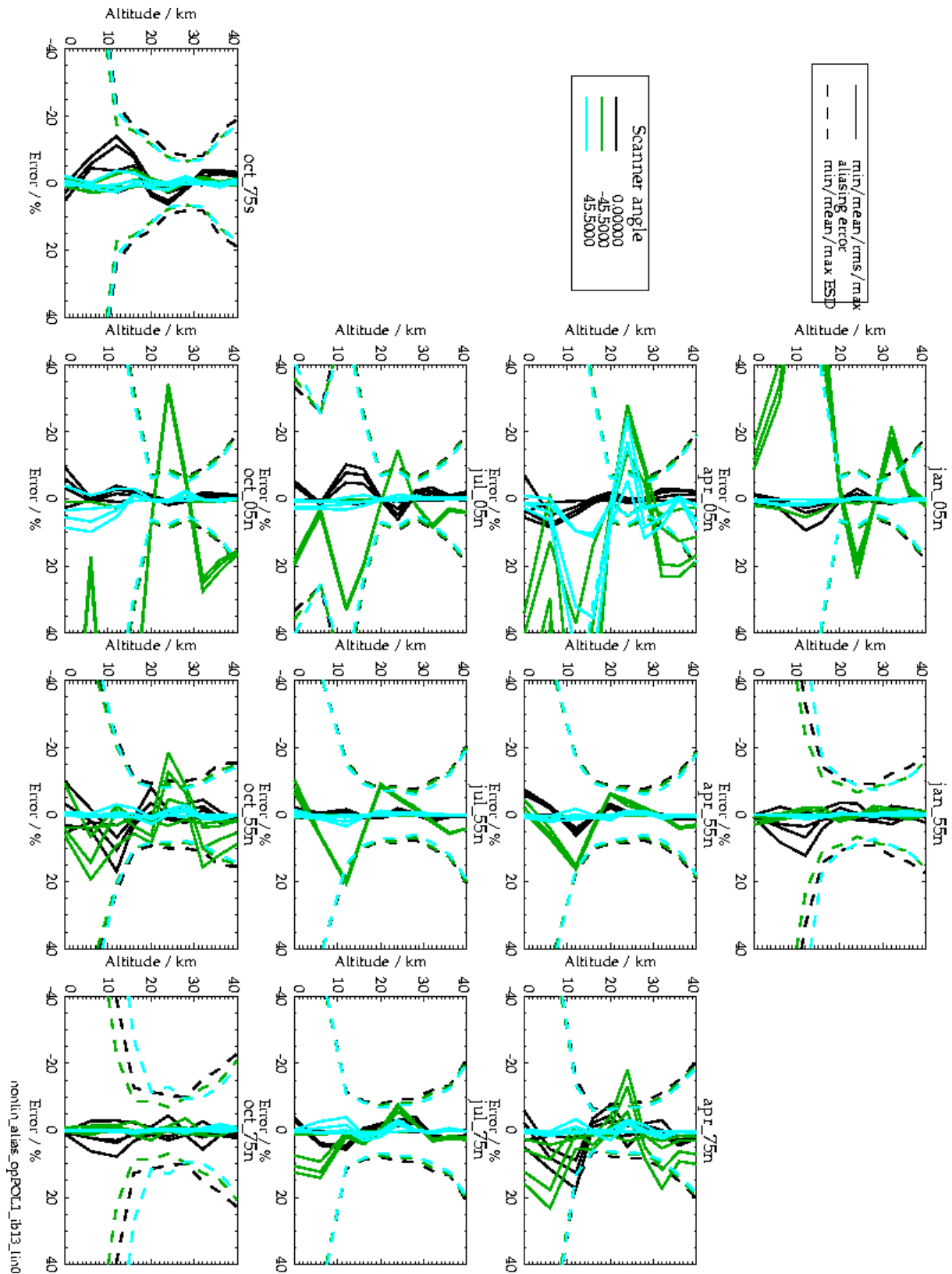
Figure 4-23:　　Aliasing errors: B1 – 265 - 307 nm; nominal readout direction B2; full error case

Task 2b: Aliasing of spatial variability into spectral variability
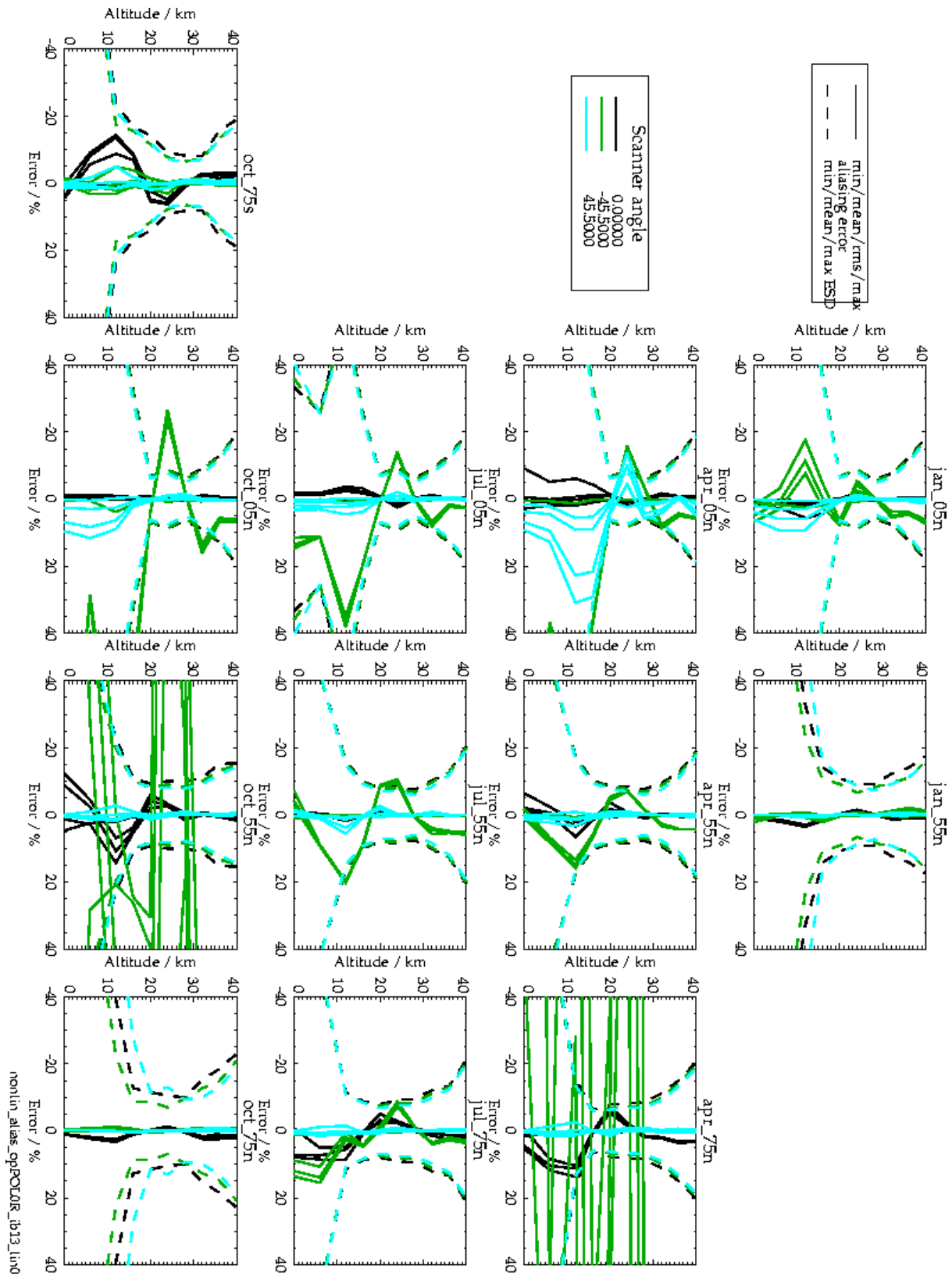
Figure 4-24: Aliasing errors: B1 – 265 - 307 nm; reverse readout direction B2; "clean" case

Figure 4-25: Aliasing errors: B1 – 265 - 307 nm; reverse readout direction B2; full error case

4.6   References

[H&Al]   Hartmann, H.W., Tanzi, C.P., Krijger, J.M., Aben, I.,
            GOME-2 polarisation study – phase C/D, July 2003

[Kur&Al]   Kurucz, , R.L., Furenlid, I., Brault, J., Testerman, L., 1984,
            National Solar Observatory Atlas No. 1

[NSF]   SO/Kitt Peak FTS data used here were produced by NSF/NOAO

[TPD02]   GOME-2 polarisation response, MO-TR-TPD-GO-0068, 16/08/2002

[ESA00]   GOME-2 PMD band selection, technical note, MO-TN-ESA-GO-0203, April 2000

[Kerr&Al]   Kerridge, B.J., R. Siddans, B.L. Latter, J.P. Burrows, M. Weber, R. De Beek, I. Aben and W.
            Hartman,   GOME-2 Error Assessment Study, Final Report EUMETSAT Contract No
            EUM/CO/01/901/DK, 2002

5 Task 2c: Requirements for Characterisation of Slit Function Shape

5.1 Introduction *(RAL)*

The GOME-2 Error Assessment Study (Ph I to Phase IV) demonstrated unequivocally that characterisation of the slit-function shape in the relevant wavelength interval of Band 2 is of critical importance to ozone profile retrieval. Use of the onboard line-lamp alone to characterise slit-function shape will not suffice because:

1. There are no suitable lamp lines in the wavelength interval between 307 nm and 333 nm

2. Lamp-lines at fixed, discrete wavelengths outside this interval do not permit the slit-function shape to be adequately resolved

Retrieval of absolute wavelength registration and slit-function width from direct-sun spectra is part of the standard RAL scheme for processing GOME-1 data. However, this approach assumes a Gaussian slit-function shape, and retrieval of additional parameters to characterise the true shape would be a difficult to formulate and ill-posed problem. Knowing the true slit-function scenario defined by the Officine Galileo (OG) analysis [OG], it can be seen that the standard RAL wavelength calibration / slit-width retrieval leads to errors in the retrieved O_3 profile in excess of 100% in the troposphere. The errors are due to inaccuracies in the assumed shape of the slit.

The recent report of TPD on slit-function shape analysis [TPD], based on the same OG analysis of the "true" slit-function, considered the possibility of parameterising the wavelength dependence of the slit-function shape in terms of some simplified shape models. In the relevant range of Band 2, the Gaussian shape was determined by TPD to be the best of the shape functions considered. Since a Gaussian shape had been assumed in the simulations of the main GOME-2 Error Study, it is therefore considered likely that the approach adopted in the TPD report would lead to errors in the O_3 profile of a similar, unacceptably large magnitude.

Pre-flight measurements of slit-function shape at sub-pixel resolution in the relevant wavelength interval of Band 2 were recommended by RAL in the Final Report of the main study, and subsequently at the GOME-2 FM1 Calibration Results Review Board (Sept '02), so as to meet user requirements on the accuracy of GOME-2 ozone profile retrieval. Such measurements would also offer a major advance on GOME-1, for which errors in knowledge of slit-function shape can now be identified to be a limiting factor on accuracy.

The purpose of Task 2c: WP2300, of the study extension (Phase V), is to quantify the requirements of pre-flight measurements to adequately characterise the GOME-2 slit-function shape.

5.2 Approach *(RAL)*

The original October 2002 proposal for Phase V outlined the following approach for WP2300:

1. Acquire information from EUMETSAT/ESA necessary to prescribe laboratory measurements of slit-function shape by:
    (a) External spectral line lamp and movable detector
    (b) Tuneable, narrowband monochromator source scanned over GOME-2 detector array

2. Iterate and agree with EUMETSAT/ESA the specifications and key error sources of the two set-ups to be simulated (WP2310).

3.   Having developed the software required as part of Task 1, synthesise measurements by the two set-ups in the Band 2 wavelength region < 350 nm and simulate derivation of slit-function shape.

4.   Simulate impacts of erroneous slit-function shape on trace gas column retrievals (WP2320) and ozone profile (WP2330). These simulations would use analogous methodologies to those used in the original study for the assessments of under-sampling and erroneous slit-function shape, respectively.

5.   Specify quantitative requirements for pre-flight measurements of slit-function shape by 1 (a) and/or 1 (b), based on error estimates from (4) (WP2340).

This proposed approach has been modified during the course of the study extension: at Progress Meeting 1, ESA ruled-out measurement concept 1 (a). Simulations were therefore only performed for concept 1 (b). Thus the measurement principle was as follows:

1.   A quasi-monochromatic source will be offered to GOME-2 and recorded by its detector arrays.

2.   The illuminating source will be scanned systematically in wavelength increments much smaller than the GOME-2 detector pixel sampling/resolution.

3.   The slit-function shape (at sub-pixel) resolution will be derived from this sequence of measurements by de-convolving from the recorded spectra, which are themselves inherently at the GOME-2 spectral resolution and sampling interval.

An approach for simulating errors in such measurements was proposed in a technical note and agreed at the 10 March meeting at RAL. It was anticipated that the technique would be limited by the stability and / or knowledge of the quasi-monochromatic source, coupled to the signal to noise of the measurements and the level to which detailed structure in the slit-function shape is important for constituent retrieval. These aspects would therefore be investigated using the following approach:

1.   True slit-function scenarios are defined. It is assumed that the slit-function is the same for both direct-sun and back-scattered observations[1].

2.   Based on the laboratory measurement approach above, linear retrieval diagnostics are used to characterise the sensitivity, Ds, of a retrieved slit-function to errors in the measurement. In the retrieval, the slit-function associated with each detector pixel is represented as a piece-wise linear function described by vector s, with elements corresponding to the value of the slit-function at regularly spaced wavelength intervals. Elements of Ds are the partial derivatives of each retrieved slit-function, $\delta s_i/\delta m_j$, where m_j is the jth measurement as the stimulus is scanner across the detectors response.

3.   N.B. Errors are derived making no assumptions about the variation of the slit-function from one detector pixel to the next (although the sensitivity is determined about a linearization state in which all detectors have the same true slit-function). Furthermore the mapping approach is insensitive to the details of the piece-wise linear representation of each slit-function.

4.   Ds is used to calculate covariance matrices, Ss(l), in the slit-function retrieval due to measurement covariance, Sm(l), arising from a number of error sources.

$$S_{s(l)} = D_s\ S_{m(l)}\ D_s^t$$

5.   The sensitivity of measurement of sun-normalised radiance simulated by the forward model used in constituent retrieval, y, to errors in the slit-function retrieved from the laboratory measurements is calculated, giving Ks, with elements$\delta y_k/\delta s_i$. In the relevant retrievals here, y = ln(I/F), where I is the back-scattered radiance and F is the solar irradiance (the profile retrieval from B1 is not considered in this analysis).

---

[1] This may not be the case and should be considered as a further error source in future work. It is intended to confirm the similarity of the direct-sun and back-scatter slit-function for OMI [Smorensburg].

i.e. $\qquad \delta y_k / \delta s_i = (\delta I_k / \delta s_i) / I_k - (\delta F_k / \delta s_i) / F_k$

Note that Ks depends on the wavelength dependent differences between I and F. In particular, Ks will be 0 if I is a wavelength independent multiple of F. Ks is large where there is structure in the atmospheric absorption, and depends on the wavelength registration of the back-scattered and direct-sun spectra.

6. The sensitivity of the constituent retrieval to perturbations in the measurement, Dy, is already known (as used extensively in simulations for the main GOME-2 Error Study).

7. The error covariance of the constituent retrieval with respect to errors in the laboratory measurements of slit-function is given by:

$$\mathbf{Sx(l) = (Dy\ Ks)\ \ Ss(l)\ (Dy\ Ks)t\ \ =\ \ Dy\ \ Sy(l)Dyt}$$

Where $S_{y(l)} = K_s S_{s(l)} K_s^t$

The square roots of the diagonal elements of S x(l) will be reported as the random errors from this source on retrieved ozone Δx(l).

8. Since the mapping is linear, the magnitude of the Δx(l) can be used to define requirements on the slit-function measurement errors represented by Sm(l).

Note that errors in the slit-function retrieval itself are not reported. These errors will be highly sensitive to the representation adopted for s, e.g. the spacing of the regular grid on which it is defined. Errors are reported only for the full mapping of slit-function measurement errors into the constituent retrieval. These will be relatively weakly sensitive to the adopted slit-representation, since the full covariance of the intermediate slit retrieval is properly taken into account. I.e. the correlation of errors in the slit-function shape retrieved from lab measurements will be fully represented in the final step to map onto the constituent retrieval.

This approach will be applied to trace-gas column retrievals in addition to O_3 profile retrieval. In the former case, slit-function errors are often mitigated in practise by the use of absorption cross-section spectra measured in the laboratory by the instrument itself. Errors reported from WP2330 for trace-gas columns will therefore be more representative of the alternative approach, in which a high-resolution laboratory absorption cross-section spectrum (e.g. from FTS) is pre-convolved with the GOME-2 slit-function for DOAS trace gas column retrieval. However, note that slit-function is used to correct for under-sampling / interpolation error in all cases, and hence the additional error when miss-registration is included in the calculation of Ks will be realistically estimated for both trace-gas column methods as well as for O_3 profile.

The simulations are not specific to a particular technique for producing the quasi-monochromatic input stimulus, but will focus on requirements on the quality / knowledge of this input source. Results will therefore be applicable to the laboratory techniques adopted for measurement of the OMI [Smor&Al] and TOMS [Har&Al] slit-functions, which generate the quasi-monochromatic input source in very different ways.

5.3 WP2310: Simulation of laboratory measurements and slit-function derivation (*RAL*)

5.3.1 General

Code to calculate Sy(l) has been developed at RAL and applied for a range of scenarios. For O_3 profile, the matrices have been calculated using sun-normalised radiances simulated by GOMETRAN at RAL. For trace-gas column retrieval CDI spectra were provided to RAL by IUP. In both cases, radiances and irradiances were simulated at 0.01 nm resolution, corresponding to that of the high-resolution solar reference spectrum of [ChSp96] and limiting the finest scales at which spectral structure exists in the monochromatic spectra before

simulated slit-function convolution. The error covariances were calculated for a number of different cases, detailed below, spanning geo-temporal observing conditions, true-slit-function, laboratory measurement characteristics and errors, a priori slit-function knowledge and wavelength registration between direct-sun and back-scatter observations.

5.3.2   Geo-temporal scenarios

Of the 12 scenarios defined for the main study spanning latitude and season the following cases were selected for the slit-function assessment:

➢ July 5°N   (a case with elevated tropospheric O_3)

➢ April 55°N   (typical mid-latitude conditions)

➢ October 75°S   (ozone-hole and elevated tropospheric BrO)

For both albedo cases (5% and 80%) were simulated.

Only direct-nadir viewing geometry is considered. There is no expectation that across-track scan position should modify the retrieval sensitivity to slit-function errors.

5.3.3   True slit-function scenarios

True slit-function scenarios were defined in which the slit-function for each detector pixel is represented by a piece-wise linear function at sub-detector pixel sampling. For the purposes of this analysis, the true slit-function is assumed to be invariant with wavelength across a given GOME channel. Two basic scenarios are adopted, corresponding to the 348 nm "focussed" and "de-focussed/vacuum" scenarios of the OG Channel 2 defocusing analysis [OG]. The spectral width of both slit-functions is similar (at 348 nm); 0.240 nm and 0.248 nm, respectively. To investigate the dependence of results on slit-function shape, independent of width, some additional simulations have been performed (for O_3 profile only) for a Gaussian slit-function with the same full-width-half maximum (FWHM) as the defocused-vacuum scenario.

Slit-functions for the other channels are defined by using the same shape scenarios, scaling the FWHM according to the channel specific pixel spectral widths (0.1103, 0.1181, 0.2085, and 0.2055 nm in Channels 1-4 from CDR optical design report, MO-RP-GAL-GO-0006, p70 [OG]).

For all simulations described here, except where explicitly mentioned, a sampling interval of 0.01 nm was chosen for the piece-wise linear representation of each slit-function.

5.3.4   Laboratory source width and measurement errors

The laboratory quasi-monochromatic source was assumed to have a Gaussian spectral shape, scanned in wavelength across the detector response. Simulations are performed for a range of source spectral widths from 0.005 nm to 0.500 nm.

The following errors on the laboratory measurements have been simulated:

N	Random measurement error
P	Error in the source power (i.e. scaling of the Gaussian shape)
S	Error in the source mean wavelength
W	Error in the source spectral width

Four ways to model each error are investigated:

U	As random (uncorrelated) from one measurement to the next as the source is scanned across the detector response, and between measurements of different detector pixels (denoted **U** in plots below).
C	As correlated over all measurements in the scan, but random from one detector pixel to the next (denoted **C** in plots). Errors due to noise and power are not modelled in this way; these would correspond to wavelength independent offset and gain errors in the retrieved slit-function and could be trivially corrected.
CB	As random over all measurements in the scan, but correlated from one detector pixel to the next (denoted **CB** in plots), corresponding to a systematic error in the measurement of all slit-functions in the fit-window 2.
CF	As correlated over all measurements in the scan and between all slit-functions (denoted **CF** in plots). Again, noise and power errors are not considered.

The simulated error terms can be translated into stability / knowledge requirements appropriate to a specific measurement concept, taking into account the observation time required to achieve the necessary signal to noise. The retrieval formulation is such that the magnitude of the simulated error on the retrieval constituent scales linearly with the magnitude of each error source. The magnitude of each error chosen for simulation purposes is therefore not critical; requirements can be derived by scaling each error magnitude such that the implied constituent error is acceptable.

The following magnitudes were assumed:

N	signal to noise of each observation is 700, when the centre of the detector pixel is illuminated (i.e. at peak signal). The same rms noise is assumed to apply to all measurements as the source is scanned across the detector pixel.
P	1% error in knowledge of source power
S	1% error in knowledge of source width
W	1% (of source width) error in knowledge of source centre wavelength (shift)

In each simulation, the source is scanned across the detector at a factor 2 finer sampling interval than that at which the sit-function is defined (usually 0.01 nm). The signal to noise quoted corresponds to a set of measurements, which scan the detector pixel at 0.005 nm sampling interval. In these simulations, the assumed noise is scaled in proportion to the inverse square-root of the sampling interval, so as to conserve signal to noise over the whole set of measurements.

5.3.5 Wavelength miss-registration

The sensitivity of sun-normalised radiance to slit-function errors depends on the extent to which spectrally dependent differences exist between back-scattered and direct-sun spectra. Changes in wavelength calibration or differences in Doppler shift between the two observations introduce significant differences in spectral structure, increasing the sensitivity of constituent retrievals to slit-function errors. Simulations have been conducted here for the ideal (but unrealistic) case of no wavelength shift between the two observations, and for a shift of 0.007 nm, corresponding to a typical Doppler shift in the direct-sun observation.

---

[2] This form of correlation is representative of e.g. measuring only one slit function and assuming the result to apply to all detector pixels in the fit-window (given a perfect model exists to model the wavelength dependence of the slit-function). Comparable correlations may exist in measurements using the OMI stimulus since a single source is used to illuminate the echelle, and there will exist correlations between then knowledge of power between the grating orders; correlations between line centre wavelength can similarly be expected.

5.3.6   A priori knowledge of slit-function shape

Initial simulations (presented at the 10 March meeting) made no a priori assumptions about slit-function shape, i.e.

$$Ds = (KmtSm(n)^{-1}Km)^{-1}KmtSm(n)^{-1}$$
$$Ss(n) = Ds\ Sm(n)\ Dst = (KmtSm(n)^{-1}Km)^{-1}$$

Where Km is the weighting function matrix for the slit-function retrieval and "(n)" denotes the random noise component of the slit-function measurement error.

It was noted that results from these initial simulations, for a realistic miss-registration between direct-sun and back-scattered spectra, exhibited a strong sensitivity to the sampling interval at which the slit-function was represented in its retrieval. I.e. fine-scale (order 0.01 nm) spectral structure in the slit-function sensitivity Ks, was propagated at significant amplitude onto O_3 profile retrieval due to errors in the retrieval of the slit-function at such fine spectral scales. (See Figure 5-1 below.).

This behaviour is considered unrealistic since the extent to which the slit-function can be spectrally structured is strictly limited by the optical performance of the instrument. The slit-function can be considered as the convolution of three functions:

> ➢ The image of the slit itself, mapped geometrically onto the detector array.

> ➢ The sensitivity of each detector as a function of position across its surface (including cross-talk).

> ➢ The point-spread function of the optics for an infinitesimally narrow slit (including aberration and diffraction).

This last function limits the extent to which the slit-function can be structured and its width is characterised (by modelling) as the spot dimension in the optical design report [OG], and subsequent Channel 2 defocusing analysis. The function broadens towards the edges of the detector array and is, of course, broader in the defocused case.

The spot dimension in the spectral direction at the centre of each channel, for the "Med. FOV" case are taken from the optical design report [OG] to define a constraint on the finest spectral scales at which structure can be expected in the slit-function. These spot dimensions are 0.022, 0.020, 0.010 and 0.006 mm, respectively in Channels 1-4, to be compared with the detector pixel spectral width of 0.025 mm, accounting for the spectral width of the detector pixel the spot widths correspond to 0.097, 0.094, 0.083 and 0.05 nm in Channels 1-4, respectively.

This a priori knowledge on slit-function shape has introduced into the slit-function retrieval according to the optimal estimation approach such that:

$$Ds = (Sa^{-1} + KmtSm(n)^{-1}Km)^{-1}KmtSm(n)^{-1}$$
$$Ss(n) = (Sa^{-1} + KmtSm(n)^{-1}Km)^{-1}$$

The a priori covariance has been defined to express a correlation length corresponding to the spot-width in each channel. Variances are set to the square of the maximum value of the true slit-function, which corresponds to a standard deviation of approximately 4 nm^{-1}, for the normalised 0.24 nm wide focussed slit.

5.3.7   Spot-width and defocusing

Defocusing the instrument leads to an increase in spot width. In physical terms, this blurring will smear out finer-scale structure in the slit-function up to a larger scale-length than for the focused instrument. To account for this mathematically, the spectral correlation length needs to be increased accordingly in the a priori covariance matrix for slit-function retrieval.

Spot dimension is not characterised explicitly for the defocused case, either in the Channel 2 defocusing document or in the FM1/2 calibration documents. The following approach has therefore been adopted to estimate the defocused spot width in this study:

The 348 nm defocused slit-function has width (defined by the Channel 2 defocusing document) of 2.10 detector pixels (0.248 nm). This width is assumed to result from the convolution of:

> ➤   The detector pixel response, given by a trapezium function with FWHM of 1 pixel and edge taper 0.5 pixels. [3]

> ➤   The image of the slit on the detector array (if perfectly focused), given by a trapezium with FWHM 1.992 pixels[4] and edge taper 0.169 pixels[5]

> ➤   A Gaussian spot-function.

The width of the Gaussian spot-function is adjusted until the convolution of the 3 functions gives the correct combined FWHM for the defocused case. This results in a defocused spot-width of 0.02695 mm (0.1273 nm).

A spot-width is similarly estimated for FM2 Channel 2 slit function (significantly broader than the "defocused" case), assuming the slit-width to be 2.4706 pixels (0.29178 nm)[6], implying a spot-width of 0.04515 mm (0.2133 nm).

Retrieval simulations have been conducted for the following scenarios:

Focused
True slit is "focused" case, a priori correlation-length based on the analysis of the focused slit from the Optical Design Report.

Defocused
True slit is "defocused-vacuum" case, a priori correlation length as focused case.

Defocused (equivalent Gaussian)
As "Defocused", but shape is Gaussian with same FWHM.

Defocused (defoc. spot-width)
As "Defocused", but a priori correlation-length based on defocusing analysis document, as described in preceding text.

Defocused (FM2 spot-width)
As "Defocused", but a priori correlation-length based on FM2 measurements, as described in preceding text.

5.3.8   Implementation of the linear mapping

The matrices Ks and Ss(l) are large, involving all elements of s, for all detector pixels in the fit window. To reduce the computational cost, the slit-function measurement is simulated for one detector pixel only (all detectors have the same true slit-function); i.e. Ss(l) is assumed block-diagonal, with identical diagonal blocks corresponding to the retrieval of slit-function shape for a single detector, by scanning the quasi-monochromatic stimulus across its response. Ks, also has block structure (measurements are independent of the slit-function in a different detector pixel). The required algebra can therefore be performed by storing and manipulating N_y x N_s and N_s x N_s matrices only, where Ns is the number of elements s (for 1 detector pixel) and N_y is the number of detectors in the constituent retrieval fit-window.

---

[3] From GOME-2 FM1 Calibration: Slit-function analysis: MO-TN-TPD-GO-0056. Edge taper refers to the interval over which the value of trapezium function varies from 0 to its maximum value.
[4] Calculated to give the correct FWHM for the Channel 2 focused slit case, assuming the quoted spot-dimension.
[5] Taper estimated from the spectral direction FOV function, p12. Optical Design Report MO-RP-GAL-GO-0006 iss.2
[6] 333 nm, Channel 2 slit function from FM2 CRR Wavelength Calibration and Slit Function MO-TR-TPD-GO-0082 iss.1, p17.

5.4   WP2310: Simulation of GOME-2 sun-normalised radiances *(IUP)*

5.4.1   General

Simulations of spectrally highly resolved nadir sun-normalised radiance spectra were provided to enable generation of error covariances by RAL.

SCIATRAN/CDI was used on a fast IBM simultaneous computer using two processes with six processors each in parallel in order to complete the required data set properly. Data was put onto the GOME-2 server for further processing at RAL.

The simulations used FTS cross-section spectra where available (BrO, O_3, HCHO and NO_2). These were prepared as described below.

The most recent SCIATRAN/CDI version (V 1.2.17) was up to apply the maximum number of spectral points required: 25902 spectral points, which have been split according to two spectral sub-windows each comprising about 13000 spectral points. The spectral sampling was 0.01 nm. In order to save storage radiances for only 20 line-of-sight zenith angles (instead of 240 as before) have been simulated to be used for generating two GOME-2 near-nadir ground pixels (east and west from nadir) for each of the 12 study scenarios and for ground albedos of 5% and 80%.

FTS cross-sections available at http://www.iup.physik.uni-bremen.de/gruppen/molspec/ have been used as input.

For O_3, polynomial coefficients (Bass-Paur parameterisation) have been fitted on the basis of the FTS cross-sections in order to serve the SCIATARAN parameterisation in the UV, below about 340 nm, which covers the spectral ranges for O_3 profile retrieval and DOAS UV fittings of O_3.

Beyond 340 nm GOME-FM O_3cross-sections have been used covering BrO and NO_2 spectral fitting windows used for DOAS.

Ring has been simulated for one scenario and has been added to the considered intensity spectra, as usual. For a qualitative check, simulations using Kurucz on 0.01 nm grid convolved with simple triangle functions, (with FWHMs of 0.24 nm for Channel 1 and 2 and FWHMs of 0.48 nm for Channel 3) have been compared with the IUP model Ring according to GOME. This was as used for previous tasks of this study. This check showed qualitatively good agreement (Figure 5-1). Discrepancies between the GOME Ring and the convolved "FTS-Ring" arise due to different parameter settings (slitfunction, ground albedo, scenario, …). Again, the dominance of the Ring effect compared to e.g. absorption structures is evident, as shown by structures of up to more than 50% observed in the Huggins range of the spectrally highly resolved radiance spectrum.
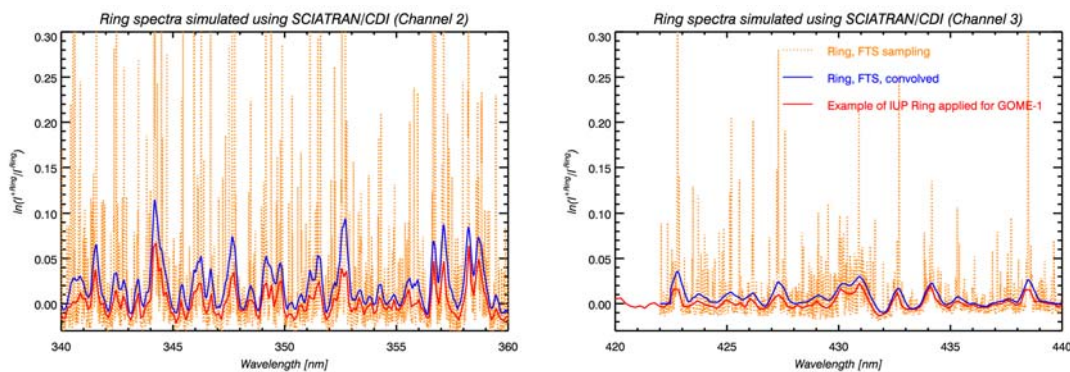
Figure 5-1:   Ring spectra simulated using SCIATRAN/CDI (sectors of Channels 2 and 3)

5.5 WP2330: Propagation of errors in slit-function shape onto ozone profiles *(RAL)*

5.5.1 General

The Sy(l) matrices have been calculated and propagated onto errors in the O_3 profile retrieval. Results for a selected set of cases are presented in figures below. In each case, the following conditions are assumed:

➢ A priori correlations are included.

➢ 0.007 nm wavelength miss-registration between direct-sun and back-scattered spectra

Figures are as follow:

Figure 5-3 for the April 55°N geo-temporal scenario, illustrates the effect of varying the true-slit-function scenario. The laboratory source is assumed to have a width of 0.04 nm, corresponding approximately to that obtainable from the measurement stimulus designed for OMI [Smor&Al][7]. Ozone-profile user requirements[8] are indicated by the dotted-black line and the factor by which the nominal error magnitude must be scaled such that mapped errors are always below the user-requirement (at all altitudes) is indicated in the caption (numbers less than 1 indicate that the slit measurement requirement implied by the nominal error magnitude can be relaxed).

Note the following:

➢ Errors are largest in the troposphere (retrieval levels 12 km and below), Errors at the O_3 peak altitude in the stratosphere are generally lower by a factor 5-10.

➢ Source width errors at the magnitudes simulated have a relatively small impact on the O_3 profile retrieval. However, note in this case the source width is smaller than the optical spot-width used to define the a priori correlation length (0.04 nm vrs. 0.094 nm). Furthermore, note the shift error magnitude of 1% of the width corresponds to an absolute shift of 0.0004 nm.

➢ O_3 errors are generally largest when slit-function measurement errors are random during the characterisation of each detector pixel, but correlated from one detector pixel to the next ("(CB)" case).

➢ O_3 errors are generally lower than this if they are correlated during the slit-function measurement but random from one detector pixel to the next ("(C)" case).

➢ A completely systematic shift (i.e. correlated during measurement of slit-function for a given detector pixel and over all detector pixels, denoted "(CF)") gives rise to the smallest shift errors. (Such an error would be expected to be accommodated by the retrieval of wavelength calibration parameters in the profile retrieval). The focused slit scenario exhibits greater sensitivity to the fully correlated shift error than either of the defocused cases.

➢ With the exception of the fully correlated (CF) errors, the magnitude of errors in the defocused case and defocused case (equivalent Gaussian) are similar, assuming the focused spot-function.

➢ Increasing the spot-width considerably reduces the impact of all errors.

---

[7] The source width of the OMI stimulus varies with wavelength from 0.028 nm at 270 nm to 0.053 nm at 500 nm. Over the range of importance to O_3 profile retrieval, the source width varies from 0.033 nm at 317 nm to 0.036 nm at 337 nm.

[8] From Ozone-SAF Science Plan, SAF/O3/FMI/ALG/PL/003 (rev.10)

Figure 5-4 illustrates the three geo-temporal scenarios, for the defocused (FM2 spot-function) case. The dependence on geo-temporal scenario is relatively small (errors are generally similar within a factor of 2). Largest errors are always in the troposphere, though the altitude of the peak error within the troposphere (0, 6 or 12 km) depends on the geo-temporal scenario.

Figure 5-5 and Figure 5-6 show the dependence of O_3 error at the 6 km retrieval altitude on the width of the laboratory source, for the defocused and focused cases, respectively. The ozone-profile User Requirement for the 6 km level is indicated by the black dashed line (but slit measurement requirement scaling factors in the legend still relate to all altitudes). Note the following:

➢ As might be expected, errors are large for a source of width comparable to or larger than the slit-function itself (> 0.2 nm).

➢ For the focused case, it is particularly noticeable that the random noise term has a plateau at source widths comparable to the a priori correlation length (0.1 nm). Other errors have a local minimum around 0.1 nm.

➢ Errors improve as source width is reduced over the range from 0.1 nm to 0.01 nm (the resolution at which monochromatic radiance/irradiance spectra have been simulated).

➢ The importance of source width errors in relation to other errors increases as source width is increased from 0.01 nm to 0.1 nm (as the width approaches that of the a priori correlation length). A similar behaviour is seen in the shift curves, though in this case note that the modelled magnitude is defined relative to the source width itself. Errors in knowledge of source power have a larger relative importance for small source widths.

➢ Errors which are random within a detector pixel but correlated between detector pixels "(CB)" are comparable in their impact to fully uncorrelated "(U)" errors, though there is a systematic tendency for "(CB)" errors to be a factor 2 larger at 0.04 nm source width (as noted in the error-profile plots referred to above).

Figure 5-7 to Figure 5-9 show comprehensive results for the focused scenario, providing error profiles for the 0.04 nm source width and error growth curves as a function of spot-width for the 6 km retrieval level. Figure 5-10 to Figure 5-15 show similar plots for the defocused (including defocused spot-function) and defocused (FM2 spot-function) cases, respectively.

5.6 WP2340: Definition of requirements for lab measurement of slit-function *(RAL)*

5.6.1 General

In the results reported above, requirements have been derived for three scenarios: focused, defocused (with defocused spot-function) and defocused (with FM2 spot-function) and are listed in Table 5-1 to Table 5-3.

Requirements for the defocused case adopting the FM2 spot-width are considered most appropriate for laboratory characterisation of the FM2 slit.

In each case and for each error type, the requirement is derived by scaling the linearly-mapped errors such that the O_3 profile User Requirements are satisfied at all altitudes, for both albedos and all three geo-temporal scenarios. The geo-temporal / albedo case which is driving each requirement (usually July 5°N and always 0.8 albedo) is indicated in the table.

Assumptions common to all derived requirements are: (1) that the source width is 0.04 nm (comparable to the OMI stimulus), and (2) that observations are scanned across the detector array in 0.005 nm steps. Quoted signal/noise values relate to this spacing. The scan-step may be relaxed to some degree without modifying other results; however the required signal/noise should then be correspondingly increased (by the square-root of the ratio of the new step-spacing to the 0.005 nm nominal value).

Refer to Section 5.8.1, below for corresponding conclusions drawn from the trace-gas column analysis.

Source error type	Error correlation			
	Uncorrelated (U)	Correlated during slit measurement (C)	Correlated between detector pixels (CB)	Fully correlated (CF)
Signal : Noise	1120 July 5N 0.8	-	1830 July 5N 0.8	-
Power	0.386% July 5N 0.8	-	0.208% July 5N	-
Shift	1.05% of width (0.000419 nm) July 5N 0.8	10.5% of width (0.00420 nm) April 55N 0.8	0.524% of width (0.000209 nm) July 5N 0.8	9% (0.00359 nm) April 55N 0.8
Width	6.37% July 5N 0.8	30.8% July 5N 0.8	3.05% July 5N 0.8	30.3% July 5N 0.8

Table 5-1: **Knowledge requirements of laboratory source assuming focussed slit**

Requirements on knowledge of laboratory source derived for source width 0.04 nm, assuming focused slit. Scenario/albedo identifies the worst-case scenario, which defines the requirement.

Source error type	Uncorrelated (U)	Correlated during slit measurement (C)	Correlated between detector pixels (CB)	Fully correlated (CF)
Signal:Noise	689 July 5N	-	843 July 5N	-
Power	0.834% July 5N 0.8	-	1.14% July 5N	-
Shift	3.06% of width (0.00122 nm) July 5N 0.8	16.5% of width (0.00660 nm) April 55N 0.8	3.26% of width (0.00131 nm) July 5N 0.8	43.1% (0.0172 nm) April 55N 0.8
Width	34.1% July 5N 0.8	127% July 5N 0.8	34.9% July 5N 0.8	109% April 55N 0.8

Table 5-2: **Knowledge requirements of lab source for defocused slit (defocusing document)**
Knowledge requirements of laboratory source derived for defocused slit (spot-width from defocusing document)

Source error type	Uncorrelated (U)	Correlated during slit measurement (C)	Correlated between detector pixels (CB)	Fully correlated (CF)
Signal:Noise	425 July 5N	-	709 July 5N	-
Power	1.2% July 5N 0.8	-	1.02% July 5N	-
Shift	4.37% of width (0.00175 nm) July 5N 0.8	16.1% of width (0.00645 nm) April 55N 0.8	3.26% of width (0.00130 nm) July 5N 0.8	54.4% (0.0218 nm) April 55N 0.8
Width	48.5% July 5N 0.8	184% April 55N 0.8	39.0% July 5N 0.8	96.9% April 55N 0.8

Table 5-3: **Knowledge requirements of lab source for defocused slit (FM2 document)**
Requirements derived for defocused slit scenario (spot-width from FM2 document).
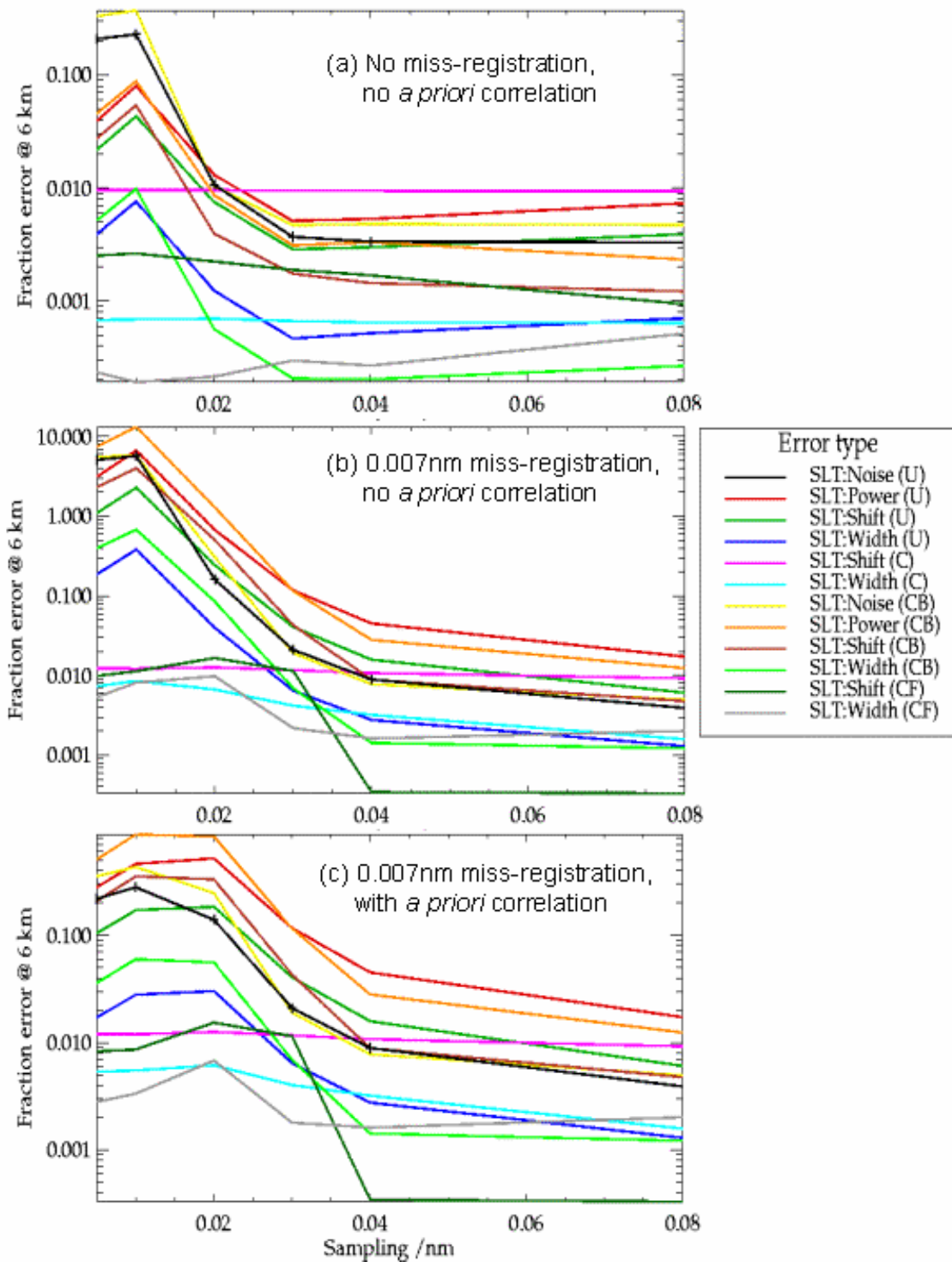
Figure 5-2: **Effect of slit-function definition sample interval on retrieved O$_3$ error at 6 km**
All panels show results for 0.04 nm wide laboratory source and correspond to July 5°N scenario. The focussed slit scenario is assumed. In each case errors increase dramatically, when sampling interval is reduced below the width of the laboratory source. This error growth is particularly evident when the Doppler shift in direct-sun spectrum induces a miss-registration between direct-sun and back-scattered spectra (compare Panels (a) & (b)). Error growth is constrained by introduction of a priori correlations, which express finite spot-width of optics (Panel (c)).
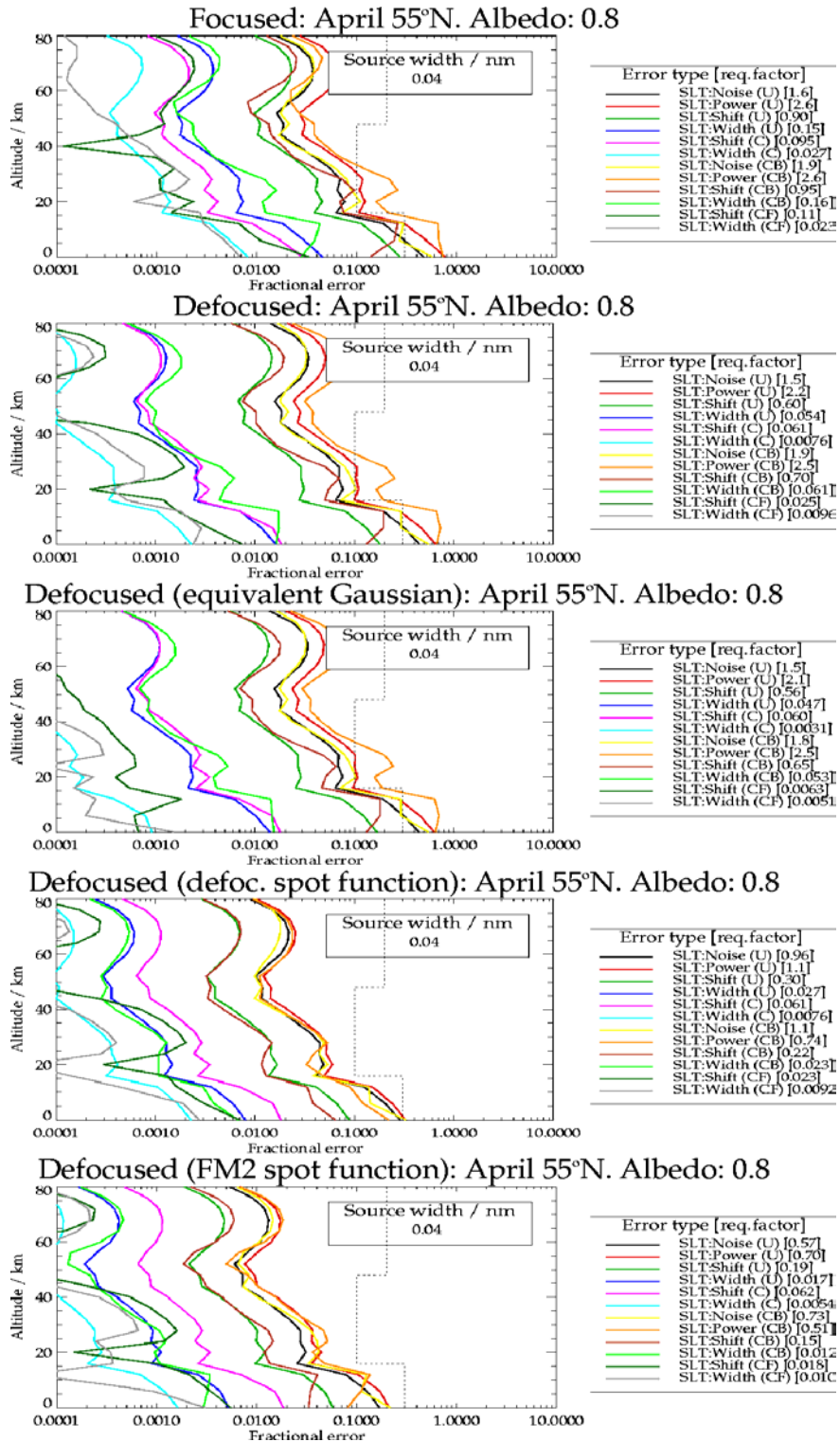
Figure 5-3: Comparison of error profiles for different slit-function scenarios

In all cases the April 55°N scenario and a 0.04 nm laboratory source are assumed.
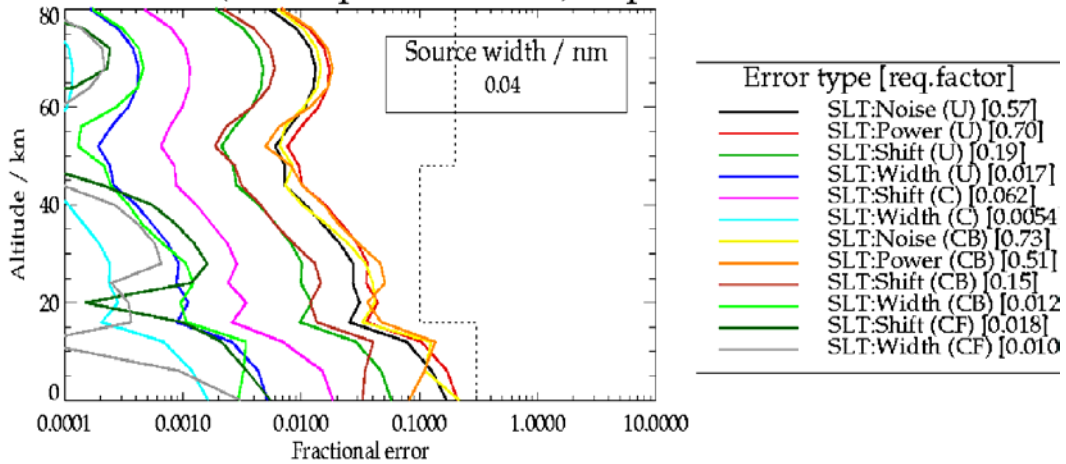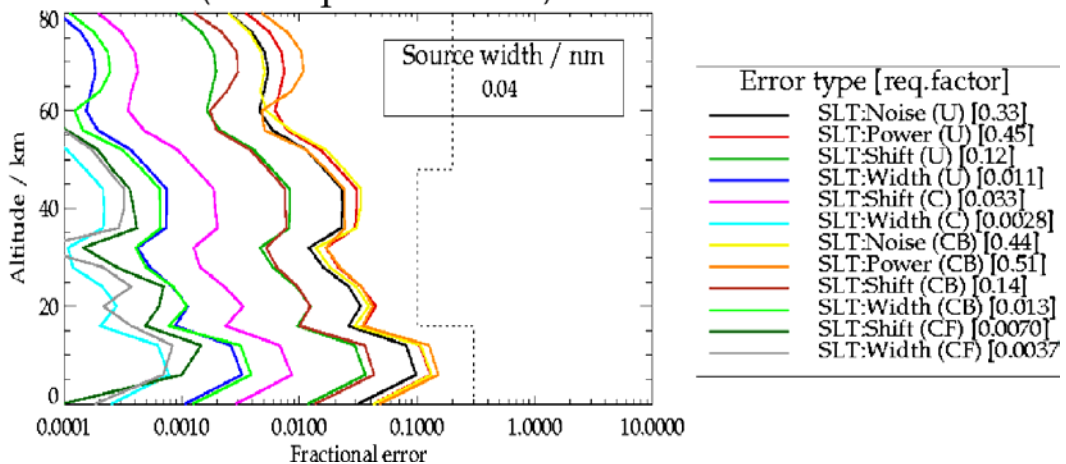
Figure 5-4: Comparison of error profiles for different atmospheric scenarios

The true slit-function is the focused case and the laboratory source width is 0.04 nm.
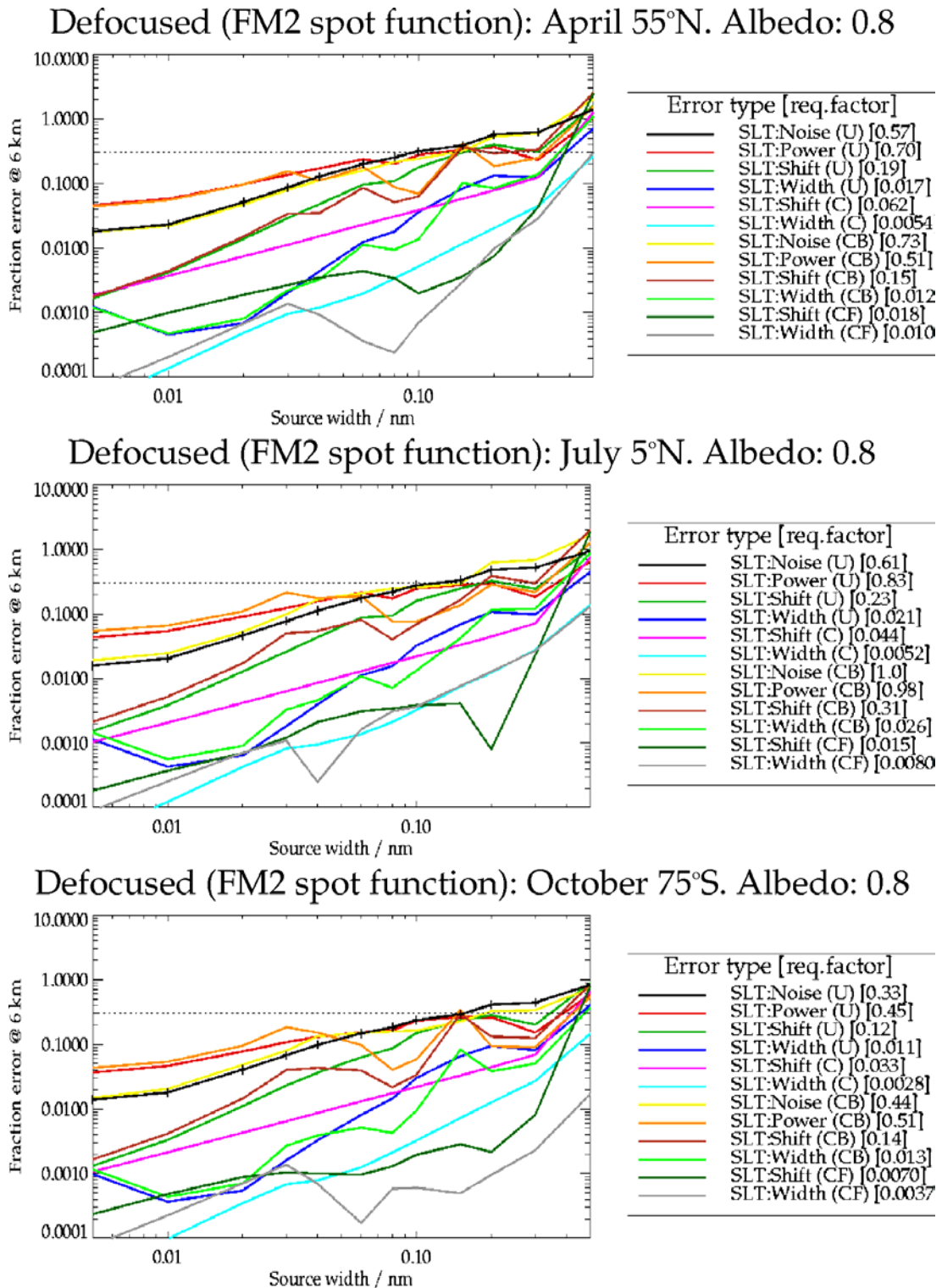
Figure 5-5: **Effect of lab source spectral width on retrieved O$_3$ error (defocused slit-function, FM2 spot-width)**

Effect of laboratory source spectral width on error in retrieved O$_3$ at 6 km for the 3 atmosphere scenarios. Defocused-vacuum slit-function (with FM2 spot-width) is assumed.

Focused: April 55°N. Albedo: 0.8

Focused: July 5°N. Albedo: 0.8

Focused: October 75°S. Albedo: 0.8
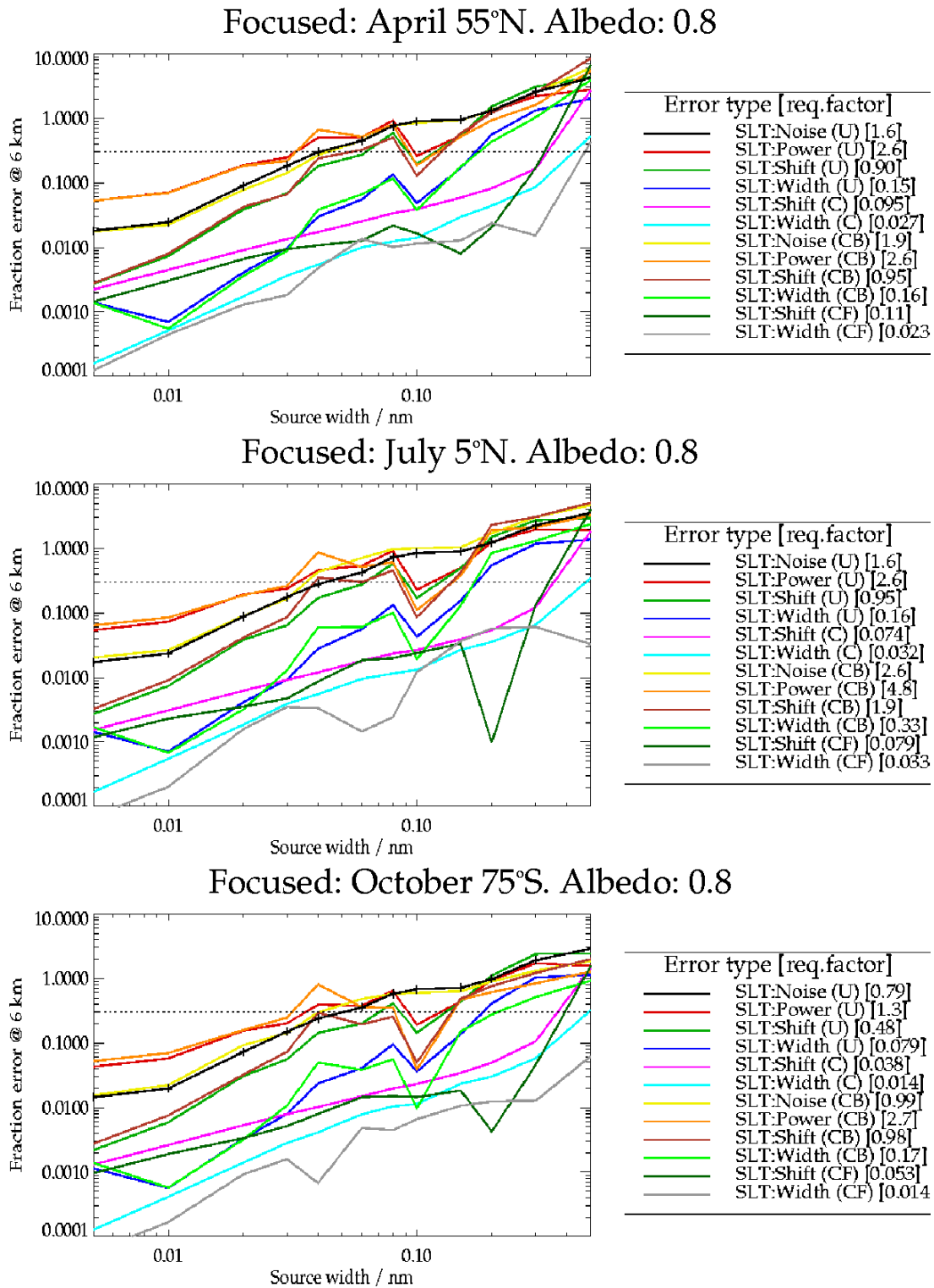
Figure 5-6:   **Effect of lab source spectral width on retrieved O$_3$ error (focused slit-function)**

Effect of laboratory source spectral width on the error in retrieved O$_3$ at 6 km for the 3 atmosphere scenarios. Focused slit-function is assumed.
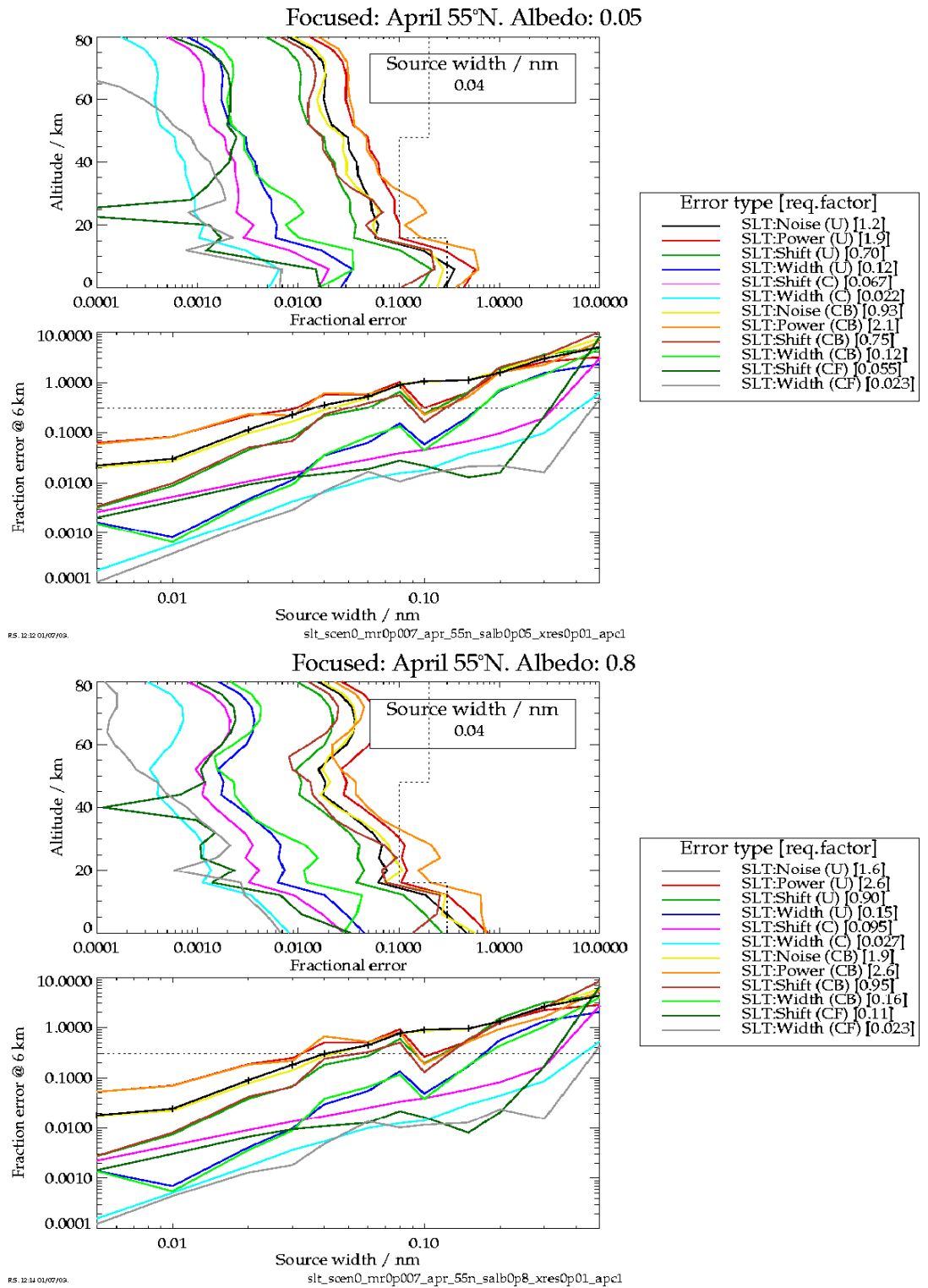
Figure 5-7: **Results for April 55°N, both albedos, focused slit case**
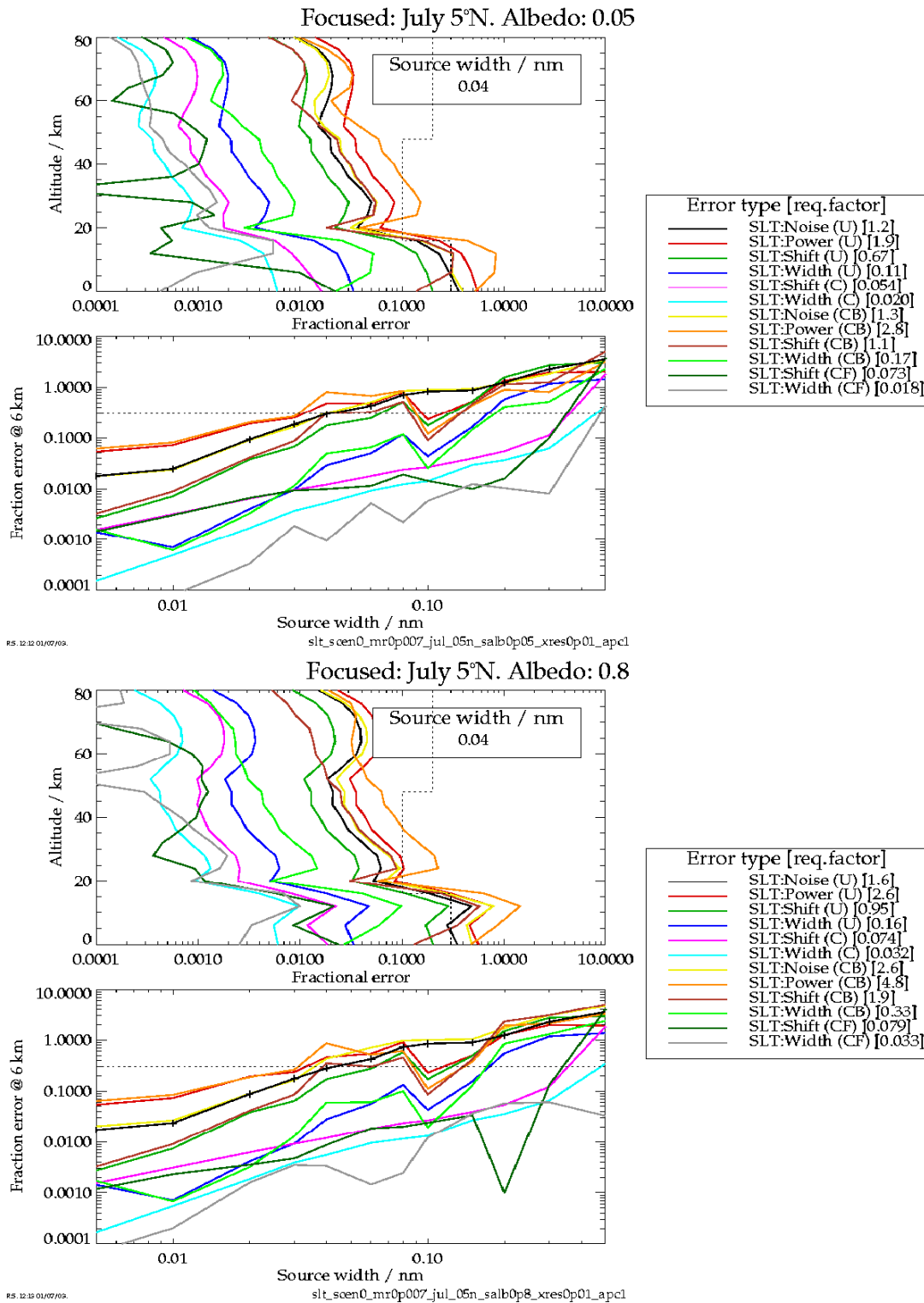
Figure 5-8:   **Results for July 5°N, both albedos, focused slit case**
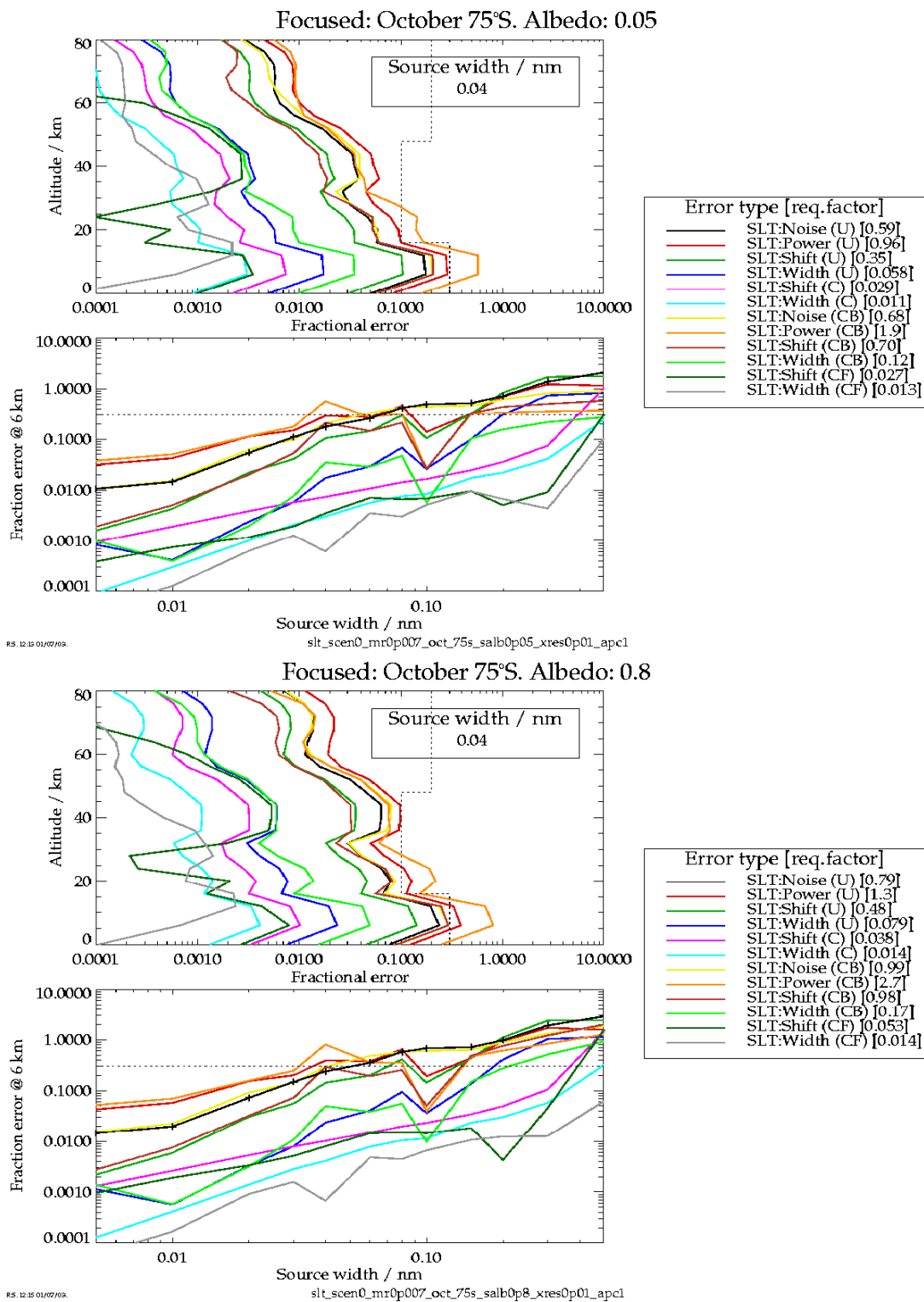
Figure 5-9: **Results for October 75ºS, both albedos, focused slit case**
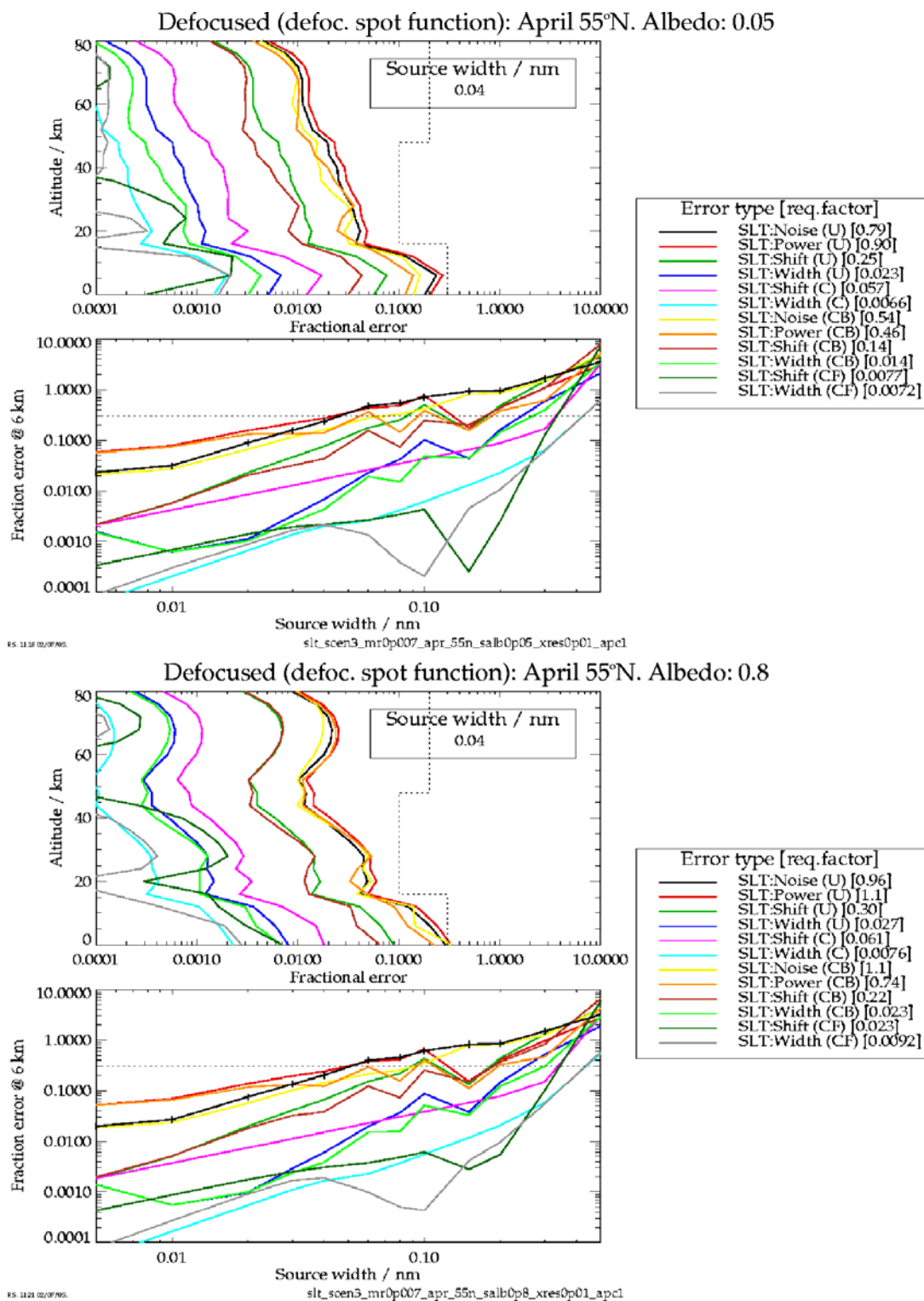
Figure 5-10: **Results for April 55°N, both albedos, defocused slit case (with defocused spot-function)**

Figure 5-11: **Results for July 5°N, both albedos, defocused slit case (with defocused spot-function)**
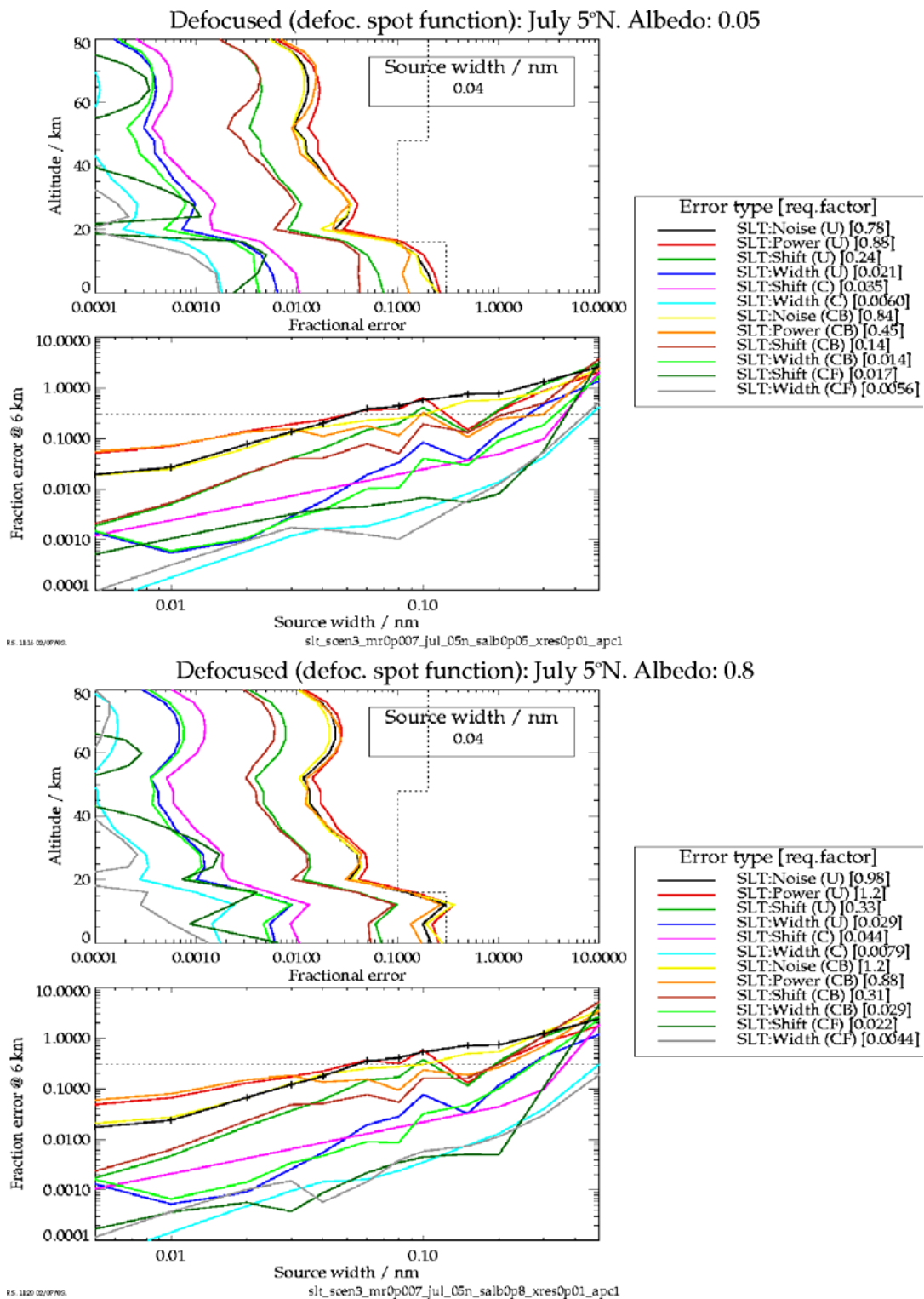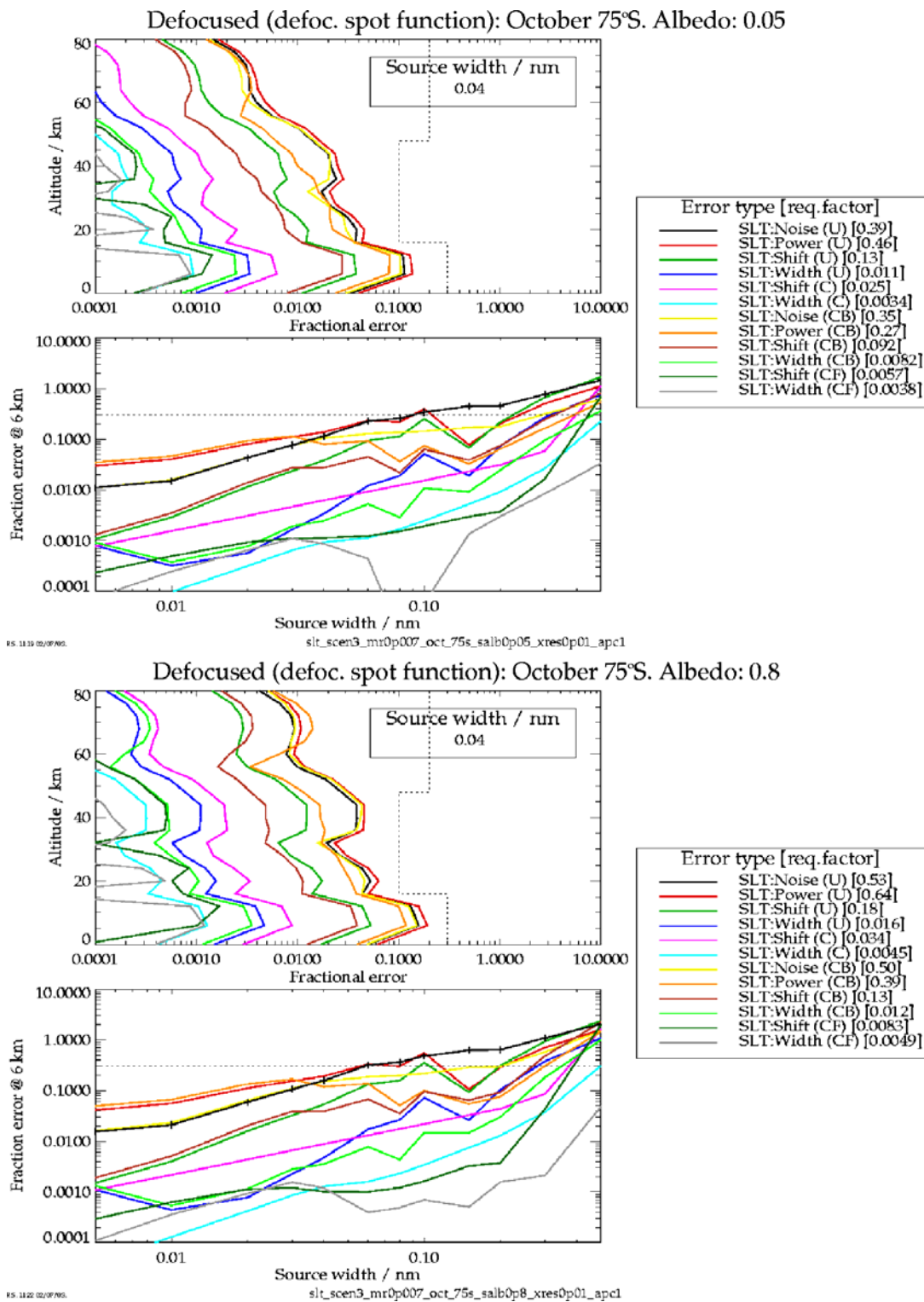
Figure 5-12: Results for Oct 75°S, both albedos, defocused slit case
(with defocused spot-function)
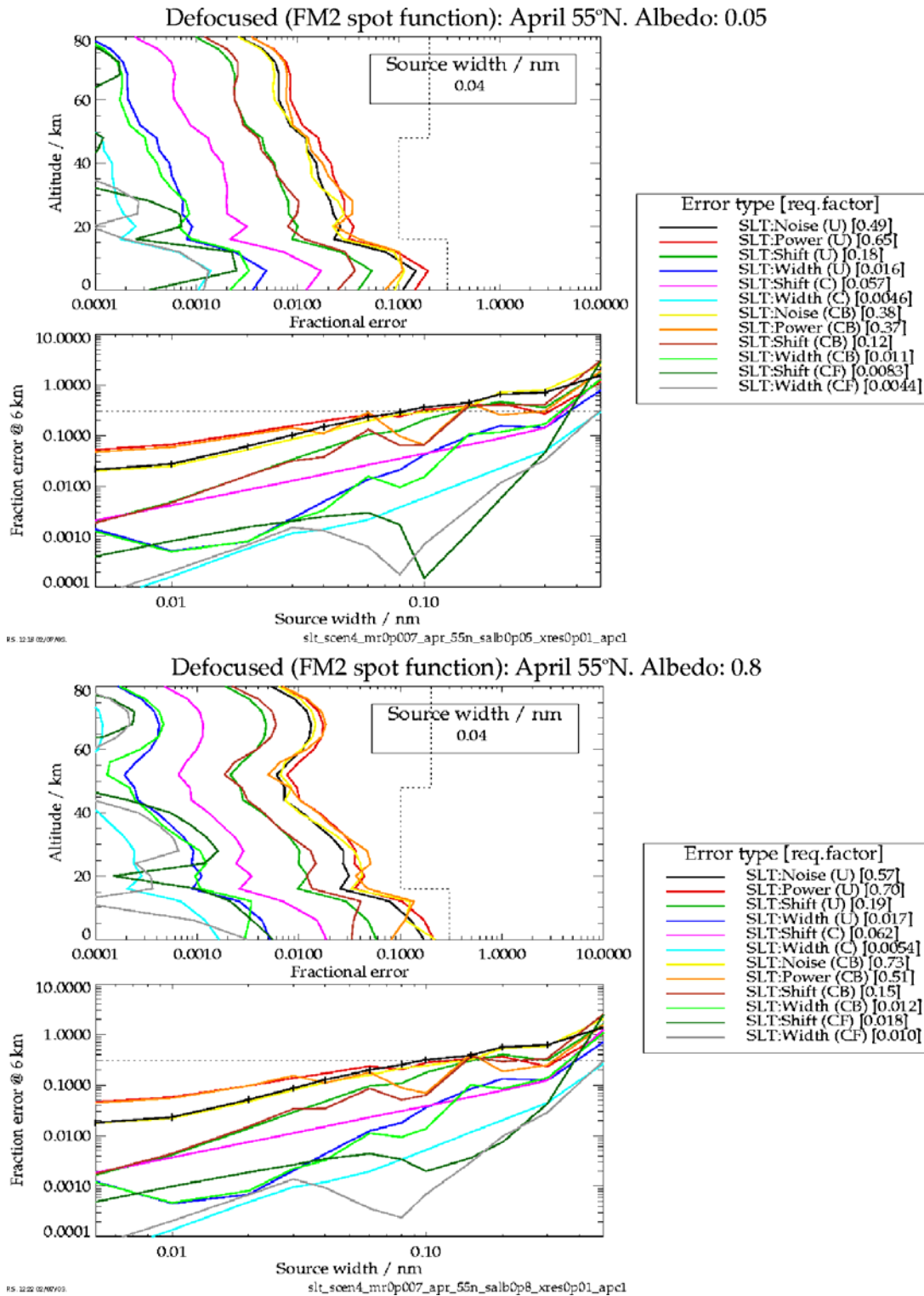
Figure 5-13: Results for April 55°N, both albedos, defocused slit case (with FM2 spot-function)
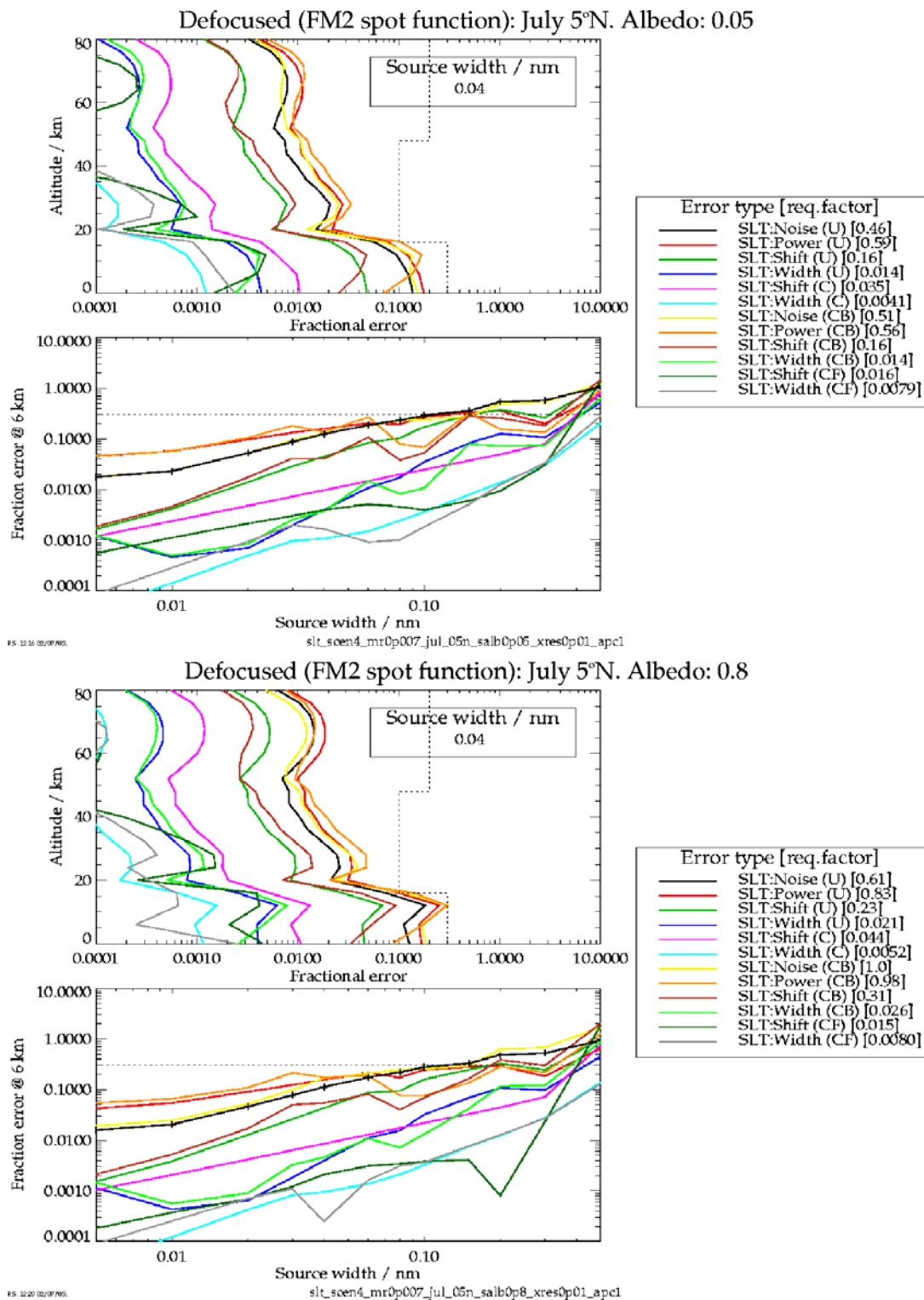
Figure 5-14: **Results for July 5°N, both albedos, defocused slit case (with FM2 spot-function)**
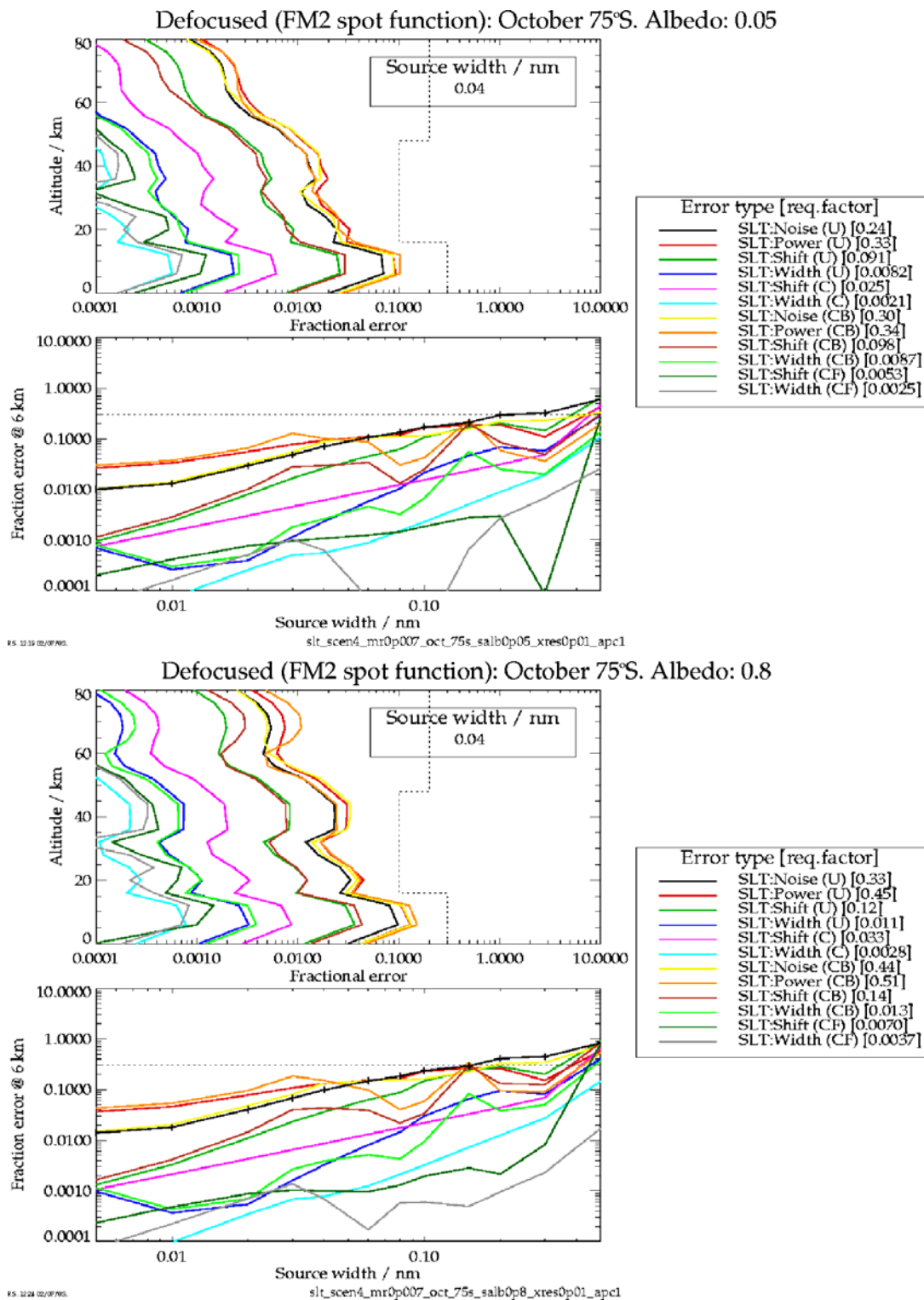
Figure 5-15:   **Results for October 75°S, both albedos, defocused slit case (with FM2 spot-function)**

5.7 WP2320: Propagation of errors in slit-function shape onto tracegas columns *(IUP)*

5.7.1 General

The Sy(l) matrices were calculated at RAL for trace-gas column retrieval, using high spectrally resolved CDI spectra provided by IUP (Section 5.5). The slant column errors have been derived using transformation involving the DOAS linear mapping matrices L as follows: $SSC = (L^T L)^{-1} L^T \cdot Sy(l) \cdot L(L^T L)^{-1}$.

The diagonal elements of SSC provide the slant column errors and the rows of L contain the various cross-sections as a function of wavelength. The ring effect as pseudo-absorber as well as the various polynomial terms $(1,1,1,\ldots)$, $(\lambda 1, \lambda 2, \lambda 3,\ldots)$, and $(\lambda 1^2, \lambda 2^2, \lambda 3^2,\ldots)$ are part of the L-matrix.

Errors have been analysed for twelve different error types. These include random measurement error (noise, N), source spectral width (width, W), source wavelength registration (shift, S), and source strength (power, P). Four different error models are provided, which are denoted U, C, CB, and CF; these account for various degree of correlation between successive monochromatic measurements by scanning through the spectral range of the detector array.

These 12 error types (which are explained in detail in Section 5.3.4. above) are as follow:

U N	Random measurement error	- uncorrelated between measurements, uncorrelated between pixels
U P	Error in the source power	- uncorrelated between measurements, uncorrelated between pixels
U S	Error in the source mean wavelength	- uncorrelated between measurements, uncorrelated between pixels
U W	Error in the source spectral width	- uncorrelated between measurements and between detector pixels
C S	Error in the source mean wavelength	- correlated between measurements, uncorrelated between pixels
C W	Error in the source spectral width	- correlated between measurements, uncorrelated between pixels
CB N	Random measurement error	- uncorrelated between measurements, correlated between pixels
CB P	Error in the source power	- uncorrelated between measurements, correlated between pixels
CB S	Error in the source mean wavelength	- uncorrelated between measurements, correlated between pixels
CB W	Error in the source spectral width	- uncorrelated between measurements, correlated between pixels
CF S	Error in the source mean wavelength	- correlated between measurements, correlated between all slit functions
CF W	Error in the source spectral width	- correlated between measurements, correlated between all slit functions

Each of these error types were applied to different slit function errors using the focused and defocused spot width dimension from FM2 calibration (0.045 mm).

In addition, the two cases were considered where Doppler shift is applied in the irradiance measurements during error propagation. For partial compensation of the Doppler shift shifted irradiance error spectra were provided by RAL that were used as additional pseudo-absorber. This inclusion did not change the results and were therefore omitted in the subsequent analysis.

Figure 5-16 shows the slant column errors for the CB model and NO_2 as a typical example for the error pattern. For NO_2 the slant column error remained below about 1% except for the source power error where maximum errors of about three percent were found. Particularly for NO_2 the errors are negligible in all cases when compared to a precision requirement of 10%. This is not the case for the other trace gases (see Table 5-4 to Table 5-7).

In general the defocused case provides slightly lower errors than the focused one. A Doppler shift in the irradiance leads to an increase of the error by about one magnitude. Without Doppler shift in the irradiance with respect to the backscatter data, all trace gases show negligible slant column errors in all correlation models. The Doppler shift can lead to errors in specific cases that are on the same order or higher than the precision requirement. In general the errors are largest with regard to the source power requirements. Stability of the order of 0.3% is required to meet the precision requirement of 0.5% and 3% for ozone in the UV and visible fitting window, respectively. For the other error types (source noise, source width, and source shift) requirements appear to be more relaxed than in the nominal case.

It is obvious that the uncorrelated case U show similar error pattern as the partially correlated case CB. Correlations between measurements while scanning individual pixels yield lower errors than in the case when they are random but correlate with other detector pixel. This is quite similar to the results for the ozone profile retrieval, which are discussed in Section 5.5. The error pattern does not vary with geo-temporal scenario (albedo and viewing geometry) in the majority of cases.
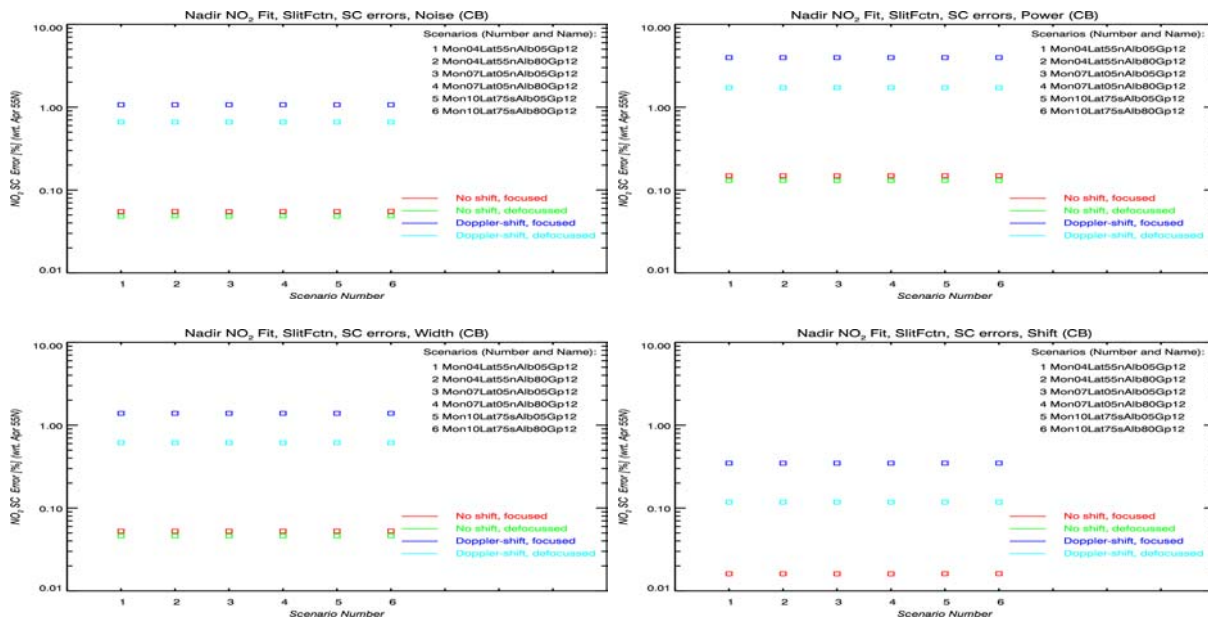
Figure 5-16: **NO_2 Slant column errors for CB error model**
From left to right and top to bottom: noise, power, shift, and width error in laboratory source for six geo-temporal scenarios and separated into four cases: focused, defocused and with and without Doppler shift. Percentage error was determined by referencing to April 55°N scenario.

O₃ UV	Focused		Defocused	
	Doppler	**No shift**	**Doppler**	**No shift**
U N	0.5	< 0.1	0.4	< 0.1
U P	1.7	0.2	1.0	0.2
U S	0.2	< 0.1	0.2	< 0.1
U W	0.6	< 0.1	0.3	< 0.1
C S	< 0.1	< 0.1	< 0.1	< 0.1
C W	< 0.1	< 0.1	< 0.1	< 0.1
CB N	0.4	0.1	0.4	0.1
CB P	1.0	0.1	1.0	0.1
CB S	< 0.1	< 0.1	< 0.1	< 0.1
CB W	0.4	< 0.1	0.3	< 0.1
CF S	< 0.1	< 0.1	< 0.1	< 0.1
CF W	< 0.1	< 0.1	< 0.1	< 0.1

Table 5-4: **O₃ UV slant column errors for the various error models**
O_3UV slant column errors for the various error models. As a precision requirement for ozone a 0.5% requirement was imposed. All errors exceeding these values are highlighted.

O₃ vis	Focused		Defocused	
	Doppler	**No shift**	**Doppler**	**No shift**
U N	3.0	0.1	3.0	0.1
U P	10.0	0.4	10.0	0.4
U S	1.0	< 0.1	0.6	< 0.1
U W	4.0	0.1	3.0	0.1
C S	0.5	< 0.1	0.2	< 0.1
C W	0.5	0.2	0.3	0.1
CB N	2.0	0.3	2.0	0.2
CB P	10.0	0.3	6.0	0.3
CB S	1.0	< 0.1	0.4	< 0.1
CB W	3.0	0.1	2.0	0.1
CF S	0.1	< 0.1	0.2	0.1
CF W	0.1	0.1	0.2	0.1

Table 5-5: **O₃ VIS slant column errors for the various error models**
O_3vis slant column errors for the various error models. As a precision requirement for ozone a 3% requirement was imposed. All errors equalling and exceeding this value are highlighted.

NO$_2$	Focused		Defocused	
	Doppler	No shift	Doppler	No shift
U N	1.0	< 0.1	1.0	< 0.1
U P	4.0	0.2	3.0	0.2
U S	0.4	< 0.1	0.2	< 0.1
U W	1.5	< 0.1	1.0	< 0.1
C S	0.2	< 0.1	< 0.1	< 0.1
C W	0.2	0.1	0.2	0.1
CB N	1.0	< 0.1	1.0	< 0.1
CB P	4.0	0.2	3.0	0.2
CB S	0.4	< 0.1	0.2	< 0.1
CB W	2.0	< 0.1	1.0	< 0.1
CF S	<0.1	< 0.1	< 0.1	< 0.1
CF W	<0.1	< 0.1	< 0.1	< 0.1

Table 5-6: **NO$_2$ slant column errors for the various error models**

NO$_2$ slant column errors for the various error models. As a precision requirement for NO$_2$ a 10% requirement was imposed. All errors equalling and exceeding this value are highlighted.

BrO	Focused		Defocused	
	Doppler	No shift	Doppler	No shift
U N	8.0	0.8	7.0	0.8
U P	30.0	3.0	20.0	2.0
U S	3.0	0.3	2.0	0.2
U W	10.0	0.9	7.0	0.7
C S	1.5	0.6	0.6	0.4
C W	0.4	< 0.1	< 0.1	< 0.1
CB N	10.0	0.8	8.0	0.7
CB P	40.0	3.0	25.0	2.0
CB S	3.0	0.3	2.0	0.1
CB W	15.0	1.0	9.0	0.8
CF S	0.3	< 0.1	0.2	< 0.1
CF W	0.3	< 0.1	0.1	< 0.1

Table 5-7: **BrO slant column errors for the various error models**

BrO slant column errors for the various error models. As a precision requirement for BrO a 20% requirement was imposed. All errors equalling and exceeding this value are highlighted.

5.8 WP2340: Definition of requirements for lab measurement of slit-function *(IUP)*

5.8.1 General

The main driver for the laboratory requirements of slit function drivers come from total ozone.

In Table 5-8 the worst-case scenarios from Table 5-4 to Table 5-7 are summarised for source error types and different correlation models separate for each trace gas. In the focused case the requirements for the monochromatic source are: SNR = 700, 0.3% stability in the power, 3% accuracy in the source width (0.0012 nm) and 1% knowledge of the centre wavelength (0.0004 nm). This only relaxes slightly in the defocused case with spot-size dimension derived from FM2.

The requirements are quite similar to the requirements defined from ozone profile retrieval. Nevertheless the requirements for the stability of the width of the monochromatic source are quite high (1%), when compared to 39% and higher for profiling. This is confirmed by looking at the error spectra and comparing them with the nominal noise pattern as shown in Figure 5-17. One should note here that only the misregistration between irradiance and radiances is responsible for enforcing such a high stability requirement. Without such a misregistration the requirements can be significantly relaxed (up to a factor of ten).

To sum up, an independent assessment of the slit function shape using a sub-pixel spectral resolution monochromatic source will benefit DOAS retrievals by:

➢ Reducing fit residuals by permitting proper convolution of high-resolution cross-section to instrument resolution

➢ Providing the possibility to verify undersampling correction schemes widely used in the DOAS community to GOME-1 data

Source error type O3UV/ O3Vis/ NO2/ BrO	Error correlation for slant column retrieval (%)			
	Uncorrelated (U)	Correlated during slit measurement (C)	Correlated between detector pixels (CB)	Fully correlated (CF)
Signal:Noise	700/ 700/ -/ -		560/ 465/ -/ 350	
Power	0.3/ 0.3 / 2.5 / 0.7		0.5/ 0.3/ 2.5/ 0.5	
Shift	5.0/ 3.0/ 25.0/ 6.7	5.0/ 6.0/ -/ 13	5.0/ 3.0/ 25/ -	5/ 15/ -/ -
Width	1.0/ 1.3/ 6.7/ 2.0	5.0/ 6.0/ -/ -	1.7/ 1.5/ 6.7/ 1.3	5/ 30/ -/ -

Table 5-8:   **Initial requirements on knowledge of the laboratory source (trace gas columns)**

Initial requirements on knowledge of the laboratory source for source width 0.04 nm for both defocused and focussed slit-function scenario. The numbers between slashes represents the four trace gas fitting windows for ozone, NO_2, and BrO, respectively. Highlighted numbers represent the worst-case scenario in each error model, while pink numbers indicate the overall requirement.
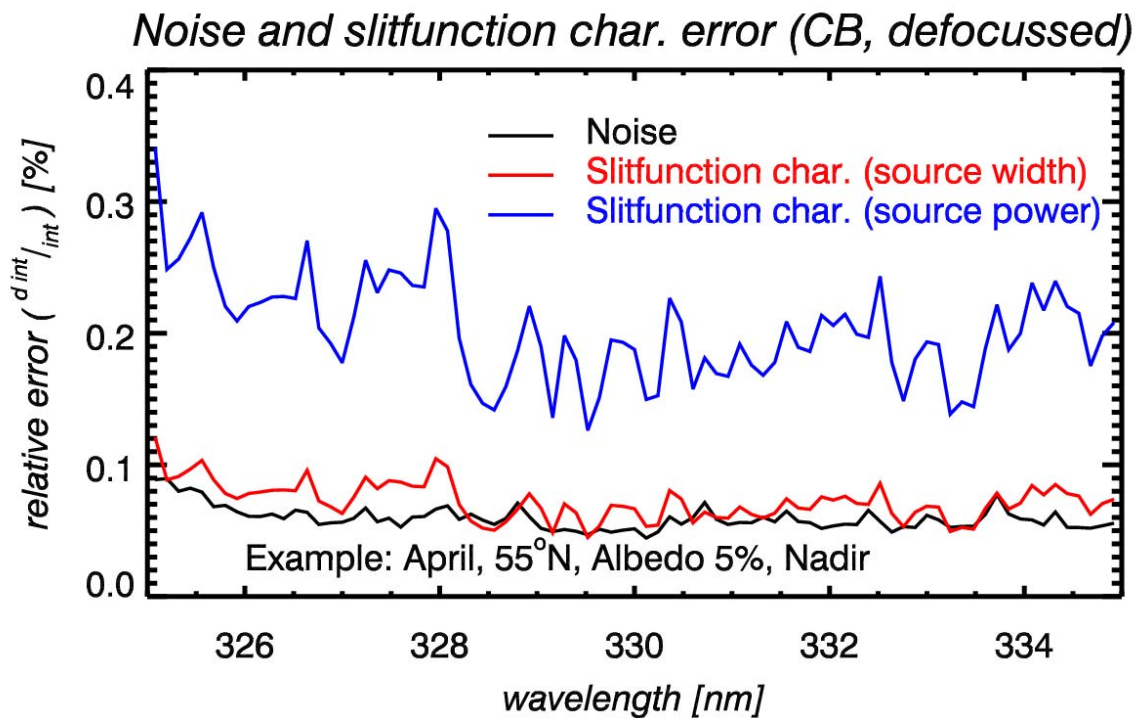
Figure 5-17   Error pattern for CB (defocused) compared to noise pattern for IT = 0.1875 sec

5.9   References

[Smor&Al]   Smorensburg, K, M. Dobber, E. Schenkeveld, R. Vink, H. Visser, Slitfunction measurement optical stimulus.

[Har&Al]   Haring, R.E., F.L. Williams U.G. Hartmann, D. Becker, G. Vanstone, H. Park, P.K. Bhartia, R.D. McPeters, G. Jaross, M. Kowalewski, Spectral Band Calibration of the Total Ozone Mapping Spectrometer (TOMS) Using a tuneable laser technique. Proc. SPIE 4135. pp421-31

[ChSp96]   Chance, K., and R. Spurr, Ring effect studies, GOME Geophysical Validation Campaign. Workshop Proceedings, ESA WPP-108, pp.69-74, 1996

[Kerr&Al]   Kerridge, B.J., R. Siddans, B.L. Latter, J.P. Burrows, M. Weber, R. De Beek, I. Aben and W. Hartman,   GOME-2 Error Assessment Study, Final Report EUMETSAT Contract No EUM/CO/01/901/DK, 2002.

[TPD]   MO-TN-TPD-GO0056i1 recent report of TPD on slit-function shape analysis

[OG]   Officine Galileo (OG) analysis MO-RP-GAL-GO-0006, iss.2

6 Task 2e: Reassessment of key instrumental errors

6.1 Introduction *(RAL)*

The GOME-2 FM1 Calibration Results Review (CRR) held in September (to which SRON, IUP and RAL all contributed, as external reviewers) concluded that further work was needed to understand and/or improve the quality of FM1 calibration data in several important respects, including:

➢ Wavelength Dependent (Absolute) BSDF

➢ Polarisation Response

Recommendations by the CRR Board in these respects were acted upon in the following months, and calibration results documentation was updated and made available to the consortium by EUMETSAT/ESA. This exercise to upgrade the FM1 and subsequently FM2 and FM3 calibration data was complemented by a scientific study on polarisation by SRON.

In this task, the assessment of "baseline instrumental errors" undertaken in the original study was updated with this improved information on errors likely to arise in GOME-2 Level-1 data (i.e. sun-normalised radiances) via wavelength dependent errors in (absolute) BSDF1 and the polarisation correction algorithm.

The work required was carried out under the headings of the following sub-tasks:

WP2410	Generation of Instrumental Error Signatures for Mapping	
	- Uncertainty in BSDF calibration	RAL
	- Uncertainty in polarisation correction algorithm	SRON
WP2420	Mapping of instrumental errors onto trace gas columns	IUP
WP2430	Mapping of instrumental errors onto ozone profile retrievals	RAL

For clarity, the work is described below in separate sections on BSDF calibration and polarisation correction, respectively.

6.2 Uncertainty in BSDF calibration

6.2.1 WP2410: Generation of BSDF error signatures *(RAL)*

The current uncertainty in knowledge of the GOME-2 BSDF was gauged from the discrepancy between the FEL and Sun simulator measurements reported by TPD for FM1 [TPD67], FM-2 [TPD85]. The FEL/Sun simulator ratio curves for FM1 and 2 were digitised by RAL from the respective reports and made available for linear mapping into ozone profile and trace-gas column retrievals. Subsequently, updated results for FM1-3 were made available by ESA, reported in [TPD64]. The curves are shown in Figure 6-1.

Deviation from 1 of the ratio of FEL/SUN simulator measurements of BSDF are considered errors in sun-normalised radiance and mapped into constituent retrieval.

---

1 "Absolute" wavelength-dependent errors in BSDF to be inferred from TPD's calibration measurements using the FEL lamp and the sun simulator (on GOME-2 and its calibration unit sub-assembly) should be distinguished from the "differential structures" associated with the Al and QVD diffusers to be addressed in Task 2a, which are an issue for DOAS retrieval of trace gas columns except ozone.
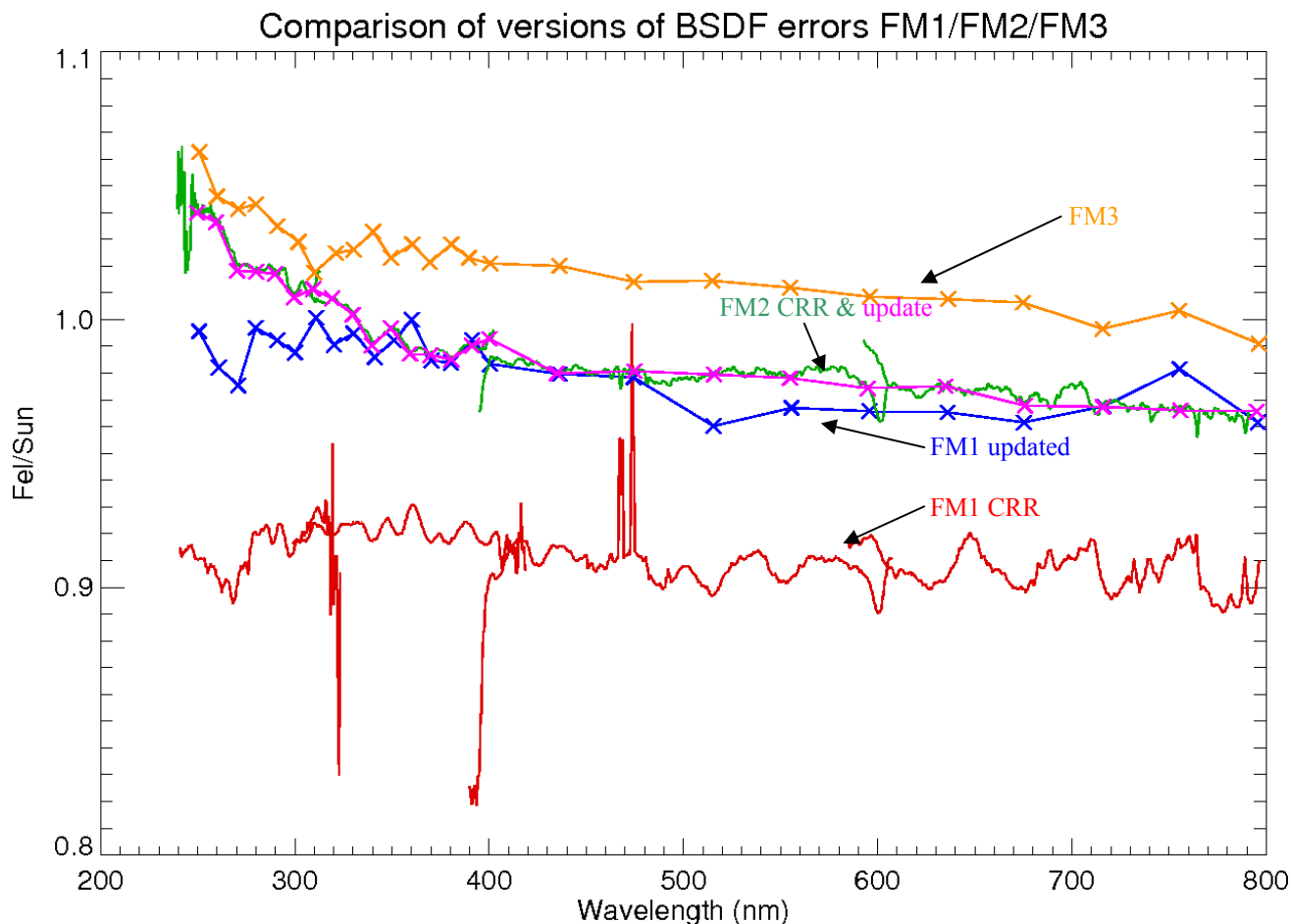
Figure 6-1: BSDF error spectra for FM1, FM2 and FM3

6.2.2   WP2420: Mapping of BSDF errors onto trace gas columns *(IUP)*

6.2.2.1   *Introduction*

The relative accuracy of the calibration of GOME-2 is important for DOAS retrieval as the trace gas absorption information is achieved using the differential structure of sun-normalized radiance.

In the calibration, instrumental polarisation features and the scattering characteristics of the scanner unit of the instrument (BSDF) have to be corrected. After calibration, any structure observed in the sun-normalized radiance has its origin in the atmosphere only, and not in the instrument. Fitting the remaining instrumental structures should yield zero slant columns after DOAS applications. The two instrumental errors mentioned and their consequences for DOAS trace gas slant column retrieval are under consideration in the following two sections.

The correction for polarisation is multiplicative with respect to radiance, and the correction for BSDF is multiplicative with respect to irradiance. These errors can be separated within the DOAS equation and have therefore been mapped into trace gas slant column space using direct DOAS fitting, e.g. see Appendix E of GOME-2 Error Study Final Report (Phase I to IV) [Kerr&Al].

The errors on atmospheric slant columns are driven by the correlation of the absorption cross-sections with the error pattern, and by the strength of the error pattern features compared to absorption features. The latter is a function of absorption cross-section and the number of molecules in the atmosphere. Errors are given with respect to a slant column of an atmospheric scenario used for the study.

6.2.2.2 Uncertainties in BSDF characterisation - propagation onto trace gas columns

The GOME-2 instrumental BSDF is determined using an absolute calibrated FEL lamp (BSDF_fel). Results are part of the instrument key data.

However, laboratory measurements of the BSDF have also been performed using a "sun-simulator" (BSDF_sun), which compared to the FEL lamp is a highly spatially uniform unpolarised light source [TPD85]. Ideally both measurements should yield the same results, in fact the ratio BSDF_fel/BSDF_sun should be 1.

In reality this is not the case as Figure 6-2 shows. Besides broad band deviations, a relatively strong differential structure can be seen. It is therefore expected that, after calibration of the GOME-2 solar irradiance using the BSDF key data, similar structures will remain in reflectance spectra to be used for DOAS trace gas column retrieval. Interferences of absorption cross-sections with this spectral error pattern lead to slant column errors.

To investigate the slant column errors, direct fittings of O_3 in the UV and VIS fitting windows, as well as BrO and NO_2, onto the error pattern have been performed as usual, using cross-section and Ring spectra as established for the study.

Figure 6-3 shows examples of spectral fittings in the BrO and NO_2 fitting windows. For both cases the residuals are of the same order of magnitude as the differential error pattern itself: the spectral response to the BSDF error is small. However, as BrO atmospheric contents are generally very tiny, the little response leads to a large relative error of –34.2%, which is much larger than the mean SNR error and is therefore significant. For NO_2 the observed error is – 4.2%, which is small compared to the mean SNR error (15%). For O_3, errors are significant in the UV and in the visible (0.3% and 5.7%, compared to 0.3% and 3% mean SNR error, respectively).

An overview of the obtained errors is given in Table 6.1.

	BrO	NO_2	O_3UV	O_3VIS
Reference [cm^{-2}]	9.097E+13	6.898E+15	2.235E+19	2.233E+19
Abs. Error [cm^{-2}]	-3.144E13	-2.805E14	6.150E+16	3.948E+18
Rel. Error [%]	-34.2	-4.1	0.3	5.7

Table 6.1: **Slant column retrieval errors due to expected solar cal inaccuracies**

Errors of slant column retrieval of BrO, NO_2 and O_3 due to expected solar calibration inaccuracies. Relative errors refer to April 55N nadir slant column.

6.2.3 WP2430: Mapping of BSDF errors for ozone profile retrievals *(RAL)*

A complete set of linearly mapped errors are included in Appendix D: "Residual polarisation error signatures (overview)" and Appendix E: "Residual polarisation error signatures (overview)". See CD-ROM "GOME- 2 Error Assessment Study – Phase V: Final Report and Supporting Documents".

A complete set of results is given in Appendix F: "Mapping of residual polarisation errors". See also CD-ROM "GOME- 2 Error Assessment Study – Phase V: Final Report and Supporting Documents".

In this report, typical results of mapping are shown in Figure 6-17. These are for the "jul_05n" geo-temporal scenario.
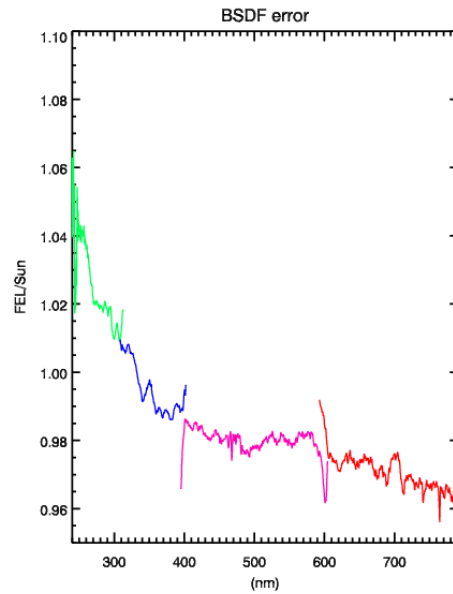
Figure 6-2: **Ratio of GOME-2 BSDF spectra – FEL lamp / Sun-simulator**

Ratio of two GOME-2 BSDF spectra determined using an FEL lamp and a Sun-simulator as light sources (data provided by RAL).
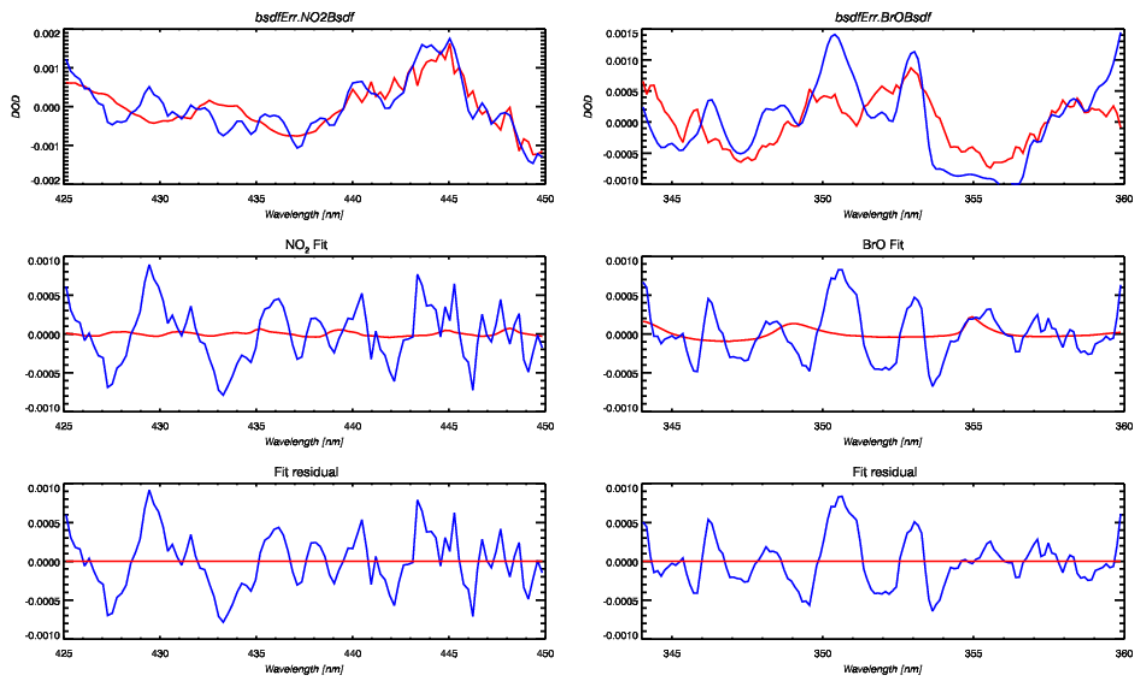
Figure 6-3: **NO₂ and BrO fittings onto FEL/Sun-Simulation BSDF error pattern**

Results for NO_2 and BrO fittings onto FEL/Sun-Simulation BSDF error pattern

Blue lines: Differential error pattern, NO_2 fit + fit residual, fit residual, respectively
Red lines: Refer to fitted cross-sections

Panels annotated '-V1' plots correspond to the errors from the CRR documents, while `-V2' correspond to the updated analyses, which are considered more realistic. The contributions due mapping errors only in Band 1a are also shown, indicated by '-B1A'. For FM1, BSDF errors in Band 1a cause oscillatory ozone errors in the mid to upper stratosphere with a peak of around 15%. This is possibly due to the step-change in the signature around 270 - 280 nm. For FM2 and FM3 the errors produce a systematic negative bias in the mid to upper stratosphere of up to 10%. The '-V2' data generally show reduced, but still significant, errors in the middle stratosphere.

For FM1, including errors in Band 2b results in large lower stratospheric and tropospheric errors which exceed the ESD (> 60% in some cases, e.g. jul_55n). For FM2 and FM3 errors at low altitude are smaller, although a bias of up to 15% is seen. The sign of the bias is not consistent between FM2 and FM3. It should be noted that error estimates are based on the assumption that the Fel/Sun ratio approximates the error on BSDF calibration. It may be the case though, that one or other measurement is more reliable than this estimate would suggest (though this is not currently known to be the case), or that there are additional errors common to both measurements.

Subject to the above caveat, it is considered that BSDF errors in Band 1 are likely to be realistically estimated by the method implemented here. However, the impact on the retrieval due to errors in Band 2 is much more sensitive to any fine-scale wavelength variations in the error signature mapped. The V1 signatures (digitised from the CRR reports) show marked fine-scale structure in Band 2 leading to significant retrieval error, whereas the V2 signatures were only analysed at a relatively coarse spectral sampling (indicated by the X symbols in Figure 6-1).

It is not clear to what extent the fine-structure evident is representative of genuine errors in the BSDF calibration or simply noise or other error in the analysis. The piece-wise linear representation of the V2 spectra is certainly unrealistic in that a step-change in the gradient of the signature occurs within the range of Band 2 used in the retrieval (315 - 334.6 nm). If the error spectra within Band 2 were smooth (i.e. could be described by a 5th order polynomial within this range) then negligible additional errors would be expected from the inclusion of Band 2 (with this ozone profile retrieval scheme). Results including the impact of BSDF errors in Band 2 are therefore not considered realistic, only indicative of the importance BSDF knowledge at fine spectral scales (or clear a priori knowledge of the smoothness of the BSDF). If fine scale structure at an amplitude comparable to that shown in the CRR analysis should really pertain to the accuracy of the Level 1 data, then errors on ozone after propagation through Band 2, or on a trace-gas column retrieval, could well be larger than any case shown here, since the spectral structure associated with the deviation between the true BSDF and the measurements could be more correlated with the trace-gas differential absorption spectrum.

6.2.4   Conclusions

Errors on ozone profile retrieval due to BSDF errors in Band 1 can be comparable to the ESD, but will be manifest as biases. It can therefore be clearly recommended that the BSDF of FM1 be better characterised, either through improved analysis of existing measurements or by additional measurements.

It also be desirable to improve characterisation of FM2 and FM3 in this spectral range, since the biases which are close to ~ 10% in the mid-upper stratosphere are significant compared to the RSS component of the base-line error budget, see Section 7: Task 3 "Optimal Error setting and error mitigation".

The propagation of errors in the other bands leads to significant errors in ozone profile and column BrO and ozone. These errors are driven by the nature of fine spectral structure in the BSDF error, but it is not clear to what extent the structure evident in the CRR analysis is representative of errors which would be applicable to calibrated Level 1 data. If it cannot be argued that such structure can be assumed to be an artefact of one or both measurement techniques, then it is clearly necessary to better characterise the BSDF at fine spectral scales in Band 2b (for ozone profile retrieval) and other spectral ranges used for trace-gas column analysis.
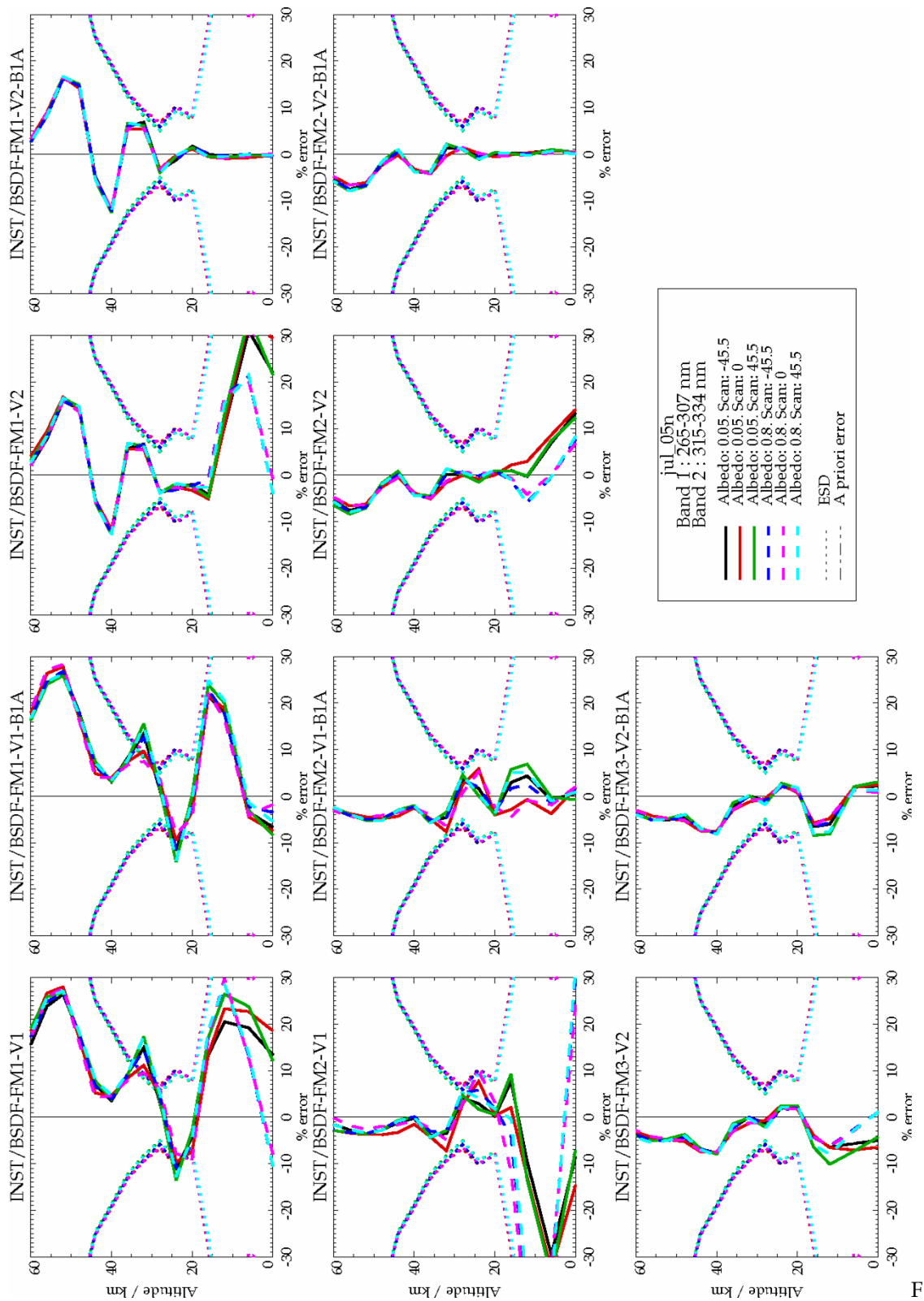
gure 6-4:   BSDF linearly mapped errors FM1-3

6.3   Imperfect polarisation correction

6.3.1   WP2410: Generation of error signatures *(SRON)*

Spectral signatures of residual error due to an imperfect polarisation correction algorithm were calculated and supplied by SRON.   Section 4.2: "Generation of Spatially Aliases Signatures in PMD Channels" gives details of the methodology of the generation and of these signatures.

A complete set of figures, which show the range of spectra calculated, are found in Appendix B: "Spectra for residual polarisation errors". See CD-ROM "GOME-2 Error Assessment Study – Phase V: Final Report and Supporting Documents".

Spatial aliasing is not included in the model calculations in these spectra. This is done by setting the time variable A(t) to zero in the equations on Page 4-3. The aliasing synchronisation step is then removed, and it is also excluded from the polarisation correction algorithm.

6.3.2   WP2420: Residual polarisation structures - propagation onto trace gas columns *(IUP)*

The error spectra for the 72 geo-temporal atmospheric cases (24 scenarios each, for east, west and nadir viewing geometries) have been investigated. The derivation of error signatures is described in more details in Section 6.3.3.

In Figure 6-5 some examples of error spectra are shown for the ozone UV fitting window. The red curves show the estimated effect on GOME-1, and the blue curves shows the estimated effect on GOME-2. In some cases the error spectra for GOME-2 appear noisier than for GOME-1. This is most likely due to singularities in the Q/I Stokes ratio. The fitting residuals for the error spectra shown in Figure 6-5, are depicted in Figure 6-6.

Figure 6-7, Figure 6-8 and Figure 6-9 show the ozone column errors of scenarios for GOME-1, GOME-2 V2 polarisation correction, and for a high PMD readout rate (hypothetical case).

For GOME-1 the errors are generally below 0.5%, which is of the same magnitude as the baseline error. For GOME-2 the errors can reach up to 1%, and are significant. There is no improvement for ozone column retrieval to be expected from the high PMD read-out rate, the latter probably affecting more strongly the overlap region between single-scatter point and 320 nm, well outside the UV fitting window.
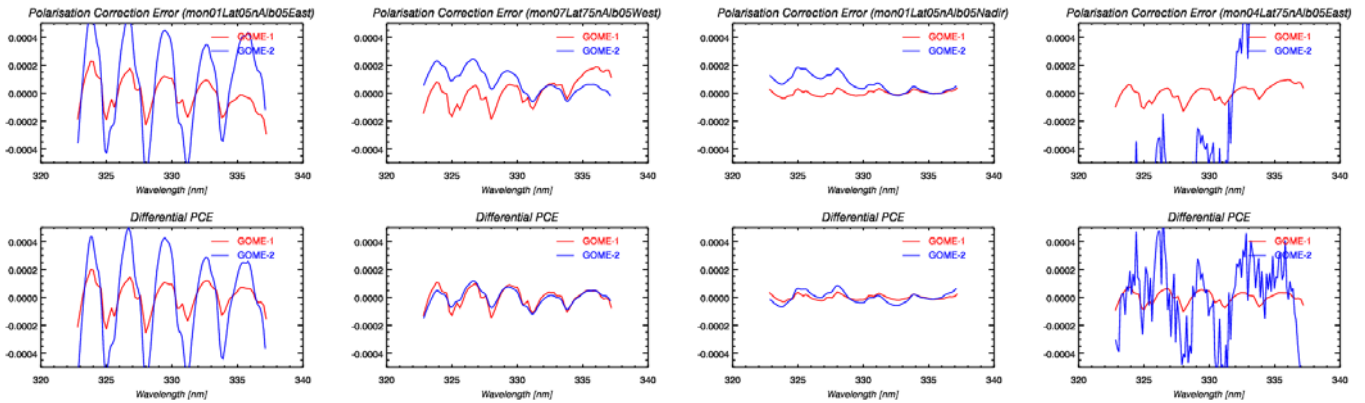
Figure 6-5: **Radiance errors and differential spectrum due to polarisation correction errors**

Relative radiance errors (top) and their differential spectrum (bottom) due to polarisation correction errors for GOME-2 estimated on the basis of GOME-1 (red curves, used for previous study, see Final Report for Ph I - IV) and for the data set updated for Phase V (radiance errors assumed to be relative without unit). As examples, four of the 72 scenarios considered are shown.
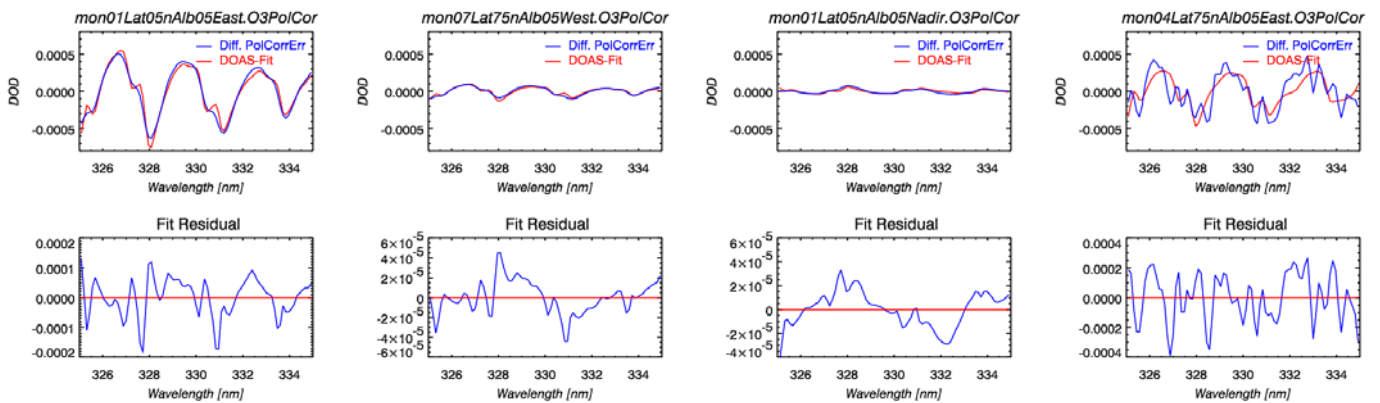
Figure 6-6: **Differential error patterns and fits and their differences (O₃)**

Differential error patterns and fits (top) as well as their differences (fit residuals, bottom) for the examples shown in Figure 6-5.
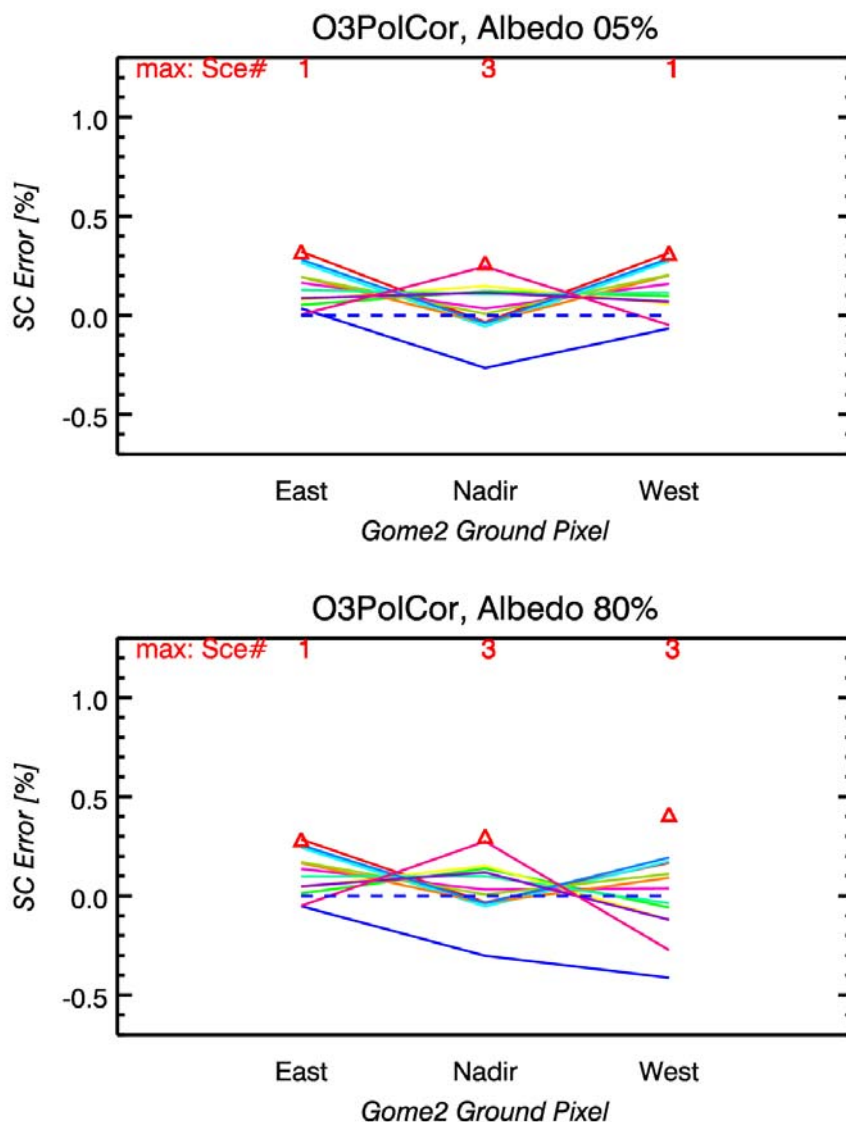
Figure 6-7: **GOME-1: O$_3$ slant column errors due to polarisation correction residuals**

O$_3$ slant column errors due to polarisation correction residuals for albedos 5% (top) and 80% (bottom). Each colour belongs to a single study scenario.

The scenario number (1-24) producing the largest error is shown at the top for each viewing direction.

Scenarios: jan_05n (1, red), oct_75s (3, blue), apr_05n (4, cyan), and oct_75n (12, pink).

See details on geotemporal scenarios in Table 2-1.
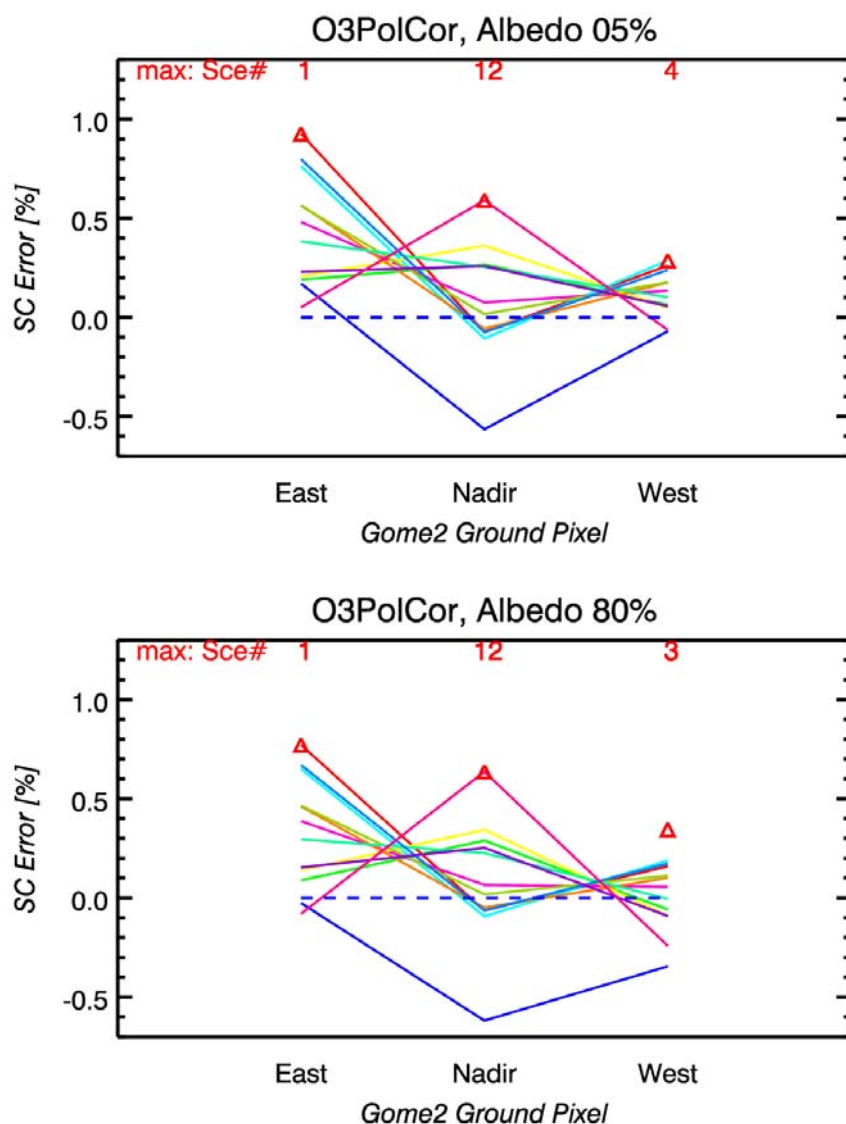
Figure 6-8   **GOME-2 V2:   O$_3$ slant column errors due to polarisation correction residuals**

O$_3$ slant column errors due to polarisation correction residuals for albedos 5% (top) and 80% (bottom). Each colour belongs to a single study scenario.

The scenario number (1-24) producing the largest error is shown at the top for each viewing direction.

Scenarios: jan_05n (1, red), oct_75s (3, blue), apr_05n (4, cyan), and oct_75n (12, pink).

See details on geotemporal scenarios in Table 2-1.
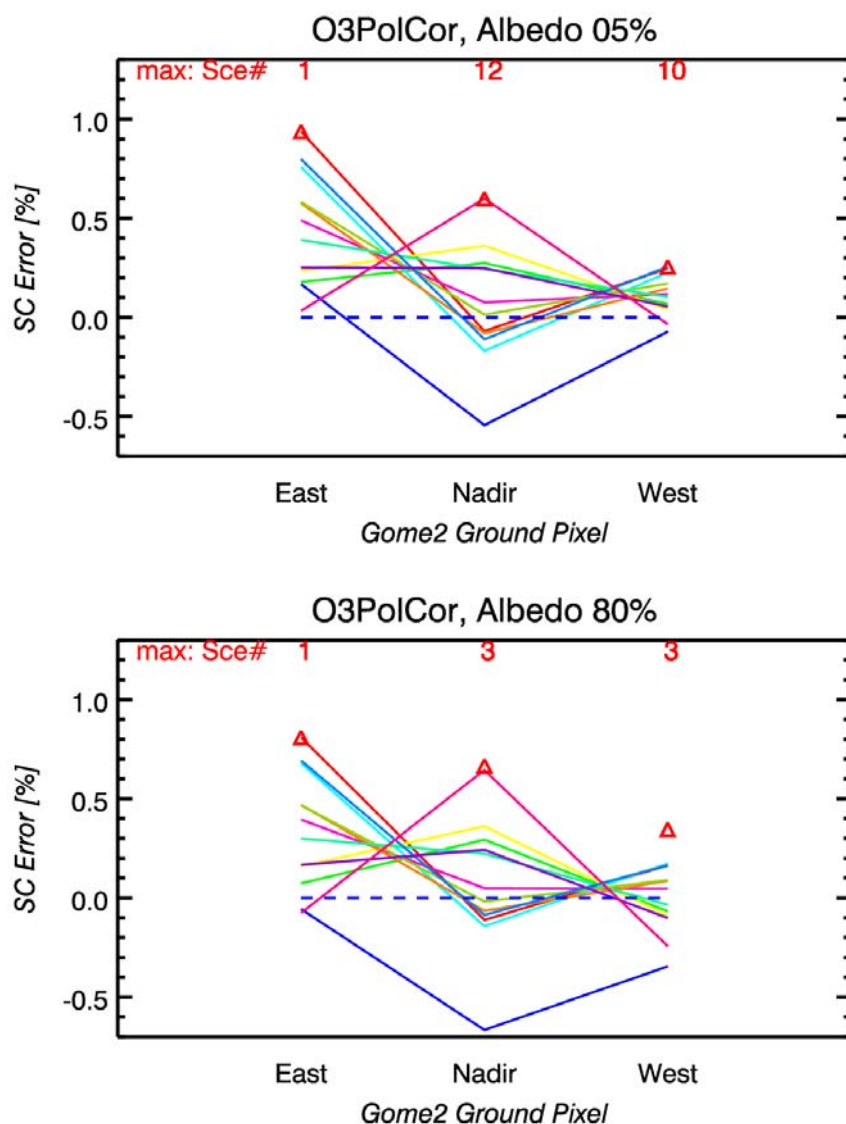
Figure 6-9: **GOME-2:** **O$_3$ slant column errors due to polarisation correction residuals by assuming a high PMD read-out rate**

O$_3$ slant column errors due to polarisation correction residuals for albedos 5% (top) and 80% (bottom). Each colour belongs to a single study scenario.

The scenario number (1-24) producing the largest error is shown at the top for each viewing direction.

Scenarios: jan_05n (1, red), oct_75s (3, blue), apr_05n (4, cyan), and oct_75n (12, pink).

See details on geotemporal scenarios in Table 2-1.

6.3.3 WP2430: Mapping of instrumental errors onto ozone profile retrievals *(RAL)*

6.3.3.1 *Error signatures in the spectral ranges of importance for ozone profile retrieval*

Error spectra for the east/nadir/west view for several measurement scenarios were made available by SRON:

> **GOME-2 "component" analysis**
> As used in the main study, an analysis based on information on a component level
>
> **GOME-1**
> An approximate estimate of GOME-1 errors for nadir geometry only, as used in the main-study
>
> **FM2**
> Updated error signatures based on CRR documentation and assuming the nominal polarisation correction algorithm
>
> **FM2-high-rate PMD readout**
> As FM2 but assuming signals from all detectors in the PMD array can be used in the correction algorithm (as opposed to the 12 "bands", formed by on-board averaging and down-link, used in the nominal scheme due to data rate limitations).

The error spectra in the wavelength range of significance for ozone profile retrieval are illustrated for all geo-temporal scenarios in the Appendix D: "Task 2e: Residual polarisation error". An example is shown in Figure 6-10.
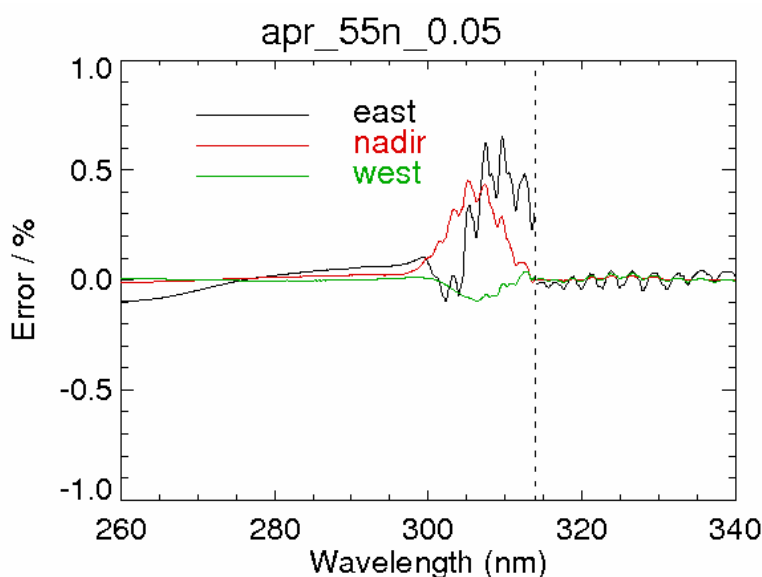
Figure 6-10   **Polarisation error signature (FM2 nominal case; apr_55n)**

The relatively large Band 1 errors at wavelengths just above 300 nm are due to interpolation between the theoretical single scattering value at ~ 300 nm and the first PMD measurement, in combination with the instrument polarisation sensitivity. Because the lowest wavelength PMD is ~ 350 nm for GOME-1, the interpolation is of relatively poor quality, causing a broad error signature in Band 1 which is often > 1% (the fitting precision in this range exploited for ozone profile retrieval). For GOME-2, the lowest analogous wavelength is ~ 311 nm, and therefore much closer to 300 nm, so the interpolation error in Band 1 is comparatively small, even though the polarisation sensitivity of GOME-2 is larger than GOME-1 at the longest wavelengths of Band 1 (eta > 2, slightly worse than for GOME-1, which was not predicted by combining component-level polarisation responses for which eta ~ 1.5).
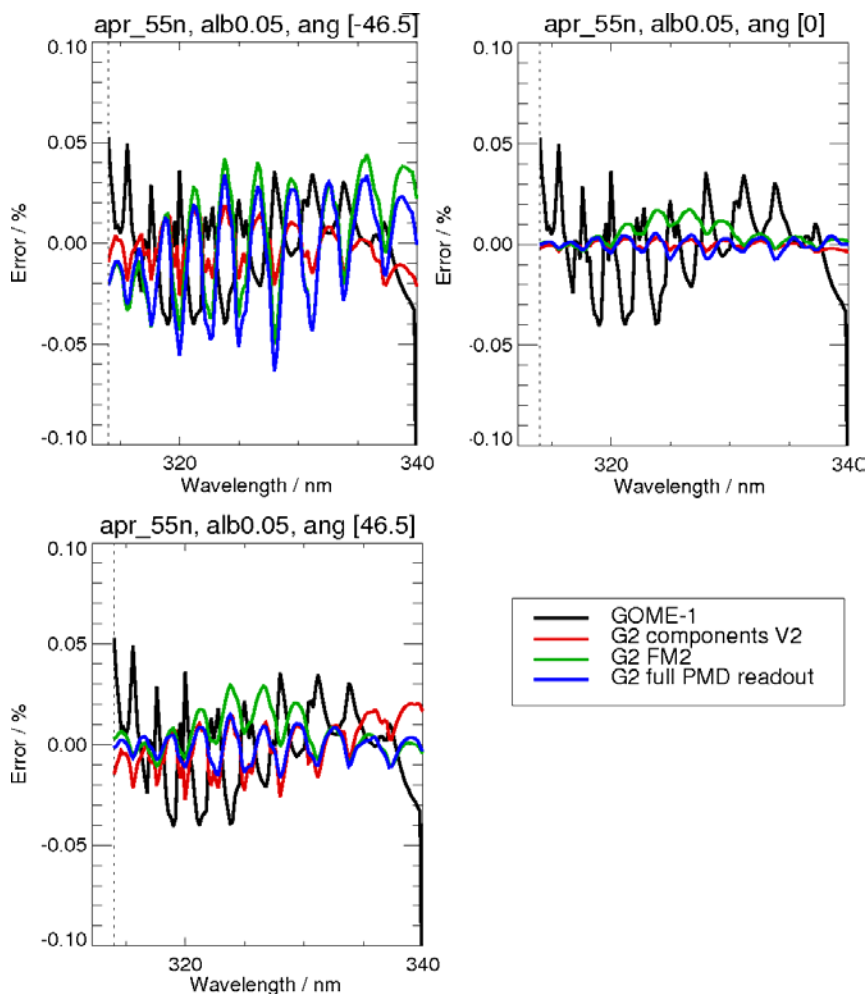
Figure 6-11   Polarisation errors - Band 2b (various)

In Band 2, the error signatures have fine-scale spectral structure in the wavelength region of the Huggins bands used for O_3 profile retrieval. Although the amplitude of this fine-scale structure is small in comparison to the broad-scale structure affecting Band 1 particularly, it can potentially have a much larger impact on O_3 profile retrievals because:

  ➢   Sun-normalised radiance spectra have to be fitted to much higher precision in Band 2 (< 0.1% c.f. 1% RMS) to retrieve useful information on O_3 in the troposphere and lower stratosphere

  ➢   Structure in the error signatures is highly correlated with (in fact determined by) the Huggins bands themselves

This structure is not significantly reduced even in the FM2 high-readout case because the resolution of the PMDs in this region is of order 4 nm. Huggins bands related structure cannot therefore be captured by the PMDs.

As noted under Task 2b, that specific problems occur in the implemented polarisation correction algorithm when the ratio of Stokes parameters Q:I is close to zero. An estimate of this ratio, under the assumption of pure Rayleigh single scattering, can be calculated purely from the view/solar geometry:

$$Q:I = (1-c^2)/(1.0657+c^2) \cdot (b^2-a^2)/(a^2+b_2)$$

Where the first ratio on the RHS is the degree of linear polarisation and the second is associated with the rotation of coordinate frame from the scattering plane,

and:

$a = \cos(\theta_0) \sin(\theta) - \cos(\theta) \sin(\theta_0) \cos(\phi)$

$b = -\sin(\theta_0) \sin(\phi)$

$c = -\cos(\theta) \cos(\theta_0) - \sin(\theta) \sin(\theta_0) \cos(\phi)$ i.e. the cosine of the scattering angle

θ = line-of-sight zenith angle

θ_0 = solar zenith angle

ϕ = relative azimuth angle

Q:I is plotted for both METOP /GOME-2 and ERS-2/GOME in Figure 6-12. The cosine of the scattering angle c is also plotted in Figure 6-13.

Note:

> The ratio reaches low absolute values in an extended area in the tropics due to the first term in the equation above (solar/view geometry close to perfect back-scatter)

> Over most of the orbit Q:I varies from positive to negative across the swath due to the second term, leaving a narrow strip of low Q:I along-track. At least one pixel across-track is therefore likely to be affected

> The impact will presumably be largest for small pixel sizes. It is noted that no averaging over the GOME-2 pixel size is simulated either in this plot, or in generating the error signatures. The impact near the low Q:I condition may be over or underestimated because of this approximation

> Of the geo-temporal / view scenarios used in this study, Apr_05n West pixel, Apr_75n East and Oct_55n East are clearly affected by low Q:I. This situation is reflected in quasi-noise structure in the polarisation correction error signatures, originating from patterns in the key-data.

> It is expected that algorithmic changes could be implemented to mitigate error signatures associated with low Q:I. These cases will therefore not to be considered in drawing conclusions relating to the limiting performance of GOME-2 with respect to polarisation correction errors

6.3.3.2   Linear mapping results

Error signatures have been linearly mapped in the same way as the original study and are shown in full in Appendix F. See CD-ROM "GOME-2 Error Assessment Study – Phase V: Final Report and Supporting Documents".

The standard wavelength ranges adopted in original study were again used here (Band 1: 265 - 307 nm, Band 2: 315 - 334.6 nm).

Original errors (GOME-2 components and GOME-1 cases), as estimated in Phase I to IV of this study, are shown in

Figure 6-14 for an 0.05 albedo.

New results for GOME-2 FM2 (with/without full read-out), as estimated in Phase V of this study, are illustrated for the two albedo cases in Figure 6-15 and Figure 6-16. Cases with low Q:I are indicated by the asterisk plot symbols.

The following points are noted:

❑ In the main-study simulations errors for GOME-2 were almost always better than GOME-1 and always less than 20% (in almost all cases < 10%).

❑ The new more reliable simulations for GOME-2 indicate that errors can be much larger than previously simulated for GOME-1 or GOME-2, particularly for Eastward pixels. In some cases, notably the East pixels of apr_05n and oct_05n, errors are unacceptably high in the troposphere.

❑ It was originally expected that the largest errors would be introduced in the Band 1 region due to the interpolation from the theoretical point. However, the mapped errors show that, for GOME-2 FM2, the largest contributions are from Band 2. This is driven by the unexpectedly large amplitude in some cases (notably extreme East pixels) of fine-structure in the error signatures which is correlated with the Huggins bands. In certain cases errors are worse than previously simulated for GOME-1.

These errors are surprisingly large given experience of real retrievals from GOME-1, though errors may genuinely be worse for GOME-2 since:

o Due to the wider swath and earlier ascending node crossing time GOME-2 views much closer to 90° scattering angle at the east of the 1920 km swath than GOME-1, with a 960 km swath (see Figure 6-13).

o Although more PMD channels are available for the correction scheme, GOME-2 does not improve upon GOME-2 in capturing polarisation structure in the Huggins bands because the resolution of the PMDs is too poor.

o Errors due to low Q:I ratio are generally large but not as significant as those driven by large amplitude Huggins structure.

6.3.4   Conclusions

It is suggested that further work be carried out with respect to residual polarisation errors, because these typically cause significant error in total column error and profile errors of 10's % in some cases. At present, errors in the extreme East view are unacceptable for ozone profile retrieval. These large errors are caused by Huggins structure in the residual polarisation error which cannot be corrected with the current scheme, even if all PMD pixels were to be available and used in the correction. This is a consequence of the low spectral resolution of the PMDs in the Huggins range. Possible approaches to mitigate these errors are:

Improve the spectral resolution of the PMDs in the Huggins bands by at least a factor of 2. A resolution of order 1 nm (c.f. PMD pixel sampling in this region of 0.7 nm) would be expected to largely remove these errors. If better resolution could be accomplished by preferentially focusing the PMDs in this spectral range then this should certainly be considered.

Reducing the GOME-2 swath-width or shifting the swath to the West might minimise the occurrence of the largest errors. Further work would be required to model full across-track dependence of this error. It is noted that errors due to the pseudo-spherical radiative transfer approximation were found, in the main study, to be significant in West pixels of the 1920 km swath leading to a suggestion that the swath be shifted Eastward. The pseudo-spherical error could, however, also be mitigated by feasible improvements in radiative transfer modelling (CDI rather than CDI-PI would be acceptable).

A significantly more complicated polarisation correction scheme might be envisaged which would make use of *a priori* knowledge of the ozone profile (possibly including a total column retrieval) to model the wavelength dependence of the polarised radiation at finer scales than captured by the PMDs. It would require significant further work to assess whether or not such an approach might be successful or feasible.

Low Q:I ratio occurs in at least 1 across-track ground pixel throughout most of the orbit. It is important to implement a polarisation correction algorithm which can cope with this specific case.
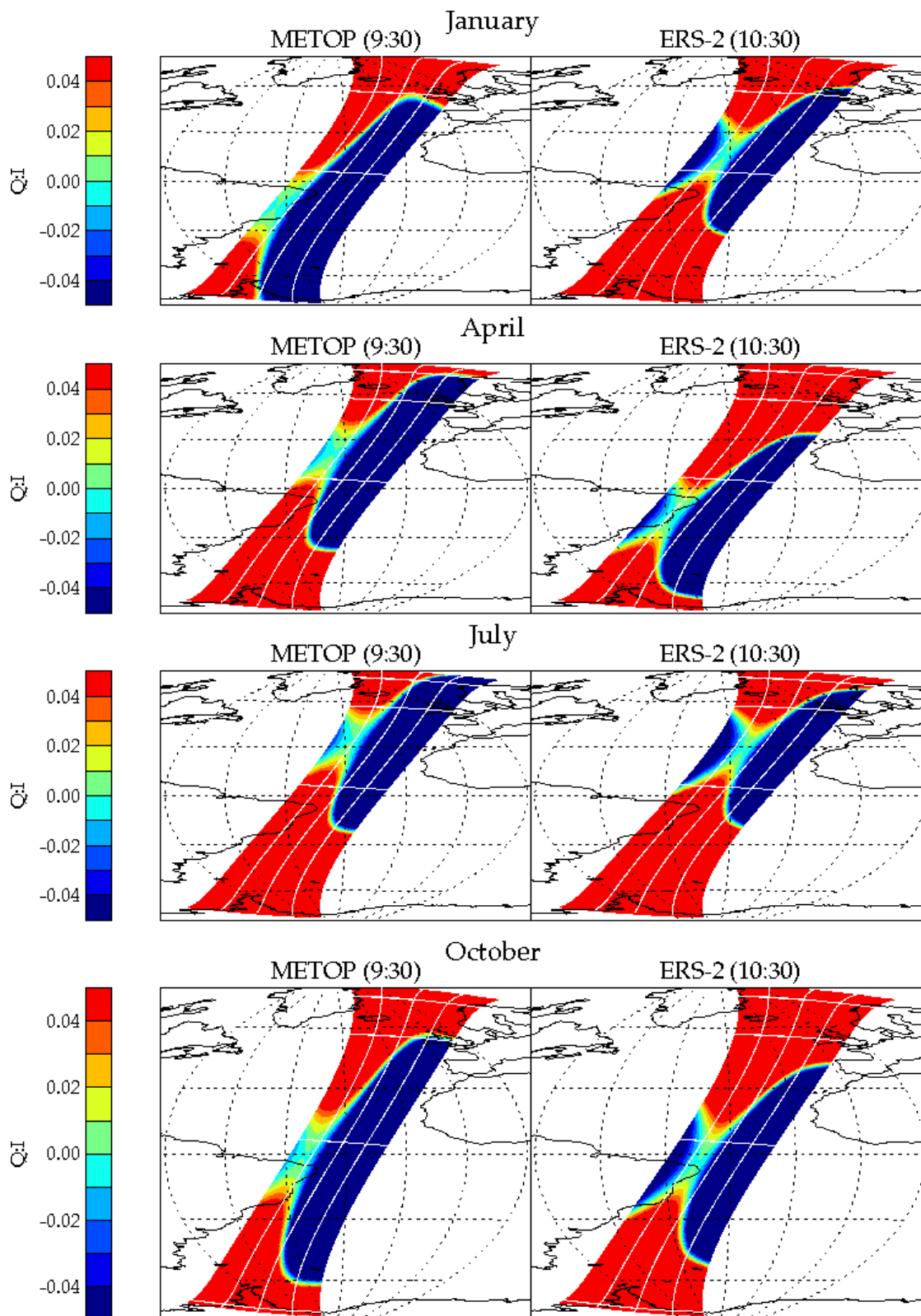
Figure 6-12:   **Polarisation ratio Q:I for METOP and ERS-2**

White lines along the orbit track indicate the nadir and 960km (i.e. actual GOME-1) swath extent. White lines across-track indicate the locations of the standard geo-temporal scenarios.
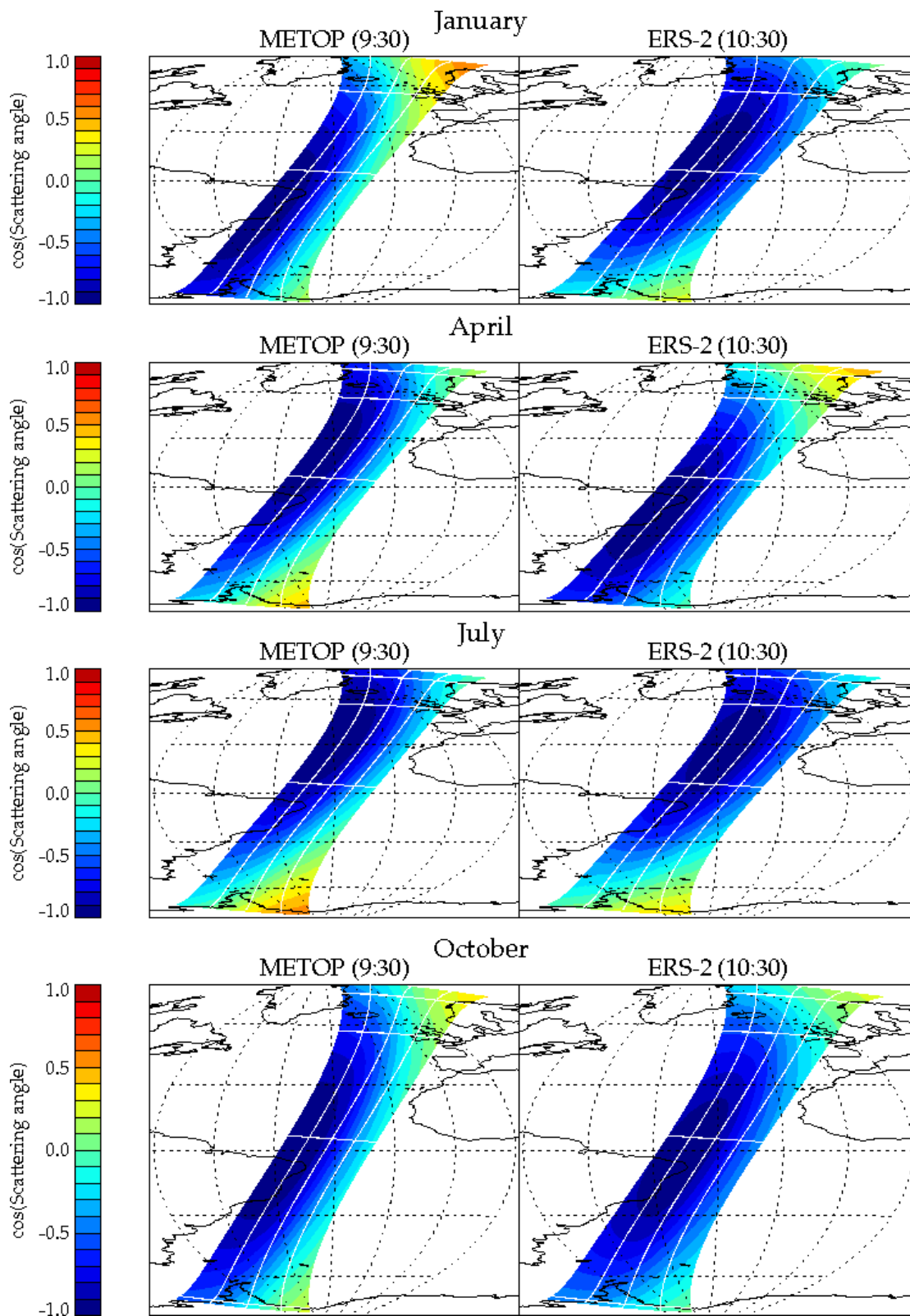
Figure 6-13:   Cosine of the scattering angle for METOP and ERS-2

White lines along the orbit track indicate the nadir and 960km (i.e. actual GOME-1) swath extent. White lines across-track indicate the locations of the standard geo-temporal scenarios.
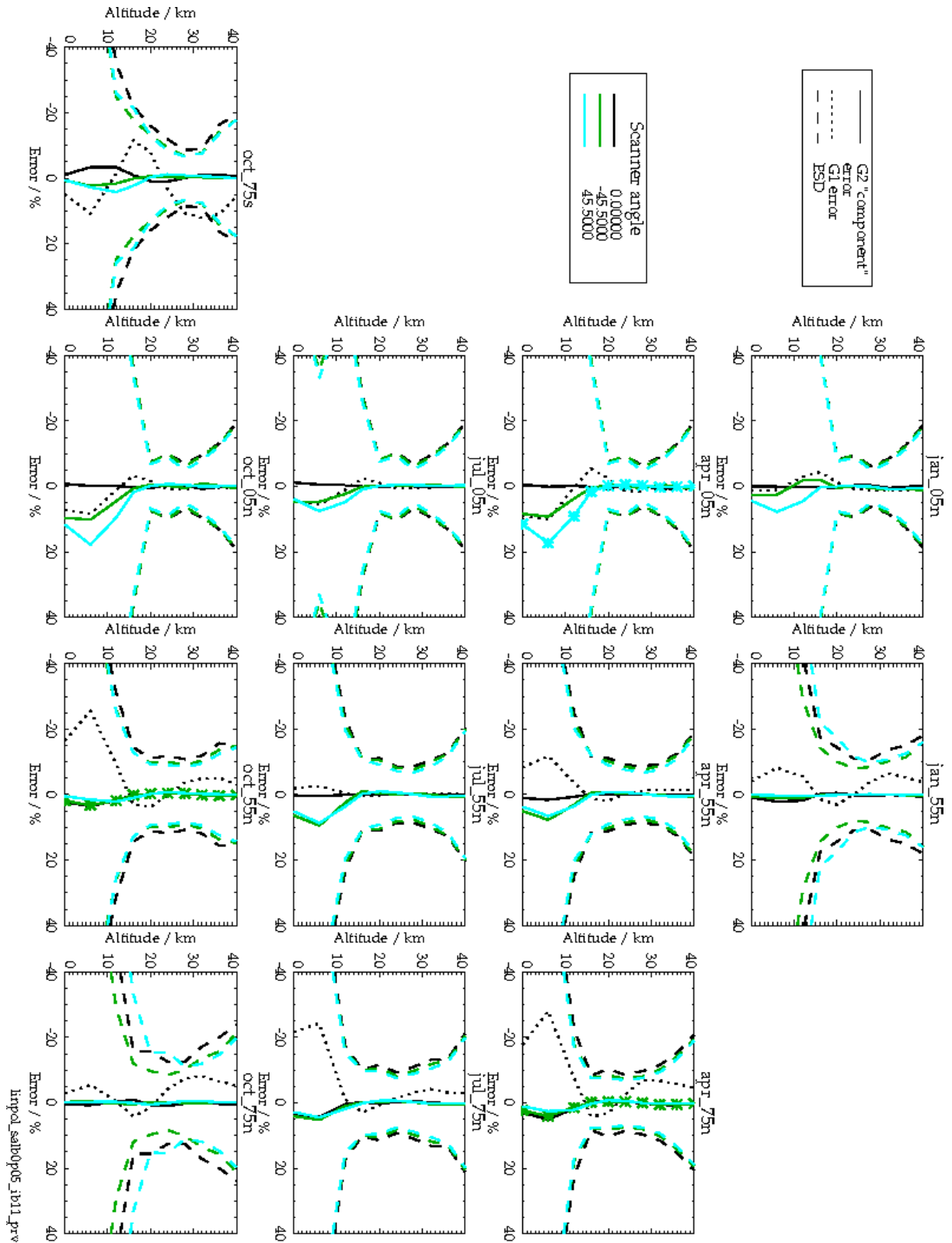
Figure 6-14:   **Polarisation correction errors for GOME-1 and GOME-2 - Albedo 0.05 case**

Main study polarisation correction errors for GOME-1 and GOME-2 "components"

Albedo 0.05 case   -   Low Q:I cases indicated by asterisk plot symbols.

Task 2e: Reassessment of key instrumental errors
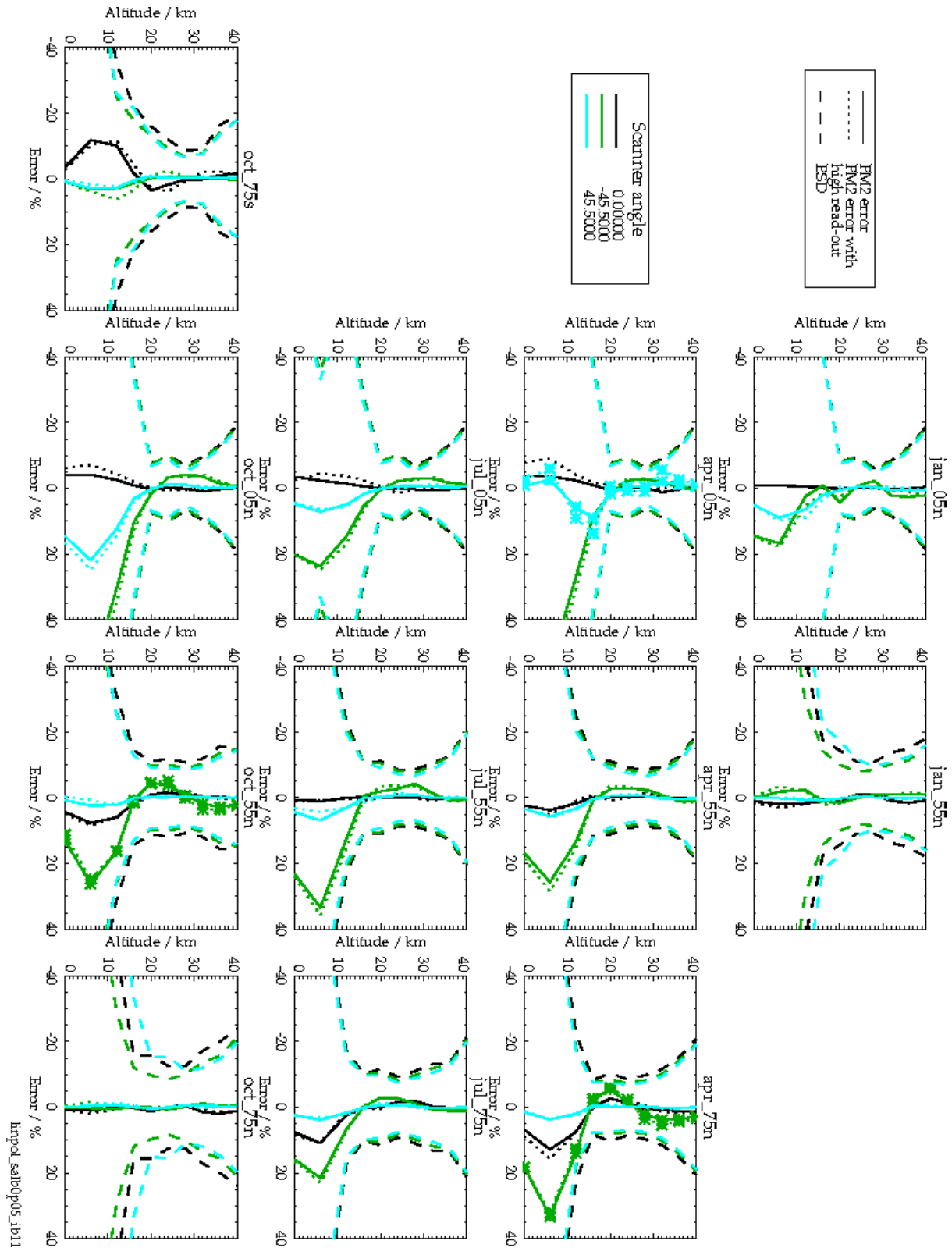
Figure 6-15: **New polarisation correction results for GOME-2 FM2**

With / without full PMD read-out   - Albedo 0.05

Low Q:I cases indicated by asterisk plot symbols.
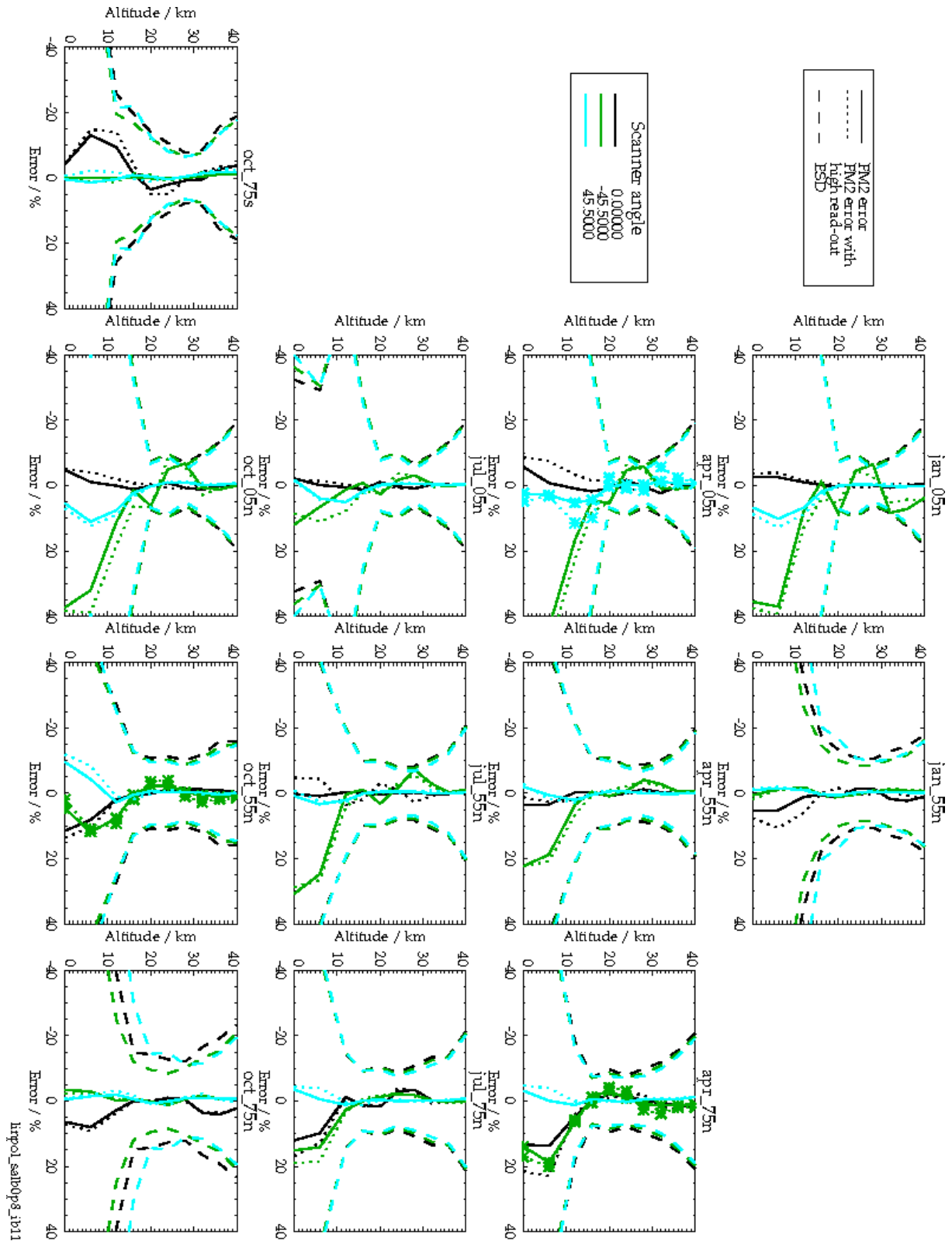
Figure 6-16: **New polarisation correction results for GOME-2 FM2**

With/without full PMD read-out - Albedo 0.8

Low Q:I cases indicated by asterisk plot symbols
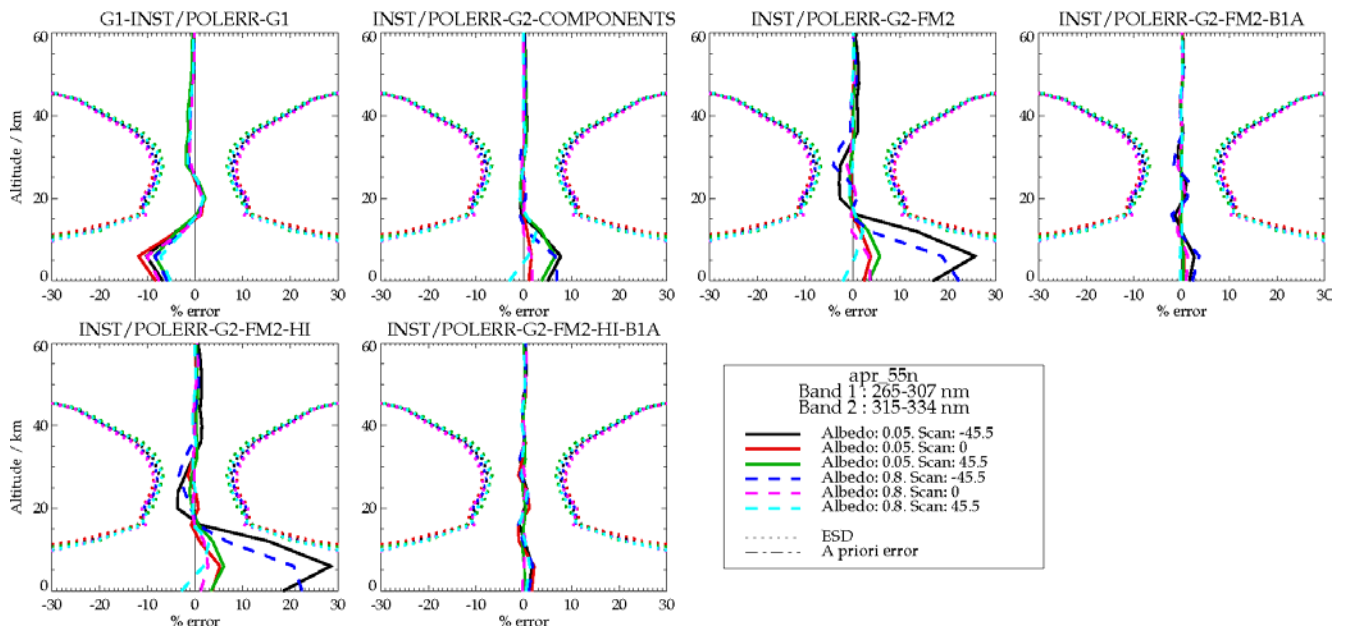
Figure 6-17:   **Polarisation corrections errors - including separation of impact from B1**

Linearly mapped polarisation corrections errors example

Including separation of impact from B1

6.4   References

[Smor&Al]   Smorensburg, K, M. Dobber, E. Schenkeveld, R. Vink, H. Visser, Slitfunction measurement optical stimulus.

[Har&Al]   Haring, R.E., F.L. Williams U.G. Hartmann, D. Becker, G. Vanstone, H. Park, P.K. Bhartia, R.D. McPeters, G. Jaross, M. Kowalewski, Spectral Band Calibration of the Total Ozone Mapping Spectrometer (TOMS) Using a tuneable laser technique. Proc. SPIE 4135. pp421-31

[ChSp96]   Chance, K., and R. Spurr, Ring effect studies, GOME Geophysical Validation Campaign. Workshop Proceedings, ESA WPP-108, pp.69-74, 1996

[Kerr&Al]   Kerridge, B.J., R. Siddans, B.L. Latter, J.P. Burrows, M. Weber, R. De Beek, I. Aben and W. Hartman,   GOME-2 Error Assessment Study, Final Report EUMETSAT Contract No EUM/CO/01/901/DK, 2002.

[TPD56]   MO-TN-TPD-GO0056i1 recent report of TPD on slit-function shape analysis

[TPD64]   MO-TN-TPD-GO-0064i1

[TPD67]   MO-TR-TPD-GO-0067i1

[TPD85]   MO-TR-TPD-GO-0085i1

[OG]   Officine Galileo (OG) analysis MO-RP-GAL-GO-0006, iss.2

7   Task 3: Optimal operational settings and error mitigation

7.1   Introduction

In this Task, error budgets for trace gas columns and ozone profiles which had been compiled in the main study (Phases I – IV) were reviewed in light of the new findings from Task 2 of the study extension (Phase V) Recommendations for optimal operational settings and error mitigation strategies were also compiled.

New error budgets for trace gas columns and ozone profiles are presented in Sections 7.2 and 7.3, respectively. The recommendations arising from Phase V are set out in Section 7.4 and the original recommendations from Phases I – IV are reviewed in Section 7.5.

7.2   Updated error budgets for tracegas columns

In Table 7-1 all error types investigated between Phase I and V are summarised. Error types investigated in Phase V are highlighted in green. As stated in FR, due to the small baseline error (based upon SNR figures) for UV ozone, most error types have some significance although UV ozone errors are generally small. Yellow marked error figures indicate same order of magnitude as baseline error; orange marked fields show errors exceeding significantly the baseline error.

Table 7-1:   Updated error budget for GOME-2 trace gas column retrieval

Error type		O3	O3 VIS	NO2	BrO	OCIO
						O3 hole, alb=0.8
Basic SNR (IT=0.1875s)		<0.5% (~0.3%)	<5% (~3%)	<30% (~15%)	<60% (~30%)	>100% (~100%)
polarisation correction		<1% (0.5%)				
Ground AI diffuser		~0.3%	? (larger than UV)	50%	70%	?
QV diffuser*		0.1%	6%	22%	67%	
*indirect estimate						
Spatial aliassing		0.2%		<2%	<1%	<15%
Spectral Resolution	Defocusing (1/2)*	0.3%	3%	18%	35%	
	Open slit (1/2)*	0.2%	2%	11%	25%	
	usampl./defoc(2.2px. FWHM)*	0.2%±0.3%		2%±15%	80%±30%	
*basic SNR included						
RTM assumption	PS vs Spherical w/ refraction	<1%	<1%	<1%	<1%	
	Spherical w/o refraction	<0.3%	<0.2%	<0.5%	<1%	
	Spherical vs. PS GRD	<1%		<1%	<1%	
	Spherical vs PS TOA	<4%		<6%	<5%	
BRDF		<0.3%	<3%	<2%	<3%	
FEL/sun simulator		0.3%	6%	4%	30%	
Pointing accuracy		<0.5%		<1%	<0.5%	

7.3   Updated error budget for ozone profiles

Figure 7-1 and Figure 7-3 are from the main study (Phase I to IV). These plots illustrate the baseline error budget for ozone profile retrieval for albedo 0.05 and albedo 0.8, respectively.

Panels indicate results for a particular geo-temporal scenario. Lines in each panel indicate results for the nadir case. The full line indicates the estimated retrieval precision or standard deviation (ESD), the dashed line shows the root-sum-squared mapped errors from the following sources:

> **Pressure:**   1% perturbation in surface pressure.
>
> **Temperature:**   Error after assimilation of IASI data into NWP model.
>
> **Res Pol Corr:**   Residual polarisation correction error ("components" case)
>
> **Radcal:**   Impact of 1% wavelength-independent bias in radiometric calibration
>
> **Aerosol:**   Impact of perturbing MODTRAN background case to an extreme tropospheric aerosol load.

The dotted line shows the RSS when the aerosol uncertainty is omitted. Shaded areas show the envelope of each line when extreme east and west viewing geometries are considered. More details are given in:

> *Kerridge, B.J., R. Siddans, B.L. Latter, J.P. Burrows, M. Weber, R. De Beek,*
> *I. Aben and W. Hartman,   GOME-2 Error Assessment Study,*
> *Final Report EUMETSAT Contract No EUM/CO/01/901/DK, 2002*

Figure 7-2 and Figure 7-4 are corresponding plots from the current extension (Phase V). They illustrate the effects of the update to the polarisation correction error based on FM2.

The new error budgets are seriously degraded from the previous results in a number of cases, particularly in the East pixel.

The following additional errors, which were also investigated in Phase V, will further degrade the error budget, if recommendations for their mitigation are not implemented:

> ➢ Errors in BSDF calibration, particularly if correlated with spectral structure in the Huggins band range
>
> ➢ Errors in slit function knowledge

Figure 7-1:   Main-study base-line error budget for O$_3$ profile - albedo 0.05
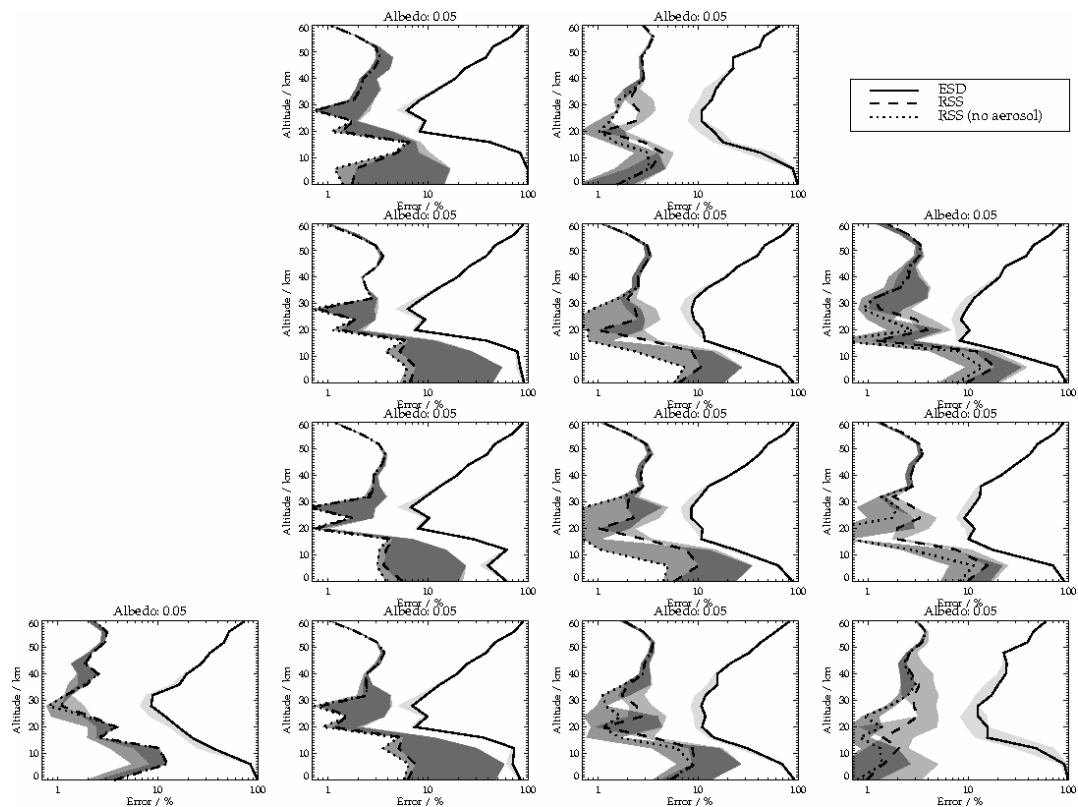
Figure 7-2:   New base-line error budget for O$_3$ profile - albedo 0.05

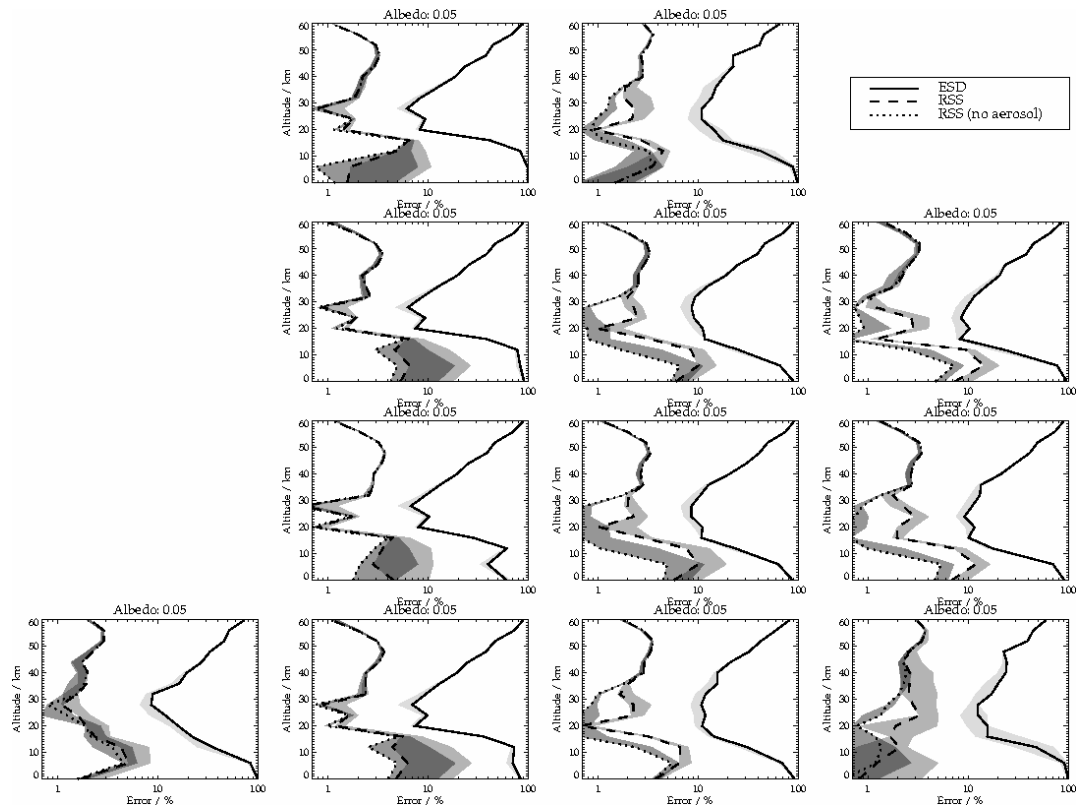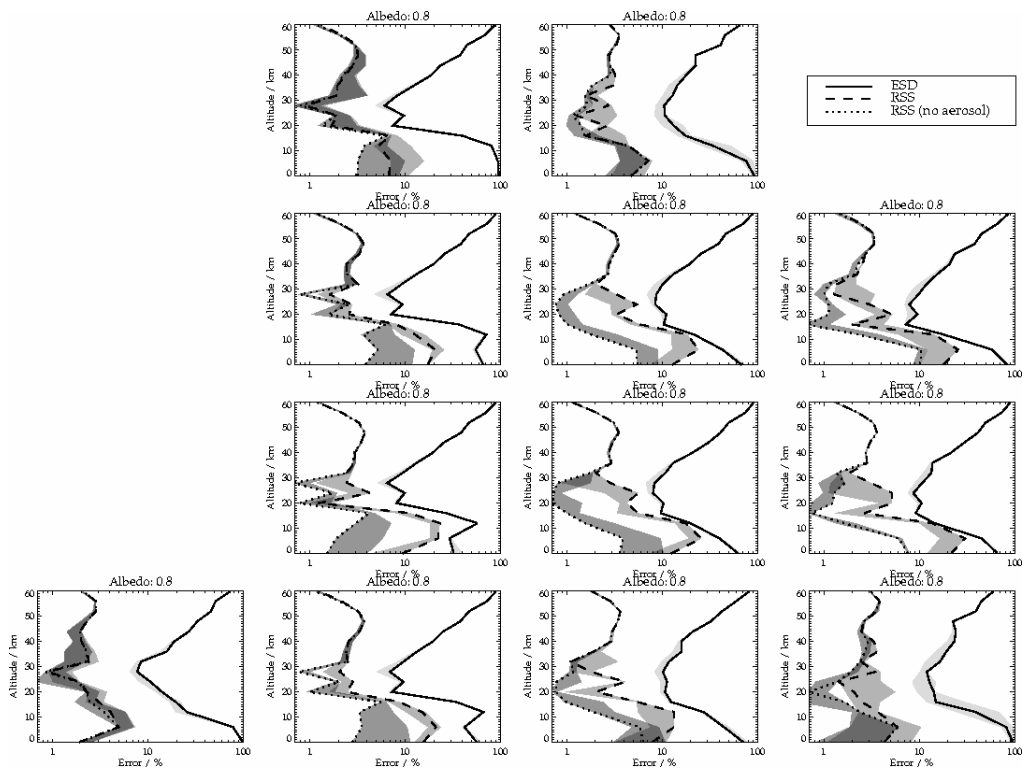**Figure 7-3:**   Main-study base-line error budget for O₃ profile - albedo 0.8
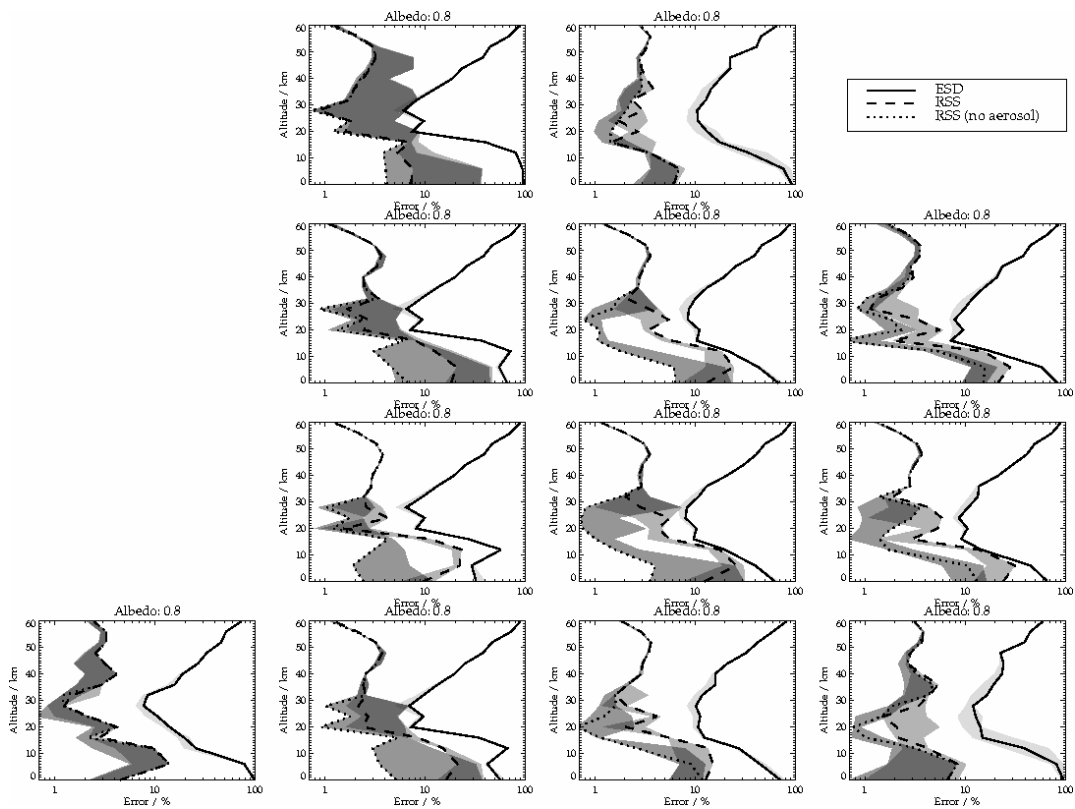

Figure 7-4:   New base-line error budget for O₃ profile - albedo 0.8

7.4 Recommendations from study extension (Phase V)

7.4.1 *General*

Recommendations arising from Phase V are given below and numbered V1 to V8

7.4.2 *Diffuser plate*

It was shown in Section 3 of this Phase V report that a replacement of the ground Al diffuser plate with the Quasi-Volume Diffuser (QVD) should reduce the diffuser related errors cited in FR by approximately a factor of four. *The replacement of the ground Al diffuser with a QVD is therefore highly recommended.*

This error is caused by differential structures that correlate with those in atmospheric absorption spectra used in the column retrieval. For GOME-1, this dependence has a clear seasonal cycle because the elevation and azimuth angles of the solar beam incident on the diffuser vary according to the sun-earth-satellite configuration. This error therefore causes a seasonally-dependent offset in the retrieved columns. However, one should keep in mind that such errors have been estimated indirectly and will need to be confirmed during operation in space.

In case offsets for the GOME-2 QVD are found to be significant, there are possibilities to reduce these. Using a single solar reference spectrum for the whole year would keep the bias constant over the seasons. Comparing GOME-2 retrieved column amounts with independent measurements from the ground or other platforms would yield the unknown bias for a given fixed solar reference. A network of ground-based measurements exists within the NDSC (Network for Detection of Stratospheric Change) that could be used for bias determination in certain cases. However, for most of the minor absorbers (particularly for H_2CO, BrO, OClO, SO_2) correlative data sets are difficult to obtain. Specific validation campaigns using airborne or ground-based measurements should be planned during the commission phase.

However, additional validation campaigns may be needed beyond the commissioning phase to evaluate possible remaining biases in the retrieved columns related to the new diffuser. For maintaining the quality of the minor trace gases for the lifetime of the three METOP missions a dedicated ground-based network with particular emphasis on (free) tropospheric measurements of the same gases will be needed.

> *Recommendation V1:* The quasi volume diffuser should be used for GOME-2
>
> *Recommendation V2:* Measurements of NO_2, BrO, OClO, H_2CO and SO_2 columns should be made regularly for several years by ground-based instruments to characterise the *seasonal-dependence* of errors arising from diffuser spectral structures for each FM in flight.

7.4.3 *BSDF Calibration*

7.4.3.1 *Trace Gas Columns*

Two independent measurements of the BSDF of the diffuser plate were available. These BSDF measurements allow an absolute radiometric calibration of the spectrometer for a set of incidence angles onto the diffuser.

One set of measurements was made using an absolute radiometric calibration source (FEL lamp) according to a standard NIST procedure. The second set of measurements was made using a Xenon lamp with a different optical set-up. The latter set was called the sun simulator (see GOME-2 CDR Report). The differences in the results lead to significant deviations in the DOAS columns that were statistically significant compared to the baseline error. This discrepancy needs to be resolved. No adequate alternative is known to compensate this effect.

In particular, the sun simulator experimental set-up must be verified to conform to a standard that is required to do an absolute radiometric calibration, as is the case with the FEL lamp set-up. It is also recommended to check that the FEL lamp set-up properly conforms to the prescribed standard procedure.

It is strongly recommended that during instrument characterisation both experimental set-ups (FEL lamp/ sun simulator) conform to standard procedures as required in absolute radiometric calibration. A better

understanding of the fine scale spectral structures observed in both set-ups would be helpful. There is no adequate correction scheme on the algorithmic side to compensate for this type of error

Additional zenith-sky and direct sun measurement with the flight models could be very useful to complement laboratory calibration. It allows, in addition, the verification of existing Level-1 and Level-2 processing algorithms, and it may improve the entire calibration procedure.

7.4.3.2   Ozone Profiles

Errors on ozone profile retrieval due to uncertainties[1] in of the FM1 BSDF can be comparable to the ESD, but it must be emphasised that they manifest as systematic, rather than random error.

It is recommended that the BSDF in Band 1 be better characterised, either through improved analysis of existing measurements or by additional measurements (e.g. with NASA sphere).

It is also desirable to improve characterisation of FM2 and FM3 in this spectral range, since the biases which are close to ~ 10% in the mid-upper stratosphere are significant compared to the RSS component of the base-line error budget.

The propagation of BSDF uncertainties in the other Bands leads to significant errors in ozone profile and column BrO and ozone. These errors are driven by fine spectral structure in the BSDF error, but it is not clear as to what extent the fine structure evident in the CRR analysis is representative of those errors which would be applicable to calibrated Level 1 data.

Unless such structure can be demonstrated to be an artefact of one (or both) measurement techniques, then it is important to better characterise the BSDF at fine spectral scales in Band 2b (for ozone profile retrieval) and other spectral ranges used for trace-gas column analysis.

It should be noted that this issue has to be resolved by careful calibration since there is no known correction scheme to compensate algorithmically for inadequate pre-flight characterisation are possible on the algorithmic side.

> **Recommendation V3**:   *Realistic error budgets should be defined for FM1, FM2 and FM3 diffuser BSDF, paying particular attention to fine-spectral scales.*

> **Recommendation V4**:   *Zenith-sky and direct-sun measurements should be made with flight models on ground to verify BSDF calibration and to test the Level-1 algorithm[2].*

7.4.4   Residual polarisation errors

7.4.4.1   Trace Gas Columns

For GOME-2 the errors in the polarisation corrections are generally below 0.5%, but in selected cases can reach 1%. This error has the same order of magnitude as the baseline error of UV ozone. It was surprising to find that the proposed and hypothetical higher PMD read-out rate did not reduce the error. In some scenarios even larger errors were found. This is maybe not surprising since the higher PMD read-out may be more beneficial in the spectral range near the single scatter point (290 - 310 nm). The fitting window for ozone column at 325-335 nm is less sensitive to the read-out rate. Other minor trace gases with absorptions less than 1/100 are not affected by the polarisation correction. In general it would be preferable to have PMD measurements at identical spectral resolution and range as the science channels, at least for Channel 1 and Channel 2 (280 – 400 nm). This would allow greater flexibility in the selection of O_3 fitting windows (column and profile retrieval), since the larger ozone absorption is the higher the polarisation correction errors gets. It may be interesting to develop a second order correction to the PCA by creating look-up-tables as a function of ozone profile shape, column and other geophysical parameters (albedo, surface height, etc.) based upon radiative transfer calculations. It is recommended to improve upon the current polarisation correction error by a factor of two to meet DOAS requirements. This may be possible by using an algorithmic correction scheme based upon radiation transfer calculation if PMD set-up and read-out cannot be altered.

---

[1] Quantified by the deviation between FEL and sun-simulator measurements of the BSDF

[2] Measurements need to be made and analysed early enough for a feasible response to be possible, if necessary (e.g. repeat measurement).

7.4.4.2   Ozone Profiles

The new analysis of residual polarisation correction errors has revealed serious consequences for ozone profile as well as trace gas column retrieval, including unacceptably large ozone errors in the troposphere for some view geometries.

Large errors are caused by:

(a)   The inappropriate handling of low Q:I cases by the current polarisation correction scheme and, more fundamentally,

(b)   Huggins structure in the residual polarisation error signature which cannot be corrected with the currently proposed L1 processor, even if signals from all PMD detector pixels were to be available and used in the correction[3].

Recommendation V5:   *The base-line polarisation correction scheme for L1 processing should be improved to accommodate low Q:I cases.*

Recommendation V6:   *To mitigate residual polarisation errors correlated with the Huggins absorption features, the following strategies should be investigated: (a)devise across-track scan pattern to avoid 90° scattering angle; (b) devise scheme to correct for fine structure in polarisation.*

7.4.5   Spatial aliasing

The consequences for ozone profile retrieval of perturbations to the polarisation correction caused by spatial aliasing are minor compared to (a) the direct impact of spatial aliasing on the signals recorded by the FPAs (modelled in the main study) and (b) other errors in polarisation correction (see Task 2e).

Other issues relating to the direct impact of spatial aliasing were identified in the main study but were not included in the SoW for this extension.

These issues still remain, and should be addressed (see below).

7.4.6   Slit function characterisation

The main study clearly identified the necessity of characterising the slit function accurately at sub-pixel spectral resolution for ozone profile retrieval.

Such characterisation will also benefit DOAS retrievals by:

(a)   Reducing fit residuals,

(b)   Permitting proper convolution of high-resolution cross-section to instrument resolution,

(c)   Provides the possibility to verify under-sampling correction schemes widely used in the DOAS community to GOME-1 data.

Work carried out in this study extension has quantified requirements for adequate laboratory measurements of slit function. It has been shown that a stimulus of the type used to measure the OMI slit-function should be acceptable for characterising the GOME-2 slit function. Requirements on slit-function measurements derived to meet End User requirements on ozone profile and column retrievals are found to be broadly comparable.

It is important to note that requirements as specified apply to a GOME-2 spot width of 0.21 nm which corresponds to a GOME-2 slit-function width of 0.3 nm, as pertains to FM2 after defocusing. Calculations performed within the study show that more stringent requirements would have to be imposed for a more focused instrument. It is therefore recommended that FM1 and FM3 be defocused to at least 0.3 nm slit-width for this reason, in addition to those given in the main study.

Recommendation V7:   *The slit function of GOME-2 (all flight models) should be determined according to the quantitative requirements specified in this study, with particular attention to the Huggins bands (315-335 nm).*

Recommendation V8:   *FM1 and FM3 should be defocused to at least the level implemented in FM2 (slit width of 0.3 nm in Huggins bands), with the same physical slit dimension*

---

[3] Due to the low spectral resolution of the PMDs in the Huggins range

Source error type	O3 Profile	Trace gas column	OMI Source
Signal:Noise	700	100	~1000[4]
Power	1%	2 %	0.5-1%[5]
Shift	3% of width (0.0012 nm)	8% of width (0.0032 nm)	0.003nm[6]
Width	40%	20%	~10's%[7]

Table 7-2:   **Requirements for laboratory measurements derived from O$_3$ profile and trace gas column analyses assuming defocused slit and FM2 spot size**

---

[4] A basic S/N of ~ 1000 can be achieved at the stimulus central wavelength.

[5] For sufficiently long integration times, and Echelle angles within 1° of the nominal angle (at 75° angle of incidence)

[6] Relative accuracy near 335 nm arising from motor drive. Bias of ~ 0.01 nm is also expected from the alignment procedure, but is not important to derivation of slit-width since it would apply to all wavelengths.

[7] Uncertainty in knowledge of stimulus width has been inferred indirectly by comparison of measured and predicted OMI slit-function widths to be ~ 10's %.

7.5 Review of Recommendations from the main study (Phases I to IV)

7.5.1 *Introduction*

The primary recommendations from the main study are restated (in italics), then reviewed below. The original numbering has been retained from the final report on the main study.

7.5.2 *Recommendation A1*

For O_3 profile retrieval, it is recommended to not use Band 1B wavelengths above 307 nm.

Retained

7.5.3 *Recommendation A2*

For O_3 profile retrieval, it is recommended that the integration times for Bands 1A and 1B be 1.5 sec and 0.1875 sec, respectively.

Retained

7.5.4 *Recommendation A3*

For O_3 profile retrieval, it is strongly recommended that the slit-function shape in Band 2 below 340 nm be measured before flight at sub-pixel resolution.

Superseded by Recommendation V7   (above)

7.5.5 *Recommendation A4*

It is recommended that the impact of spatial aliasing be assessed more thoroughly:

> *a) Impact on O_3 profiles and trace-gas columns via use of PMD measurements to correct polarisation response of detector arrays*
>
> *b) Global statistical analysis of O_3 profiles and tracegas columns using ATSR-2 images*
>
> *c) Impact on geophysical products retrieved from PMD measurements*
>
> *d) Impact on multi-wavelength aerosol retrieval*

Recommendation A4 (a):   Completed in Phase V

Recommendations A4 (b), (c) and (d):   Retained

7.5.6 *Recommendation A5*

Recommendation A5: It is recommended that an Observing System Simulation Experiment (OSSE) be undertaken for GOME-2 to decide on optimum ground-pixel size and swath width
It is envisaged that although such an OSSE might be conducted using the O_3 assimilation scheme of an NWP centre, the "figure of merit" should be the 4D O_3 field itself, and possibly the surface UV flux, rather than the usual NWP forecast variables. I.e. ground-pixel size and swath would be optimised by minimizing (time-evolving) deviations between assimilated and true O_3 fields, taking into account the likelihood of cloud obscuration for different ground pixel sizes and known variations with integration time and scan-angle of random and systematic errors on retrieved O_3.

Retained

7.5.7 *Recommendation B1*

For retrieval of trace gases other than ozone, it is strongly recommended to switch to a diffuser plate with peak-to-peak spectral signatures of less than 10^{-4}.

Superseded by recommendation V1   (above)

7.5.8   Recommendations B2/C3

B2: For retrieval of trace gas columns other than ozone, it is recommended to open the slit in preference to the defocusing option.

C3: More studies are needed to investigate the impacts of: (a) defocusing, (b) opening the slit and (c) opening the Band 3/4 aperture stop, in particular with respect to hardware implications.

The significant reduction in column error by opening the slit as proposed in B2 is due to the fact that the gain in signal-to-noise-ratio more than outweighs the decreased spectral resolution (less differential structures). Opening the slit in Band 2 could, however, potentially degrade the accuracy of the ozone profile. Further work would therefore be required to assess the trade-off between the signal to noise benefits of opening the slit and degrading spectral resolution for the ozone profiling. The current optical design of the current GOME-FMs limits the maximum amount of slit opening and may require an optical re-design of the instruments that may be out of scope for the current generation of GOME-2. Nevertheless, the slit opening may become an important issue for future instrumentations

In the main study, it was recognised that a reduction in the GOME-2 ground pixel size for a given swath width could potentially improve the quality of tropospheric composition sounding. The possibility has recently been identified that onboard data compression might offer a means to increase the number of ground-pixels measured across-track within the currently specified GOME-2 data downlink rate. Recommendations B2 and C3 are therefore now combined into the following:

It is recommended to review the feasibility of doubling the number of ground pixels sampled across-track, so as to halve ground pixel size for a given swath-width, in order to maximize the number of cloud-free scenes observed and hence the quality of O_3 and minor trace gas distributions in the troposphere.

This would require Band 2b, Band 3 and Band 4 integration times to be halved from 0.1875 sec to 0.09375 sec. Onboard data compression might offer a means to double the number of ground-pixels without doubling the GOME-2 data downlink capacity. If not, an alternative would be to halve the integration times and downlink alternate ground-pixels across the swath. This would still permit the frequency of cloud-free pixels to be increased substantially, although at the expense of losing half the total measurement time.

The slit width and level of defocusing as implemented for FM2 are adequate, provided that Recommendation V7 is carried out. It is however important to note that the quantitative requirements for laboratory measurements defined in Phase V depend upon the assumed level of defocusing. It should be recognised that if the slit-image is focused more sharply for FM1 or FM3 than for FM2, requirements on slit-function characterisation would need to be considerably more stringent. Recommendation C3 is therefore replaced by Recommendation V8 (above). If Recommendation V8 is not followed, then requirements for laboratory characterisation of the slit function must be carefully reconsidered.

7.5.9   Recommendation C1

Specify requirements for laboratory measurements of slit-function shape and quantify the benefits for the Band 2 step of O_3 profile retrieval.

Done in Phase V

7.5.10 Recommendation C2

It is recommended that the impact of errors in knowledge of slit-function shape be quantified for:

(a) The Band 1 step of O_3 retrieval
(b) Trace gas column retrievals
(c) Aerosol and cloud retrievals using the O_2 A-band

(a) Done
(b) Done
(c) Retained

7.5.11 Recommendation C3

More studies are needed to investigate the impacts of: (a) defocusing, (b) opening the slit and (c) opening the Band 3/4 aperture stop, in particular with respect to hardware implications.

Modified and merged with B2, See above in Subsection 7.5.8

7.5.12 Recommendation C4

Investigate and quantify the benefits of algorithm improvements for ozone profile retrieval to mitigate errors from wavelength-dependent degradation in the UV.

Undertaken for GOME-1 in parallel work to Phase V

7.5.13 Recommendation C5

Assess possible use of onboard white light source to monitor wavelength-dependent degradation in the uv

Retained

7.5.14 Recommendation C6

Implement and quantify the benefits to ozone profile and trace gas column retrievals of algorithm improvements to mitigate errors due to sun-glint.

Retained

7.5.15 Recommendation C7

Quantify errors arising from non-linear radiative transfer in conjunction with static scene inhomogeneities in cloud and surface reflectance.

Retained

7.5.16 Recommendation C8

Assess errors on ozone profiles from the assumed vertical distribution of aerosol more thoroughly, in order to better gauge instrumental errors

Retained

7.5.17 Recommendation C9

Assess the impact on ozone profile and ozone column error budgets of adding visible wavelengths

Retained

7.5.18 Recommendation C10

Assess errors from uncertainties in absorption cross-sections of ozone and other trace gases, the high-resolution solar reference spectrum and polarised atmospheric radiative transfer, in order to better gauge instrumental errors

Retained

7.6   Consolidated list of recommendations

New recommendations from this study extension and those deriving from the main study are consolidated in the tables below.

	New recommendations from Phase V of study
V1	The quasi volume diffuser should be used for GOME-2.
V2	Measurements of NO_2, BrO, OClO, H_2CO and SO_2 columns should be made regularly for several years by ground-based instruments to characterise the *seasonal-dependence* of errors arising from diffuser spectral structures for each FM in flight.
V3	Realistic error budgets should be defined for FM1, FM2 and FM3 diffuser BSDF, paying particular attention to fine-spectral scales.
V4	Zenith-sky and direct-sun measurements should be made with flight models on ground to verify BSDF calibration and to test the Level-1algorithm
V5	The base-line Level 1 polarisation correction scheme should be improved to accommodate low Q:I cases
V6	To mitigate residual polarisation errors correlated with the Huggins absorption features, the following strategies should be investigated: (a)devise across-track scan pattern to avoid 90° scattering angle; (b) devise scheme to correct for fine structure in polarisation.
V7	The slit function of GOME-2 (all flight models) should be determined according to the quantitative requirements specified in this study, with particular attention to the Huggins bands (315 - 335 nm).
V8	FM1 and FM3 should be defocused to at least the level implemented in FM2 (slit width of 0.3 nm in Huggins bands), with the same physical slit dimension.

	Retained recommendations from Phases I to IV of study
A1	For O_3 profile retrieval, it is recommended to not use Band 1B wavelengths above 307 nm.
A2	For O_3 profile retrieval, it is recommended that the integration times for Bands 1A and 1B be 1.5 sec and 0.1875 sec, respectively.
A4	It is recommended that the impact of spatial aliasing be assessed more thoroughly: a) Global statistical analysis of O_3 profiles and trace gas columns using ATSR-2 images b) Impact on geophysical products retrieved directly from PMD measurements c) Impact on multi-wavelength aerosol retrieval.
A5	It is recommended that an Observing System Simulation Experiment (OSSE) be undertaken for GOME-2 to decide on optimum ground-pixel size and swath width.
B2/C3	It is recommended to review the feasibility of doubling the number of ground pixels sampled across-track, so as to halve ground pixel size for a given swath-width, in order to maximize the number of cloud-free scenes observed and hence the quality of O_3 and minor trace gas distributions in the troposphere[8].

---

[8] This would require Band 2B, 3 and 4 integration times to be halved from 0.1875 sec to 0.09375 sec. On-board data compression might offer a means to double the number of ground-pixels without doubling the GOME-2 data downlink capacity. If not, an alternative would be to halve the integration times and downlink alternate ground-pixels across the

	Retained recommendations from Phases I to IV of study (continued)
C2	It is recommended to quantify the impacts of: (a) scene inhomogeneity on radiometric response and slit-function shape[9] and (b) errors in knowledge of slit-function shape on aerosol and cloud retrievals using the O_2 A-band.
C5	Assess possible use of onboard white light source to monitor wavelength-dependent degradation in the UV
C6	Implement and quantify the benefits to ozone profile and trace gas column retrievals of algorithm improvements to mitigate errors due to sun-glint.
C7	Quantify errors arising from non-linear radiative transfer in conjunction with static scene inhomogeneities in cloud and surface reflectance.
C8	Assess errors on ozone profiles from the assumed vertical distribution of aerosol more thoroughly, in order to better gauge instrumental errors
C9	Assess the impact on ozone profile and ozone column error budgets of adding visible wavelengths
C10	Assess errors from uncertainties in absorption cross-sections of ozone and other trace gases, the high-resolution solar reference spectrum and polarised atmospheric radiative transfer, in order to better gauge instrumental errors

7.7 Recommendation for Further Scientific Studies

- **Scientific review of calibration plan from pre-flight to in-flight (Level-0 to Level–1 processing)**

    With the vast experience form GOME-1, SCIAMACHY and OMI many calibration procedures have been developed to best characterise UV/VIS backscatter instruments. Nevertheless, problems in the retrieval of trace gases (see GOME-1 and SCIAMACHY) have been mostly related to calibration issues. Particularly for the ozone profiling and minor trace gas retrieval this has been very critical. A thorough review in form of an extensive study to investigate current calibration plans and the use of key data in data processing in a more coherent way would extremely beneficial. An outcome of such a study could provide an optimised calibration definition in combination with improved Level-1 and Level-2 data processing.

- **Study of the implementation of CCD arrays for spectral and polarisation measurements**

    Detector technology has advanced in recent years and an exploration of the use of CCD technology for spectral and polarisation measurements by future UV/VIS space instruments may bring improvements with respect to spatial resolution and signal-to-noise requirements for minor trace gas retrieval. Particularly, for tropospheric measurements the highest possible spatial resolution will be beneficial to establishing emission inventories.

---

swath. This would still permit the frequency of cloud-free pixels to be increased substantially, although at the expense of losing half the total measurement time. In the redesign of a future UV/VIS satellite-borne spectrometer, it would benefit photometric S/N on trace gas column retrievals for individual ground pixels to have a slit-function wider than that of GOME-2: ~ 0.5 nm in Band 2 and ~ 1 nm in Band 3.

[9] Non-uniform illumination of the entrance slit in conjunction with non-uniform detector pixel spatial response will modify signal level and variation in illumination along the cross-dispersion axis (i.e. along-track direction) will modify slit-function shape.